

SPATIALLY DEPENDENT TRANSFER
FUNCTION OF NUCLEAR SYSTEMS
BY CROSS CORRELATION METHODS

By
CHESTER D. KYLSTRA

A DISSERTATION PRESENTED TO THE GRADUATE COUNCIL OF
THE UNIVERSITY OF FLORIDA
IN PARTIAL FULFILLMENT OF THE REQUIREMENTS FOR THE
DEGREE OF DOCTOR OF PHILOSOPHY

UNIVERSITY OF FLORIDA
December, 1963

ACKNOWLEDGMENTS

The author wishes to express his appreciation to the members of his graduate committee for their advice and assistance. In particular, Dr. R. Uhrig and Dr. R. Selfridge have provided continued aid and guidance during this study.

The author wishes to thank the technicians and graduate assistants of the Department of Nuclear Engineering for their help. Aid in checking out equipment, building special circuits, and running the experiments was provided by: F. Primo, H. Diaz, K. Fawcett, R. Lyttle, T. McCall, A. Tuthill, R. Hartley, R. Kavipurapu, G. Fogle, P. Hunter, W. Nelson, J. Muller, D. Butterfield, J. Moore.

Special thanks are due his wife, Pat, for the many hours she spent drawing and inking figures, inserting Greek letters in the text, proofreading, and typing the manuscript.

The author also wishes to extend his thanks to Dr. M. Moore, Dr. R. Perez, and Dr. R. Dalton for their advice and many helpful comments.

TABLE OF CONTENTS

	Page
ACKNOWLEDGMENTS	ii
LIST OF TABLES	v
LIST OF FIGURES	vi
ABSTRACT	ix
Chapter	
I. INTRODUCTION	1
II. THEORY	4
Transfer Function	4
Statistical Theory	30
III. EXPERIMENTAL METHOD AND ANALYSIS	45
Experimental Method	45
Data Analysis	53
IV. EXPERIMENTAL EQUIPMENT	62
Input System	62
Nuclear Systems	66
Output System	70
V. RESULTS	75
Theoretical Results	75
Experimental Results	87
VI. CONCLUSION	114
Appendix	
A. FOURIER TRANSFORM OF A PERIODIC DELTA FUNCTION	119
B. COMBINATION OF TRIGONOMETRY FUNCTIONS, EQUATION (50)	121

TABLE OF CONTENTS (Cont'd)

Appendix		Page
C.	ROOTS OF THE CHARACTERISTIC EQUATION . .	123
D.	COMPUTER CODES	129
E.	COUNT RATE CIRCUIT DESIGN	151
BIBLIOGRAPHY	157
BIOGRAPHY	161

LIST OF TABLES

Table		Page
1.	Count Rate Meter	71
2.	Nuclear Parameters Used for the Theoretical Results	76
3.	Number of Terms Required for Four Per Cent Error in Equation (57)	86
4.	Design Criteria	153
5.	Count Rate Circuit Components	155

LIST OF FIGURES

Figure		Page
1.	Definition of functions for statistical theory	35
2.	Block diagram of the experimental equipment	46
3.	Typical maximum length sequence and its auto correlation function	48
4.	Auto power spectrum of the maximum length input sequence	51
5.	An eight-stage, maximum length sequence, pseudo-random binary signal generator .	64
6.	Light water subcritical assembly	67
7.	Heavy water subcritical assembly	69
8.	Block diagram of the data acquisition system	74
9.	Theoretical transfer function for light water	77
10.	Theoretical transfer function for light water, $z = 100$ cm	79
11.	Theoretical transfer function for heavy water	80
12.	Theoretical transfer function for a light water subcritical assembly	82
13.	Theoretical transfer function for a heavy water subcritical assembly	83
14.	Auto power spectrum of the shift register	89
15.	Cross correlation of two detectors, light water	91
16.	Cross correlation of two detectors, heavy water	93

LIST OF FIGURES (Cont'd)

Figure		Page
17.	Cross correlation of two detectors, light water subcritical assembly	94
18.	Cross correlation of two detectors, light water subcritical assembly	97
19.	Auto power spectrum of Detector 1, light water subcritical assembly	98
20.	Amplitude of the cross power spectra, light water subcritical assembly	99
21.	Phase shift of the cross power spectra, light water subcritical assembly	100
22.	Amplitude of the transfer function between two detectors, light water subcritical assembly	102
23.	Phase shift of the transfer function between two detectors, light water subcritical assembly	103
24.	Cross correlation between two detectors, heavy water subcritical assembly	105
25.	Cross correlation between two detectors, heavy water subcritical assembly	108
26.	Auto correlation of Detector 1, heavy water subcritical assembly	109
27.	Amplitude of the cross power spectra, heavy water subcritical assembly	110
28.	Phase shift of the cross power spectra, heavy water subcritical assembly	111
29.	Amplitude of the transfer function between two detectors, heavy water subcritical assembly	112
30.	Phase shift of the transfer function between two detectors, heavy water subcritical assembly	113
31.	Typical roots of the characteristic equation	125
32.	Count rate circuit diagram	152

LIST OF FIGURES (Cont'd)

Figure		Page
33.	Amplitude of the transfer function for the count rate circuit	156

Abstract of Dissertation Presented to the Graduate Council
in Partial Fulfillment of the Requirements for the Degree of
Doctor of Philosophy

SPATIALLY DEPENDENT TRANSFER FUNCTION
OF NUCLEAR SYSTEMS USING CROSS CORRELATION METHODS

By

Chester D. Kylstra

December 21, 1963

Chairman: Dr. Robert E. Uhrig
Major Department: Nuclear Engineering

The concept of a transfer function for a nuclear system is extended to include spatial effects. The general equation is derived using the time-dependent Fermi age and diffusion theories for a single-region, isotropic, homogeneous medium. The fluctuation of the thermal neutron density at any point in the assembly is related to the variation of the fast neutron source intensity.

The general transfer function equation is specialized for several cases, including the case of a point source in a cylindrical medium. Theoretical curves are calculated for multiplying and non-multiplying media and compared with the commonly used lumped parameter transfer function.

The results indicate, in general, that the lumped parameter model predicts the correct behavior of the nuclear system only if the output detector is located a specific distance from the source. If the detector is located elsewhere, the lumped parameter model is not capable of accurate results.

Experiments were performed on light and heavy water subcritical assemblies to measure the spatially dependent transfer function between two detectors. The input to the assemblies was provided by a neutron generator which was turned on and off in a pseudo-random manner by the maximum length output sequence generated by a shift register. Two neutron detection systems provided analog output voltages proportional to the neutron density fluctuations at different locations in the assembly. The voltages were sampled at a high rate by a data acquisition system, which stored the data on magnetic tape. The data was analyzed by cross correlating the two outputs and calculating the cross power spectra.

Statistical equations are developed which show that the transfer function may be obtained by computing the ratio of the cross power spectra for two different runs, with one detector moved to a new location for the second run. This method of statistical analysis has several advantages. Among them is the ability to eliminate the effects of the source spectra and the effects of the measuring system from the results.

A comparison of the experimental and theoretical transfer functions provided inconclusive evidence as to the validity of the theoretical model. Other effects, such as reflection of the neutrons from the surroundings, prevented complete agreement. The equations used to predict the behavior of a light water system clearly must take

into account the effects of a distributed source, rather than a point source. The heavy water data was affected by the small size of the system and the nearness of other structures, but the theoretical curves still agreed very well with the experimental data.

CHAPTER I

INTRODUCTION

The principal purpose of this study is to develop a spatially dependent transfer function for nuclear systems, using the time dependent Fermi age and diffusion theories. The effects of neutron energy, time, space, and delayed neutrons are considered. The experimental spatially dependent transfer function of a light water and a heavy water subcritical assembly was measured and compared with the theoretical transfer function. The multiplication factor of both systems was varied from zero to near one.

The data collected for the measurement of the experimental transfer function was processed by cross correlation methods. A secondary purpose of this thesis is to demonstrate the advantages and accuracy of the particular method used.

The transfer function equations commonly used for nuclear reactors are derived from the time dependent diffusion equation, after the spatial dependence has been removed by assuming that the flux shape is the fundamental spatial mode. The reactor is treated as a "black box", or as a lumped parameter model (1, 2). This transfer function works surprisingly well (3), especially for low frequencies where the neutron flux appears to respond

simultaneously throughout the entire reactor and for critical systems, where the band width is narrow and the higher frequencies are greatly attenuated.

A reactor, however, is not actually a lumped parameter system. The distance between the input and output devices, as well as their relative locations in the system, can have a large effect on the measured attenuation and phase shift of a disturbance as it propagates through the system. As higher frequencies are present and of interest, as in neutron wave and random noise experiments, the time and spatially dependent solution of the neutron flux behavior is needed to adequately describe experimental results. Weinberg and Schweinler (4), in 1948, were the first to discuss the solution for a reactor driven by an oscillating absorber. Other papers (5, 6) have presented results for neutron wave propagation in both multiplying and non-multiplying media, showing the dispersion nature of the process, and the attenuation and phase shift of the neutron flux disturbance.

Further evidence of the spatial effect on the propagation of a neutron flux disturbance was provided by Badgley (7) and Boynton (8). In their work with random noise measurements, both used a transfer function for a two point reactor model to represent the twin slab University of Florida training reactor. Boynton (8) was able to measure the transit time of a neutron flux disturbance as it travelled between the two slabs.

Statistical correlation techniques were used as early as 1946, by deHoffman (9), to measure the dynamic parameters of a chain reactor. This work was extended by Albrecht (10) and Velez (11) to include the reactivity, neutron lifetime, and delayed neutron effects in the theoretical auto correlation function of the neutron density fluctuations.

Moore (12, 13) showed how the power spectrum of the reactor noise is related to the reactor transfer function, where the power spectrum and the auto correlation function are Fourier transform pairs. Power spectra measurements of the reactor noise were performed by Cohn (14) and Griffin (15) to obtain the reactor dynamic parameters as expressed by a theoretical transfer function. Griffin was able to compare the noise results with pile oscillator data.

Certain disadvantages inherent in the reactor noise power spectrum and auto correlation function measurements, particularly the uncertainty in the system input, the effects of external instrument noise, and the lack of phase shift information, are not present in the cross power spectrum and the cross correlation function. Several investigators (8, 16, 17), using random reactivity inputs and cross correlating the input and output signals of the nuclear reactor, have measured the reactor dynamic parameters quite easily, even with input signals that were small compared to the power level of the reactor.

CHAPTER II

THEORY

The theory presented in this chapter consists of two parts. First, the general spatially dependent transfer function for nuclear systems is developed. It is then adapted for several special cases and applications. It is written for a point source, compared with the common lumped parameter transfer function, and converted to an alternate form that converges faster for large systems. This conversion is easily made for a non-multiplying medium, but for a multiplying medium, the solution of a complex transcendental equation is required. A completely analytical solution in terms of the elementary functions is not possible, but numerical methods may be used to obtain the theoretical transfer function for specific applications.

In the second part, the statistical theory that relates the cross correlation and cross power spectrum of three neutron detectors to the spatially dependent transfer function is developed.

Transfer Function

The theoretical spatially dependent transfer function relates the thermal neutron density fluctuations at

the point r in a nuclear system to the fluctuations of an artificial source of fast neutrons having a known spatial distribution.

In the model used, the nuclear system, which is isotropic and homogeneous, consists of a single region. The driving function or input to the system is a time varying source of fast neutrons. The fast neutrons experience a slowing down phase, represented by the time dependent Fermi age theory. Upon reaching thermal energy, the neutrons enter a diffusion phase at constant energy, represented by the time dependent diffusion theory. If the medium is a multiplying one, additional neutrons are created by fission, and join the source neutrons in the slowing down process.

It is assumed that the neutrons from the artificial source, the prompt neutrons from fission, and the delayed neutrons have the same energy at birth. This energy is defined as the zero point on the lethargy scale.

The transfer function is limited by the same restrictions and assumptions inherent in the Fermi age and diffusion theories, which may be found in Reference (19), and by the mathematical approximation used in representing the neutron source condition.

Basic equations

The time dependent Fermi age equation for continuous slowing down, absorption, and leakage (2, 18) is

$$\frac{1}{v(u)} \frac{\partial \phi(r, u, t)}{\partial t} = - \frac{\partial q(r, u, t)}{\partial u} - \Sigma_a(u) \phi(r, u, t)$$

$$\begin{aligned}
& + D(u) \nabla^2 \phi(r, u, t) + S_a(r, t) \delta(u) \\
& + \nu \Sigma_f \epsilon (1 - \beta) \phi_t(r, t) \delta(u) + \sum_{i=1}^6 \lambda_i C_i(r, t) \delta(u)
\end{aligned}
\tag{1}$$

$u \geq 0$

Neutrons starting the slowing down process at zero lethargy are contributed by an artificial source $S_a(r, t)$, by prompt fission, $\nu \Sigma_f \epsilon (1 - \beta) \phi_t(r, t)$, and by the decay of the neutron precursors $\lambda_i C_i(r, t)$. The slowing down neutron flux is $\phi(r, u, t)$, at position r , at lethargy u , and time t , in units of neutron /cm² sec (unit lethargy). The neutron velocity is $v(u)$, corresponding to lethargy u , and $q(r, u, t)$ is the slowing down density at r and t , in units of (neutrons passing lethargy u) /cm³ sec. The macroscopic absorption cross section, $\Sigma_a(u)$, and the diffusion coefficient, $D(u)$, are both functions of the neutron lethargy. The average number of neutrons produced per fission is symbolized by ν , the thermal fission cross section is Σ_f , the fast fission factor is ϵ , and β is the fraction of neutrons produced by fission that appear as delayed neutrons. The thermal flux, $\phi_t(r, t)$, is not a function of lethargy, but is a function of position r and time t , with units of neutrons/cm² sec. The six neutron precursors are represented by $C_i(r, t)$, $i = 1$ to 6, with units of precursors/cm³, and the decay constants are λ_i , with units 1/sec. The Dirac delta function, $\delta(u)$, is used to insure that all the neutron sources are considered mathematically as an initial condition in lethargy.

The time dependent diffusion equation is (2, 18)

$$\frac{1}{v_t} \frac{\partial \phi_t(r,t)}{\partial t} = - \sum_{at} \phi_t(r,t) + D_t \nabla^2 \phi_t(r,t) + q(r, u_t, t) \quad (2)$$

with the symbols previously defined. The subscript t signifies the value of the variable at thermal energy. If desired, the model used here could be changed to include an artificial thermal neutron source. The source term would be added to the diffusion equation.

The equations for the six delayed neutron precursors are (2, 18)

$$\frac{\partial C_i(r,t)}{\partial t} = \beta_i \nu \Sigma_f \epsilon \phi_t(r,t) - \lambda_i C_i(r,t) \quad i = 1 \text{ to } 6 \quad (3)$$

where

$$\sum_{i=1}^6 \beta_i = \beta \quad (3a)$$

The three basic equations describing the neutron behavior are coupled. The diffusion equation is coupled to the slowing down equation by $q(r, u_t, t)$, the precursor equation is coupled to the diffusion equation by

$\beta_i \nu \Sigma_f \epsilon \phi_t(r,t)$, and the slowing down equation is coupled to both the diffusion equation and precursor equation by $[\nu \Sigma_f \epsilon (1 - \beta) \phi_t(r,t) + \sum_{i=1}^6 \lambda_i C_i(r,t)] \delta(u)$.

The slowing down equation may be written in terms of $q(r,u,t)$ by using an approximation relating $\phi(r,u,t)$ and $q(r,u,t)$ (18)

$$q(r,u,t) = \xi \sum_t(u) \phi(r,u,t) \quad (4)$$

This is a reasonable assumption if $\sum_s(u) \phi(u)$ is slowly varying with u , and $\sum_s(u) \gg \sum_a(u)$ (18).

The average loss in the logarithm of the neutron energy per collision, ξ , has units of (average gain in lethargy) per collision, and $\sum_t(u)$ is the total cross section at lethargy u .

The relation between the thermal neutron density and the thermal flux is (18)

$$\phi_t(r,t) = v_t n_t(r,t) \quad (5)$$

Separation of time varying and steady state components. The time varying quantities in the basic equations may be separated into steady state components and time dependent components. The latter vary positively and negatively about the steady state value. Using the Δ to represent this variation, the quantities of interest, after substitution of Equations (4 and 5) in the first three equations, are

$$\begin{aligned} n_t(r,t) &= n_{t0}(r) + \Delta n_t(r,t) \\ q(r,u,t) &= q_0(r,u) + \Delta q(r,u,t) \\ C_i(r,t) &= C_{i0}(r) + \Delta C_i(r,t) \\ S_a(r,t) &= S_{a0}(r) + \Delta S_a(r,t) \end{aligned} \quad (6)$$

Since the basic equations are linear with respect to the time variable, they may be separated into the steady state and the time varying equations.

For the steady state components, the slowing down equation is

$$\begin{aligned}
 0 = & - \frac{\partial q_0(r, u)}{\partial u} - \frac{\sum_a(u) q_0(r, u)}{\xi \sum_t(u)} + \frac{D(u)}{\xi \sum_t(u)} \nabla^2 q_0(r, u) \\
 & + s_{a0}(r) \delta(u) + \nu \sum_f \epsilon (1 - \beta) v_t n_{t0}(r) \delta(u) \\
 & + \sum_{i=1}^6 \lambda_i c_{i0}(r) \delta(u) \quad (7)
 \end{aligned}$$

the diffusion equation is

$$0 = - \sum_a v_t n_{t0}(r) + D_t v_t \nabla^2 n_{t0}(r) + q_0(r, u_t) \quad (8)$$

and the precursor equations are

$$\begin{aligned}
 0 = & \beta_i \nu \sum_f \epsilon v_t n_{t0}(r) - \lambda_i c_{i0}(r) \\
 & i = 1 \text{ to } 6 \quad (9)
 \end{aligned}$$

The time varying components satisfy the following equations. The slowing down equation is

$$\begin{aligned}
 \frac{1}{\xi \sum_t(u) v(u)} \frac{\partial \Delta q(r, u, t)}{\partial t} = & - \frac{\partial \Delta q(r, u, t)}{\partial u} \\
 & - \frac{\sum_a(u)}{\xi \sum_t(u)} \Delta q(r, u, t) + \frac{D(u)}{\xi \sum_t(u)} \nabla^2 \Delta q(r, u, t) \\
 & + \Delta s_a(r, t) \delta(u) + \nu \sum_f \epsilon (1 - \beta) v_t \Delta n_t(r, t) \delta(u)
 \end{aligned}$$

$$+ \sum_{i=1}^6 \lambda_i \Delta C_i(r, t) \delta(u) \quad (10)$$

the diffusion equation is

$$\frac{\partial \Delta n_t(r, t)}{\partial t} = - \sum_{at} v_t \Delta n_t(r, t) + D_t v_t \nabla^2 \Delta n_t(r, t) + \Delta q(r, u_t, t) \quad (11)$$

and the precursor equations are

$$\frac{\partial \Delta C_i(r, t)}{\partial t} = \beta_i \nu \sum_f \epsilon_{v_t} \Delta n_t(r, t) - \lambda_i \Delta C_i(r, t) \quad i = 1 \text{ to } 6 \quad (12)$$

Solutions of time dependent equations

Equations (10, 11, and 12) are now solved for the transfer function, which is defined as the variation or perturbation in the thermal neutron density, $\Delta n_t(r, \omega)$, at position r , caused by a variation in the artificial source, $\Delta S_a(r, \omega) \delta(u)$.

Laplace transform in time. A Laplace transformation of Equations (10, 11, and 12) is now performed, which transforms the equations from the time domain to the frequency domain and removes the time derivatives from the equations. The time varying components are restricted to bounded functions, which may be composed of sinusoidal components. Thus the Laplace transform converges with the real part of the Laplace variable, $s = \sigma + j\omega$, equal to zero, or $s = j\omega$ (19).

Using the initial condition that all the time dependent variables are zero at time equal zero, which eliminates the transient solutions, Equations (10, 11, and 12) become respectively

$$\begin{aligned}
 \frac{j\omega \Delta q(r,u,\omega)}{\xi \sum_t(u) v(u)} = & - \frac{\partial \Delta q(r,u,\omega)}{\partial u} - \frac{\sum_a(u) \Delta q(r,u,\omega)}{\xi \sum_t(u)} \\
 & + \frac{D(u)}{\xi \sum_t(u)} \nabla^2 \Delta q(r,u,\omega) + \Delta S_a(r,\omega) \delta(u) \\
 & + \nu \sum_f \epsilon (1 - \beta) v_t \Delta n_t(r,\omega) \delta(u) \\
 & + \sum_{i=1}^6 \lambda_i \Delta C_i(r,\omega) \delta(u)
 \end{aligned} \tag{10a}$$

$$\begin{aligned}
 j\omega \Delta n_t(r,\omega) = & - \sum_a v_t \Delta n_t(r,\omega) + D_t v_t \nabla^2 \Delta n_t(r,\omega) \\
 & + \Delta q(r,u_t,\omega)
 \end{aligned} \tag{11a}$$

$$\begin{aligned}
 j\omega \Delta C_i(r,\omega) = & \beta_i \nu \sum_f \epsilon v_t \Delta n_t(r,\omega) - \lambda_i \Delta C_i(r,\omega) \\
 & i = 1 \text{ to } 6
 \end{aligned} \tag{12a}$$

The independent time variable, t , is replaced by an independent frequency variable, ω , in all the terms.

Spatial expansion. The slowing down density, the thermal neutron density, the precursor density, and the artificial source are now expanded in terms of complete, orthogonal functions that satisfy the Helmholtz equation (19)

$$\nabla^2 H(r, B_p) = - B_p^2 H(r, B_p) \tag{13}$$

over the volume of the system. The function $H(r, B_p)$ may be sines and cosines for Cartesian coordinates, and for cylindrical coordinates the function may be Bessel functions and sines and cosines. The requirement that the slowing down density, thermal neutron density, and precursor concentration be equal to zero at the extrapolated boundaries of the system is satisfied by $H(r, B_p)$. The eigenvalues, B_p^2 , which correspond to the familiar buckling in reactor analysis terminology, may be composed of one component for each space dimension; for example

$$B_p^2 = B_{n1}^2 + B_{n2}^2 + B_{n3}^2 \quad (14)$$

in general, or

$$B_p^2 = \left[\frac{n_1 \pi}{2a} \right]^2 + \left[\frac{n_2 \pi}{2b} \right]^2 + \left[\frac{n_3 \pi}{2c} \right]^2$$

n_1, n_2, n_3 all odd (14a)

for a rectangular parallelepiped.

Performing the expansions, the four frequency dependent variables become

$$\Delta q(r, u, \omega) = \sum_p \bar{q}_p(u, \omega) H(r, B_p)$$

$$\Delta n_t(r, \omega) = \sum_p \bar{n}_p(\omega) H(r, B_p)$$

$$\Delta c_i(r, \omega) = \sum_p \bar{c}_{ip}(\omega) H(r, B_p)$$

$$\Delta S_a(r, \omega) = \sum_p \bar{S}_p(\omega) H(r, B_p) \quad (15)$$

The bar symbolizes the expansion coefficients.

To solve Equations (10a, 11a, and 12a) for the transfer function, it is necessary that the spatial distribution of the artificial neutron source be known. Therefore, \bar{S}_p may be found by using the orthogonality property of $H(r, B_p)$ (19).

$$\begin{aligned} \int_{Vol} \Delta S_a(r, \omega) H(r, B'_p) d(Vol) &= \int_{Vol} \sum_p \bar{S}_p(\omega) H(r, B_p) \\ &\quad (\cdot) H(r, B'_p) d(Vol) \\ &= \bar{S}_p(\omega) A_p \end{aligned} \quad (16)$$

since (19)

$$\begin{aligned} \int_{Vol} H(r, B_p) H(r, B'_p) d(Vol) &= A_p \\ B'_p &= B_p \\ &= 0 \\ B'_p &\neq B_p \end{aligned} \quad (17)$$

A_p is a constant dependent on p only.

Substituting Equation (15) into Equations (10a, 11a, and 12a), and using Equation (13) where applicable, the slowing down equation becomes

$$\sum_p H(r, B_p) \left[-\bar{q}_p(u, \omega) \left\{ \frac{j\omega}{\xi \sum_t(u) v_t(u)} + \frac{\sum_a(u)}{\xi \sum_t(u)} + \frac{D(u)}{\xi \sum_t(u)} \frac{B_p^2}{v_t(u)} \right\} - \frac{\partial \bar{q}_p(u, \omega)}{\partial u} + \left\{ \sum_{i=1}^6 \lambda_i \bar{c}_{ip}(\omega) + \nu \sum_f \epsilon (1 - \beta) v_t \bar{n}_p(\omega) + \bar{s}_p(\omega) \right\} \delta(u) \right] = 0 \quad (18)$$

the diffusion equation becomes

$$\sum_p H(r, B_p) \left[-\bar{n}_p(\omega) \{j\omega + \sum_a v_t + D_t v_t B_p^2\} + \bar{q}_p(u_t, \omega) \right] = 0 \quad (19)$$

and the precursor equations become

$$\sum_p H(r, B_p) \left[-\bar{c}_{ip}(\omega) \{j\omega + \lambda_i\} + \beta_i \nu \sum_f \epsilon v_t \bar{n}_p(\omega) \right] = 0$$

$$i = 1 \text{ to } 6 \quad (20)$$

By use of Equation (13), the spatial divergence term has been replaced by $-B_p^2 H(r, B_p)$ from the Helmholtz equation. Equation (18) is the only one still containing a derivative.

Since the sums in Equations (18, 19, and 20) must equal zero independently of r , each coefficient of $H(r, B_p)$ must be equal to zero (19). Thus, the terms enclosed by the square brackets can be set equal to zero individually.

Slowing down solution. The slowing down equation has now been reduced (from Equation (18)) to

$$\begin{aligned}
\frac{\partial \bar{q}_p(u, \omega)}{\partial u} = & -\bar{q}_p(u, \omega) \left[\frac{j\omega}{\xi \sum_t(u) v(u)} + \frac{\sum_a(u)}{\xi \sum_t(u)} \right. \\
& + \left. \frac{D(u) B_p^2}{\xi \sum_t(u)} \right] + \left[\bar{S}_p(\omega) + \nu \sum_f \epsilon (1 - \beta) v_t \bar{n}_p(\omega) \right. \\
& + \left. \sum_{i=1}^6 \lambda_i \bar{\sigma}_{ip}(\omega) \right] \delta(u) \quad (21)
\end{aligned}$$

$u \geq 0$

where the bracket multiplied by $\delta(u)$ is the initial condition on $\bar{q}_p(u, \omega)$.

The solution to this equation, subject to the boundary conditions, is easily found and is

$$\begin{aligned}
\bar{q}_p(u, \omega) = & \bar{q}_p(0, \omega) \exp \left[-j\omega \int_0^u \frac{du}{\xi \sum_t(u) v(u)} \right. \\
& - \left. \int_0^u \frac{\sum_a(u) du}{\xi \sum_t(u)} - B_p^2 \int_0^u \frac{D(u) du}{\xi \sum_t(u)} \right] \quad (22)
\end{aligned}$$

The first integral in the exponential function can be identified as the average time required to slow down from zero lethargy to lethargy u . This time is defined as $l_T(u)$, with the slowing down lifetime to thermal lethargy defined as

$$l_T(u_t) = l_T \quad (23)$$

The exponential function raised to the power represented by the second integral is known in reactor analysis as the resonance escape probability $P(u)$ (18).

The third integral is defined in reactor analysis as the Fermi age, $\tau(u)$, (18). The Fermi age to thermal lethargy is defined as

$$\tau(u_t) = \tau \quad (23a)$$

Thus, Equation (22) becomes

$$\bar{q}_p(u, \omega) = \bar{q}_p(0, \omega) P(u) \exp[-j\omega \tau(u) - \tau(u) B_p^2] \quad (24)$$

The slowing down density at zero lethargy, $\bar{q}_p(0, \omega)$, may be found from the initial condition

$$\begin{aligned} \bar{q}_p(0, \omega) = \bar{S}_p(\omega) + \nu \sum_f \epsilon (1 - \beta) v_t \bar{n}_p(\omega) \\ + \sum_{i=1}^6 \lambda_i \bar{\sigma}_{ip}(\omega) \end{aligned} \quad (25)$$

Precursor terms. A relation between the precursors and the thermal neutron density is provided by Equation (20)

$$\bar{\sigma}_{ip}(\omega) = \frac{\beta_i \nu \sum_f \epsilon v_t \bar{n}_p(\omega)}{j\omega + \lambda_i} \quad (26)$$

The number of unknown variables in the basic set of equations may be reduced by substituting this relation into Equation (25), obtaining

$$\bar{q}_p(0, \omega) = \bar{S}_p(\omega) + \nu \sum_f \epsilon v_t \left[1 - \beta + \sum_{i=1}^6 \frac{\beta_i \lambda_i}{j\omega + \lambda_i} \right] \bar{n}_p(\omega) \quad (27)$$

For convenience, Equation (27) may be simplified by defining

$$\beta_c = 1 - \beta + \sum_{i=1}^6 \frac{\beta_i \lambda_i}{j\omega + \lambda_i} \quad (28)$$

Slowing down density terms. Substitution of Equation (27) into Equation (24), then Equation (24) into Equation (19) further reduces the basic equations by eliminating the slowing down density, $\bar{q}_p(u, \omega)$, resulting in

$$\bar{n}_p(\omega) [j\omega + \sum_{at} v_t + D_t v_t B_p^2] + [\bar{S}_p(\omega) + \nu \sum_f \epsilon \beta_c v_t \bar{n}_p(\omega)] P(u_t) \exp[-j\omega l_\tau - \tau B_p^2] = 0 \quad (29)$$

Solving for $\bar{n}_p(\omega)$, and using the following definitions (18)

$$\begin{aligned} L^2 &= \frac{D_t}{\sum_{at}} \\ l_s &= \frac{1}{\sum_{at} v_t} \\ k_\infty &= \frac{\nu \sum_f P(u_t) \epsilon}{\sum_{at}} \end{aligned} \quad (30)$$

for the square of the thermal diffusion length, thermal lifetime in an infinite medium, and multiplication factor in an infinite medium, respectively, gives

$$\bar{n}_p(\omega) = \frac{\bar{S}_p(\omega) P(u_t) l_s}{(1 + L^2 B_p^2 + j\omega l_s) \exp(j\omega l_\tau + \tau B_p^2) - k_\infty \beta_c} \quad (31)$$

General transfer function

An expression for the thermal neutron density may be constructed using Equations (15 and 31).

$$\Delta n_t(r, \omega) = P(u_t) \ell_s \sum_p \frac{\bar{S}_p(\omega) H(r, B_p)}{[1 + L^2 B_p^2 + j\omega \ell_s \exp(j\omega \ell \tau + \tau B_p^2) - k_\infty \beta_c]} \quad (32)$$

$\bar{S}_p(\omega)$ is found using Equation (16) and β_c is defined by Equation (28).

This is the general transfer function, showing the perturbation in the neutron density at location r caused by a source $\Delta S_a(r, \omega)$.

General point source transfer function

The transfer function can be obtained in a more explicit form if the artificial neutron source is a point source located at r_o . Then, from Equation (16)

$$\begin{aligned} \bar{S}_p(\omega) A_p &= \int_{Vol} \Delta S_a(r, \omega) \delta(r - r_o) H(r, B'_p) d(Vol) \\ &= \Delta S_a(r_o, \omega) H(r_o, B'_p) \end{aligned} \quad (33)$$

The correct form of the Dirac delta function corresponding to the geometry of interest must be used.

Therefore, Equation (32) becomes

$$\begin{aligned}
\frac{\Delta n_t(r, \omega)}{\Delta S_a(r_o, \omega)} &= G(r, r_o, \omega) \\
&= P(u_t) \ell_s \sum_p \frac{1}{A_p} \frac{H(r_o, B_p) H(r, B_p)}{[(1 + L^2 B_p^2 + j\omega \ell_s) \exp(j\omega \ell \tau + \tau B_p^2) - k_\infty \beta_c]} \quad (34)
\end{aligned}$$

Thus, the perturbation of the thermal neutron density at r , caused by a fast neutron source at r_o , is equal to an infinite sum. Each term of the sum is composed of the product of the orthogonal eigenfunctions, divided by the characteristic equation for the Fermi age, diffusion theory model used in this study. The characteristic equation corresponds to the dispersion function of classical physics. When set equal to zero, this function is called the dispersion law (42). Equation (34) is also the Green's function for this model, and could be used as a kernel in integrating over a source occupying a finite volume (27).

Equation (34) can be written in another form, using the more easily measured quantities

$$\ell_s^* = \frac{\ell_s}{1 + L^2 B_1^2} \quad (35)$$

$$k_{\text{eff}} = \frac{k_\infty \exp(-\tau B_1^2)}{1 + L^2 B_1^2} \quad (36)$$

which are the thermal neutron lifetime and multiplication factor for a finite medium.

Then

$$G(r, r_o, \omega) = [P(u_t) \ell_s^* \exp(-\tau B_1^2)]$$

$$(\cdot) \sum_p \frac{1}{A_p} \frac{H(r_o, B_p) H(r, B_p)}{\left[\left\{ 1 + \frac{L^2(B_p^2 - B_1^2)}{1 + L^2 B_1^2} + j\omega \ell_s^* \right\} \exp[j\omega \ell \tau + \tau(B_p^2 - B_1^2)] - k_{\text{eff}} \beta_c \right]} \quad (37)$$

There are several interesting features about the transfer function as written in Equations (34 and 37). The denominator, which is the characteristic equation of the system, is readily available for stability and control studies. The transcendental equation can be solved numerically for its roots, or an approximate form can be used (see Appendix C).

The approach used above to find the expansion coefficients for the source may still be used even if the source is located on one face of the assembly. The eigenfunction, $H(r, B_p)$, would then be defined over the actual medium and its mirror image, putting the source at the center of the mathematical problem.

The quantity defined by Equation (28), β_c , is simplified at the two extremes of the frequency range. As the frequency goes to zero, β_c approaches one. As the frequency goes to infinity, β_c approaches $1 - \beta$. Only in the frequency range 0.001 cps to 0.5 cps is β_c changing significantly. Thus, β_c may often be replaced by its limiting value, depending on which frequencies are of interest.

Both forms of the transfer function, Equations (34 and 37), have the disadvantage that the convergence of the series is slow, particularly if the size of the system is greater than the diffusion length and/or the Fermi age. Since one of the assumptions of the Fermi age and diffusion theories (18) is that the system is large compared to the characteristic nuclear dimensions, many terms must be included for a numerical analysis of Equation (34) or Equation (37). An alternate form of the transfer function that converges faster as the size of the system increases is developed after the next section.

Comparison with the lumped parameter transfer function

It is interesting to note that Equation (34) can be readily converted to the lumped parameter transfer function commonly used for nuclear reactors.

First, let all the quantities associated with the Fermi age model go to zero, that is, τ to 0, u_t to 0, and l_T to 0. Second, all terms in the series beyond $p=1$ may be ignored, or better yet, it may be assumed that the intensity of the artificial source is given by

$$\Delta S_a(r, \omega) = \Delta S(\omega) H(r, B_1) \quad (38)$$

which is the fundamental mode of the system. Then \bar{S}_p is zero for all p greater than one, and

$$\begin{aligned}
 \frac{\Delta n_t(r, \omega)}{\Delta S(\omega)} &= \frac{l_s H(r, B_1)}{1 + B_1^2 L^2 + j\omega l_s - k_{\infty} \beta_c} \\
 &= \frac{H(r, B_1)}{j\omega + \frac{1 - k_{\text{eff}} \beta_c}{l_s^*}} \quad (39)
 \end{aligned}$$

If the thermal neutron density is measured at the center of the system, where $H(0, B_1) = 1$, then Equation (39) is identical with the lumped parameter transfer function (5) for a subcritical system; otherwise, they differ by a constant. As k_{eff} goes to one, the correct form for a critical reactor is obtained

$$\frac{\Delta n(r, \omega)}{\Delta S(\omega)} = \frac{H(r, B_1)}{j\omega + \frac{1}{l_s^*} \left[\beta - \sum_{i=1}^6 \frac{\lambda_i \beta_i}{j\omega + \lambda_i} \right]} \quad (40)$$

Alternate form for the point source transfer function

The general transfer function may be converted to another form that converges much faster for large systems. The procedure followed is known as the inversion theory of series (20), and as Poisson's summation formula (4). In general, the method may be applied in three dimensions in any coordinate system. However, for the specific approach described below, it is necessary that the eigenvalue of Equation (13) be periodic.

Specialized problem. In order to show the inversion in some detail, the geometry of the medium is specified as cylindrical, the same geometry as that used in the experi-

ments (see Chapter IV). Since the axial eigenvalue is the only one that is periodic in cylindrical coordinates, the inversion is performed in one dimension only.

The artificial neutron source is located on the centerline of the experimental assembly and approximated by a point source. The origin of the coordinate system is located at the source.

For the cylindrical geometry described in Chapter IV, the eigenfunction is

$$H(r, B_p) = J_0(\nu_n \rho) \cos \frac{m\pi z}{2c} \quad (41)$$

with

$$\begin{aligned} B_p^2 &= B_n^2 + B_m^2 \\ &= \left[\frac{\nu_n}{R} \right]^2 + \left[\frac{m\pi}{2c} \right]^2 \\ m &= 1 \text{ to } \infty, \text{ odd only} \\ n &= 1 \text{ to } \infty \end{aligned} \quad (42)$$

The variable ρ is the radial coordinate divided by the maximum radius, R . The n^{th} zero of the J_0 Bessel function is ν_n , and c is the distance from the source to the end of the assembly in the positive z direction, even if the source is on one face of the cylinder. Under the assumptions listed above, the solution is valid only for $0 < z < c$ if the source is not in the center of the medium.

Using Equation (16) to find A_p and \bar{S}_p , Reference (21) gives for cylindrical geometry

$$\begin{aligned}
 A_p &= R^2 \left[\int_{Vol} J_0(\nu_n \rho) J_0(\nu'_n \rho) \cos \frac{m\pi z}{2c} \cos \frac{m'\pi z}{2c} \right. \\
 &\quad \left. (\cdot) 2\pi \rho d\rho dz \right] \\
 &= R^2 \pi c J_1^2(\nu_n)
 \end{aligned} \quad (43)$$

For the point source at $r = 0$,

$$\begin{aligned}
 A_p \bar{S}_p(\omega) &= R^2 \left[\int_{Vol} \Delta S(\omega) \frac{\delta(\rho)}{\rho} \delta(z) J_0(\nu_n \rho) \right. \\
 &\quad \left. (\cdot) \cos \frac{m\pi z}{2c} 2\pi \rho d\rho dz \right] \\
 &= 2\pi R^2 \Delta S(\omega)
 \end{aligned} \quad (44)$$

therefore,

$$\bar{S}_p(\omega) = \frac{2 \Delta S(\omega)}{c J_1^2(\nu_n)} \quad (45)$$

and Equation (32) becomes

$$\begin{aligned}
 G(r, 0, \omega) &= \frac{\Delta n_t(r, \omega)}{\Delta S(\omega)} = \frac{2P(u_t) l_s}{c} \\
 (\cdot) \sum_{n=1}^{\infty} \sum_{m=1}^{\infty} &\frac{J_0(\nu_n \rho)}{J_1^2(\nu_n)} \frac{\cos \frac{m\pi z}{2c} \sin^2 \frac{m\pi}{2}}{\left[(1 + L^2 B_p^2 + j\omega l_s) \exp(j\omega l_T) \right.} \\
 &\quad \left. + \tau B_p^2 - k_{\infty} \beta_c \right] } \quad (46)
 \end{aligned}$$

where $\sin^2(\frac{m\pi}{2})$ has been included in the numerator so that m may take all values, from one to infinity.

Inversion procedure. The first step is to replace B_m^2 in Equation (46) by a continuous variable, ξ^2 . To compensate for this replacement, Equation (46) must now be multiplied by the periodic delta function

$$\sum_{q=-\infty}^{\infty} \delta\left(\xi - \frac{q\pi}{2c}\right) \quad (47)$$

The sum over the index m is replaced by one half of the integral over ξ from minus infinity to plus infinity. Equation (46) becomes

$$G(r, o, \omega) = \frac{P(u_t) l_s}{c} \sum_n \frac{J_0(\nu_n \rho)}{J_1^2(\nu_n)} \quad (.) \int_{-\infty}^{\infty} \frac{d\xi \cos \xi z \sin^2 \xi c \sum_{q=-\infty}^{\infty} \delta\left(\xi - \frac{q\pi}{2c}\right)}{\left[(1 + L^2 B_n^2 + L^2 \xi^2 + j\omega l_s) \exp(j\omega l_\tau + \tau B_n^2 + \tau \xi^2) - k_\infty \beta_c \right]} \quad (48)$$

The periodic delta function may now be replaced by its Fourier expansion. It is shown in Appendix A that

$$\sum_{q=-\infty}^{\infty} \delta\left(\xi - \frac{q\pi}{2c}\right) = \frac{2c}{\pi} \sum_{m=-\infty}^{\infty} \exp(j4mc\xi) \quad (49)$$

Assuming that the summation over m and the integration commute, their order may be interchanged. The integral is seen to have the form of a Fourier transform in the ξ variable.

Since Equation (48) is an even function of the ξ variable, the cosine functions may be replaced by $\exp(j\theta)$, or vice versa. Doing this, the summation

$$f(\xi) = \sum_{m=-\infty}^{\infty} \cos \xi z \sin^2 \xi c \cos 4mc\xi \quad (50)$$

may be reduced to a simpler form as shown in Appendix B.

The result is

$$f(\xi) = \frac{1}{2} \sum_{m=-\infty}^{\infty} (-1)^m \cos \xi (z + 2cm) \quad (51)$$

$$= \frac{1}{2} \sum_{m=-\infty}^{\infty} (-1)^m \exp[j\xi (z + 2cm)] \quad (52)$$

Equation (48) becomes

$$G(r, \omega, \omega) = \frac{P(u_t) l_s}{\pi} \sum_{n=1}^{\infty} \frac{J_0(\nu_n \rho)}{J_1^2(\nu_n)}$$

$$(\cdot) \sum_{m=-\infty}^{\infty} (-1)^m \int_{-\infty}^{\infty} \frac{\exp[j\omega(z + 2cm)] d\xi}{[(1 + L^2 B_n^2 + L^2 \xi^2 + j\omega l_s) \exp(j\omega l_s \tau + \tau B_n^2 + \tau \xi^2) - \kappa_{\infty} \beta_c]} \quad (53)$$

Thus, the original cosine eigenfunctions have been replaced by positive and negative "sources" located periodically along the z axis.

The integral in Equation (53) may be evaluated by the residue theorem of complex variables (19), as applied to real integrals. The main steps in performing the integration are:

1. The real variable ξ is replaced by the complex variable ζ .

2. The poles of the integrand are found, corresponding in this case to the roots of the denominator of Equation (53)

$$DF = (1 + L^2 B_n^2 + L^2 \zeta^2 + j\omega L_s) \exp(j\omega L_T + \tau B_n^2 + \tau \zeta^2) - k_{\infty} \beta_c \quad (54)$$

3. The residues are evaluated at the poles in the upper half plane when $z + 2cm$ is positive and at those in the lower half plane when $z + 2cm$ is negative. The variable z is restricted to values between 0 and c .

4. The value of the integral is equal to the sum of the residues multiplied by $2\pi j$.

The roots of the denominator cannot be found in terms of elementary functions, since the denominator is a transcendental equation having an infinite number of complex roots. Representing these roots by

$$\zeta_i = \pm jR_i = \pm j(A_i + jB_i) \quad i = -\infty \text{ to } \infty \quad (55)$$

allows a symbolic solution of the integral, with the smallest value of R_i corresponding to $i = 0$. Appendix C presents a discussion of the characteristic equation, its roots, and how they may be found.

The residue contributed by the roots of DF are

$$\text{Res}_i = \frac{\exp(-j\omega L_T - \tau B_n^2 + \tau R_i^2) \exp[-R_i(z + 2cm)]}{2jR_i [L^2 + \tau(1 + L^2 B_n^2 - L^2 R_i^2 + j\omega L_s)]} \quad (56)$$

where L'Hospital's rule has been used. It is possible for

a root of DF to lie on the real axis, if $k_{\text{eff}} \geq 1$. For this case, the residue is equal to one half the value obtained using Equation (56).

Summing the residues, the transfer function becomes

$$G(r, \phi, \omega) = P(u_t) l_s \exp(-j\omega l_T) \sum_{n=1}^{\infty} \frac{J_0(\nu_n \rho)}{J_1^2(\nu_n)}$$

$$(\cdot) \sum_{i=-\infty}^{\infty} \frac{\exp(-T B_n^2 + T R_i^2)}{R_i [L^2 + T(1 + L^2 B_n^2 - L^2 R_i^2 + j\omega l_s)]} \left[\exp(-R_i z) \right.$$

$$\left. + \sum_{m=1}^{\infty} (-1)^m \left\{ \exp[-R_i(z + 2cm)] + \exp[R_i(z - 2cm)] \right\} \right] \quad (57)$$

Thus, the transfer function for a point source in a cylindrical medium, with a detector located at r , is equal to the product of the sum over n , the radial coordinate index; the sum over i , the roots of the characteristic equation (Equation (54)) in the upper half plane; and the sum over m , the position index on the z axis.

The transfer function (Equation (57)) for systems that are large compared to the characteristic nuclear dimensions (T and L^2) will ordinarily be adequately represented by just a few of the possible number of terms.

Alternate form for the non-multiplying medium transfer function

For the case where k_{∞} is equal to zero, Equation (46) may be easily inverted, producing a result written in terms of the elementary functions. The problem will be restricted

to a cylindrical geometry containing a point source, as discussed in the previous section.

Inversion Procedure. The procedure followed in the previous section is applicable to the case for which k_{∞} is equal to zero. Thus Equation (53) may be re-written

$$G(r, \theta, \omega) = \frac{P(u_t) l_s}{\pi} \sum_{n=1}^{\infty} \frac{J_0(\nu_n \rho)}{J_1^2(\nu_n)} \exp(-j\omega l_T - \tau_{B_n}^2) \\ (\cdot) \sum_{m=-\infty}^{\infty} (-1)^m \int_{-\infty}^{\infty} \frac{\exp(-\tau \xi^2) \exp[j\xi(z + 2cm)] d\xi}{1 + L^2 B_n^2 + L^2 \xi^2 + j\omega l_s} \quad (58)$$

The roots of the denominator are easily found, and are

$$\zeta = \pm \frac{j}{L} (1 + L^2 B_n^2 + j\omega l_s)^{\frac{1}{2}} \quad (59)$$

$$= \pm j(\alpha_n + j\gamma_n) \quad (60)$$

where

$$\alpha_n = \left[\frac{[(1 + L^2 B_n^2)^2 + \omega^2 l_s^2]^{\frac{1}{2}} + 1 + L^2 B_n^2}{2L^2} \right]^{\frac{1}{2}} \quad (61)$$

and

$$\gamma_n = \left[\frac{[(1 + L^2 B_n^2)^2 + \omega^2 l_s^2]^{\frac{1}{2}} - (1 + L^2 B_n^2)}{2L^2} \right]^{\frac{1}{2}} \quad (62)$$

Integrating around the upper half plane when $z + 2cm$ is positive, and the lower half plane when $z + 2cm$ is

negative, the transfer function becomes

$$\begin{aligned}
 G(r, 0, \omega) &= \frac{P(u_t) l_s}{L^2} \exp \left[\frac{\tau}{L^2} + j\omega \left(l_s \frac{\tau}{L^2} - l_\tau \right) \right] \\
 (\cdot) \sum_{n=1}^{\infty} \frac{J_0(\nu_n \rho)}{J_1^2(\nu_n)} \frac{1}{\alpha_n + j\gamma_n} &\left[\exp[-z(\alpha_n + j\gamma_n)] \right. \\
 + \sum_{m=1}^{\infty} (-1)^m &\left\{ \exp[-(z + 2cm)(\alpha_n + j\gamma_n)] \right. \\
 + \exp[(+z - 2cm)(\alpha_n + j\gamma_n)] &\left. \left. \right\} \right] \quad (63)
 \end{aligned}$$

Equation (63) applies for a non-multiplying medium containing a fast source located on the centerline of the assembly and for $0 < z < c$.

Appendix D contains a description of the computer code used to evaluate Equations (57 and 63), and Chapter V contains the theoretical results.

Statistical Theory

The statistical correlation and power spectrum equations used in obtaining and processing the experimental data are developed in this section.

If a nuclear system, represented by its spatially dependent transfer function, is driven by a random input (the fast neutron source), the output is also a random function. The statistical relations between the output and the input, or between several outputs, may be expressed in terms of the system's transfer function.

In this study, the cross power spectrum is calculated from the cross correlation of two outputs, which are the neutron density variations at two different locations in the medium. Repeating the experiment with one output relocated and using the equations developed in this section, the experimental transfer function of the medium can be obtained.

Definitions

There are several definitions that are basic to the statistical analysis of random functions. One that is very important is the cross correlation function (22)

$$\Phi_{12}(\tau) = \lim_{T \rightarrow \infty} \frac{1}{2T} \int_{-T}^T f_1(t) f_2(t + \tau) dt \quad (64)$$

It is seen that this is just the average over all time t of the product of two functions, with one function delayed relative to the other by the time τ . The cross correlation function is frequently written

$$\Phi_{12}(\tau) = \overline{f_1(t) f_2(t + \tau)} \quad (65)$$

to signify the averaging process. For a stationary process, the time average may be replaced by an ensemble average if desired (22).

The Fourier transform of the cross correlation function is (22)

$$\Phi_{12}(\omega) = \frac{1}{2\pi} \int_{-\infty}^{\infty} \Phi_{12}(\tau) \exp(-j\omega\tau) d\tau \quad (66)$$

and is defined as the cross power spectrum density.

An important relationship in system analysis is the convolution integral, which can be used to relate the system characteristics and the input to the output of the system (22)

$$f_o(t) = \int_{-\infty}^{\infty} h(\nu) f_i(t - \nu) d\nu \quad (67)$$

where $f_o(t)$ and $f_i(t)$ are the input and output functions, respectively, and $h(\nu)$ is the impulse response function of the system (22).

The impulse response function and the system frequency function, $H(\omega)$, of the system are related by the Fourier transform, and they form a Fourier transform pair (22)

$$\begin{aligned} h(t) &= \frac{1}{2\pi} \int_{-\infty}^{\infty} H(\omega) \exp(j\omega t) d\omega \\ H(\omega) &= \int_{-\infty}^{\infty} h(t) \exp(-j\omega t) dt \end{aligned} \quad (68)$$

For the class of functions considered here, the system frequency function and the transfer function, defined by the Laplace transform, are essentially the same thing, since $h(t)$ is equal to zero for times less than zero, and the real part of the Laplace variable is zero.

Equation (67) may be used to show the relationship between the cross correlation of the input and output of a system and its impulse response function. If $f_i(t)$ and

$f_2(t)$ in Equation (64) represent the input and output signals, $f_1(t)$ and $f_0(t)$, respectively, then substitution of Equation (67) for $f_0(t)$ gives

$$\begin{aligned} \Phi_{10}(\tau) = \lim_{T \rightarrow \infty} \frac{1}{2T} \int_{-T}^T dt f_1(t) \int_{-\infty}^{\infty} h(\nu) f_1(t) \\ + \tau - \nu) d\nu \quad (69) \end{aligned}$$

Assuming that the two integrations commute, their order may be interchanged. Realizing that Equation (64) also defines an auto correlation function if $f_1(t)$ and $f_2(t)$ are the same, Equation (69) becomes

$$\Phi_{10}(\tau) = \int_{-\infty}^{\infty} h(\nu) \Phi_{11}(\tau - \nu) d\nu \quad (70)$$

This equation has the same form as Equation (67), but relates the statistical correlation functions rather than the actual input and output.

The Fourier transformation of Equation (70) may be performed by multiplying both sides of the equation by $\exp(-j\omega\tau) d\tau/2\pi$ and integrating over all time τ . Using Equation (68) for $H(\omega)$ gives

$$\Phi_{12}(\omega) = H(\omega) \Phi_{11}(\omega) \quad (71)$$

Equation (71) relates the system frequency function and the auto power spectrum of the input to the cross power spectrum of the input and output of the system (22).

Cross power spectrum between two outputs

Referring to Figure 1, the experimental setup is represented by an input function, $S(t)$; three spatially dependent transfer functions between the source and detectors 1, 2, and 3; three measuring system transfer functions; and a black box that performs the cross correlation of the incoming functions. See Chapter IV for a description of the experimental equipment.

Functions f_1 , f_2 , and f_3 represent the neutron density variation at each of the detectors when the variation is caused by the source, while f_4 , f_5 , and f_6 are uncorrelated variations in the neutron density at the detectors, or noise as far as the experiment is concerned. Functions f_7 , f_8 , and f_9 are instrument noise added to the signal as it passes through the measuring system. Functions f_{10} , f_{11} , and f_{12} are the resultant signals that are cross correlated. From this system, the experimental transfer function is obtained

$$H_{D3D2}(\omega) = \frac{\Delta n_t(r_3, r_o, \omega)}{\Delta n_t(r_2, r_o, \omega)} \quad (72)$$

Using Equation (67), the neutron density variation at each detector is

$$\begin{aligned} f_{D1}(t) &= f_1(t) + f_4(t) \\ &= \int_{-\infty}^{\infty} h_1(u) S(t - u) du + f_4(t) \end{aligned} \quad (73)$$

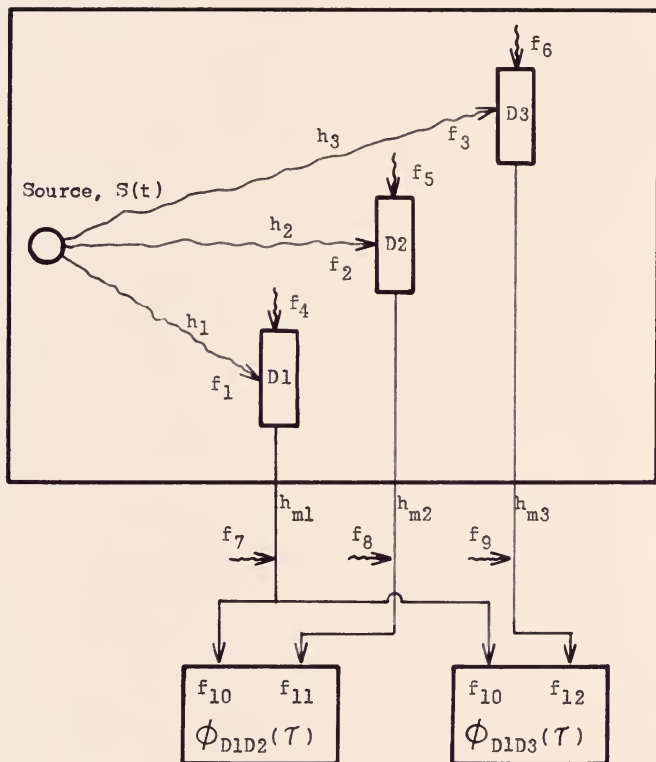


Figure 1. Definition of functions for statistical theory

$$\begin{aligned}
 f_{D2}(t) &= f_2(t) + f_5(t) \\
 &= \int_{-\infty}^{\infty} h_2(v) S(t - v) dv + f_5(t) \quad (74)
 \end{aligned}$$

$$\begin{aligned}
 f_{D3}(t) &= f_3(t) + f_6(t) \\
 &= \int_{-\infty}^{\infty} h_3(w) S(t - w) dw + f_6(t) \quad (75)
 \end{aligned}$$

The signals which are cross correlated, f_{10} , f_{11} , and f_{12} , are affected by the impulse response function of the measuring system and are

$$\begin{aligned}
 f_{10}(t) &= f_7(t) + \int_{-\infty}^{\infty} h_{m1}(x) dx f_{D1}(t - x) \\
 &= f_7(t) + \int_{-\infty}^{\infty} h_{m1}(x) dx \left[f_4(t - x) \right. \\
 &\quad \left. + \int_{-\infty}^{\infty} h_1(u) du S(t - x - u) \right] \quad (76)
 \end{aligned}$$

$$\begin{aligned}
 f_{11}(t) &= f_8(t) + \int_{-\infty}^{\infty} h_{m2}(y) dy \left[f_5(t - y) \right. \\
 &\quad \left. + \int_{-\infty}^{\infty} h_2(v) S(t - y - v) dv \right] \quad (77)
 \end{aligned}$$

$$f_{12}(t) = f_9(t) + \int_{-\infty}^{\infty} h_{m3}(z) dz \left[f_6(t - z) + \int_{-\infty}^{\infty} h_3(w) S(t - z - w) dw \right] \quad (78)$$

Thus, the functions that are cross correlated are related to the system input through two impulse response functions, one for the nuclear system and one for the measuring system, and to the noise present in the two systems.

Equation (64) may be used to obtain the two cross correlation functions

$$\Phi_{D1D2}(\tau) = \lim_{T \rightarrow \infty} \frac{1}{2T} \int_{-T}^T f_{10}(t) f_{11}(t + \tau) dt \quad (79)$$

and

$$\Phi_{D1D3}(\tau) = \lim_{T \rightarrow \infty} \frac{1}{2T} \int_{-T}^T f_{10}(t) f_{12}(t + \tau) dt \quad (80)$$

Substituting Equations (76 and 77) in Equation (79) results in

$$\begin{aligned} \Phi_{D1D2}(\tau) &= \lim_{T \rightarrow \infty} \frac{1}{2T} \int_{-T}^T dt \left[f_7(t) \right. \\ &\quad \left. + \int_{-\infty}^{\infty} h_{m1}(x) dx \left[f_4(t - x) + \int_{-\infty}^{\infty} h_1(u) du S(t - x - u) \right] \right] \\ &(\cdot) \left[f_8(t + \tau) + \int_{-\infty}^{\infty} h_{m2}(y) dy \left[f_5(t + \tau - y) \right. \right. \end{aligned}$$

$$+ \int_{-\infty}^{\infty} h_2(v) dv S(t + \tau - y - v) \Big] \quad (81)$$

Performing the multiplication, separating terms, and using the definition of the cross correlation function (Equation (65)), gives

$$\begin{aligned} \phi_{D1D2}(\tau) = & \overline{f_7(t) f_8(t + \tau)} \\ & + \int_{-\infty}^{\infty} h_{m1}(x) dx \overline{f_4(t') f_8(t' + \tau + x)} \\ & + \int_{-\infty}^{\infty} h_{m2}(y) dy \overline{f_7(t) f_5(t + \tau - y)} \\ & + \int_{-\infty}^{\infty} h_{m1}(x) dx \int_{-\infty}^{\infty} h_1(u) du \overline{S(t') f_8(t' + \tau + x + u)} \\ & + \int_{-\infty}^{\infty} h_{m2}(y) dy \int_{-\infty}^{\infty} h_2(v) dv \overline{f_7(t) S(t + \tau - y - v)} \\ & + \int_{-\infty}^{\infty} h_{m1}(x) dx \int_{-\infty}^{\infty} h_{m2}(y) dy \overline{f_4(t') f_5(t' + \tau + x - y)} \\ & + \int_{-\infty}^{\infty} h_{m1}(x) dx \int_{-\infty}^{\infty} h_{m2}(y) dy \int_{-\infty}^{\infty} h_2(v) dv \\ & \quad (\cdot) \overline{f_4(t') S(t' + \tau + x - y - v)} \\ & + \int_{-\infty}^{\infty} h_{m1}(x) dx \int_{-\infty}^{\infty} h_{m2}(y) dy \int_{-\infty}^{\infty} h_1(u) du \\ & \quad (\cdot) \overline{S(t') f_5(t' + \tau + x - y + u)} \end{aligned}$$

$$+ \int_{-\infty}^{\infty} h_{m1}(x) dx \int_{-\infty}^{\infty} h_{m2}(y) dy \int_{-\infty}^{\infty} h_1(u) du \int_{-\infty}^{\infty} h_2(v) dv$$

$$(\cdot) \frac{S(t') S(t' + \tau + x - y + u - v)}{(82)}$$

Now, if f_4, f_5, f_6, f_7, f_8 , and f_9 , are uncorrelated noise functions, and satisfy (22)

$$\int_{-\infty}^{\infty} f(t) dt = 0 \quad (83)$$

then the cross correlations in the first eight terms of Equation (82) are zero. This illustrates one of the advantages of the cross correlation function, the ability to eliminate the uncorrelated noise from the final answer.

Equation (82) is now

$$\phi_{D1D2}(\tau) = \int_{-\infty}^{\infty} h_{m1}(x) dx \int_{-\infty}^{\infty} h_{m2}(y) dy \int_{-\infty}^{\infty} h_1(u) du$$

$$(\cdot) \int_{-\infty}^{\infty} h_2(v) dv \phi_{ss}(\tau + x - y + u - v) \quad (84)$$

The cross power spectrum density of $\phi_{D1D2}(\tau)$ may be obtained by using Equation (66). Multiplying both sides of Equation (84) by $\exp(-j\omega\tau) d\tau/2\pi$ and integrating over τ gives

$$\Phi_{D1D2}(\omega) = \frac{1}{2\pi} \int_{-\infty}^{\infty} \phi_{D1D2}(\tau) \exp(-j\omega\tau) d\tau \quad (85)$$

Using the variable

$$\mu = \tau + x - y + u - v \quad (86)$$

in Equation (85) gives

$$\begin{aligned}\Phi_{D1D2}(\omega) &= \int_{-\infty}^{\infty} h_{m1}(x) \exp(j\omega x) dx \\ (\cdot) &\int_{-\infty}^{\infty} h_{m2}(y) \exp(-j\omega y) dy \int_{-\infty}^{\infty} h_1(u) \exp(j\omega u) du \\ (\cdot) &\int_{-\infty}^{\infty} h_2(v) \exp(-j\omega v) dv \frac{1}{2\pi} \int_{-\infty}^{\infty} \Phi_{ss}(\mu) \exp(-j\omega \mu) d\mu\end{aligned}\quad (87)$$

Using Equations (66 and 68), Equation (87) becomes

$$\Phi_{D1D2}(\omega) = H_{m1}^*(\omega) H_{m2}(\omega) H_1^*(\omega) H_2(\omega) \Phi_{ss}(\omega) \quad (88)$$

The cross power spectrum of two detectors depends on the transfer functions of the two measuring systems, the transfer function of the nuclear system, and the auto power spectrum of the source.

Moore (38) has independently developed a general equation for the auto power spectra of a noise field that is similar to Equation (88). Moore, however, ignores the effects of the measuring system.

Repeating the same development as that above for $\Phi_{D1D3}(\omega)$ gives

$$\Phi_{D1D3}(\omega) = H_{m1}^*(\omega) H_{m3}(\omega) H_1^*(\omega) H_3(\omega) \Phi_{ss}(\omega) \quad (89)$$

If Equation (89) is now divided by Equation (88), the result is

$$\frac{\Phi_{D1D3}(\omega)}{\Phi_{D1D2}(\omega)} = \frac{H_{m1}^*(\omega) H_{m3}(\omega) H_1^*(\omega) H_3(\omega) \Phi_{ss}(\omega)}{H_{m1}^*(\omega) H_{m2}(\omega) H_1^*(\omega) H_2(\omega) \Phi_{ss}(\omega)} \quad (90)$$

It is clear, if the third measuring system has the same transfer function as the second, and if $\Phi_{ss}(\omega)$ is the same for both cross power spectrum measurements, that Equation (90) reduces to

$$\frac{\Phi_{D1D3}(\omega)}{\Phi_{D1D2}(\omega)} = \frac{H_3(\omega)}{H_2(\omega)} = H_{32}(\omega) \quad (91)$$

where

$$\begin{aligned} H_{32}(\omega) &= \frac{G(r_3, r_o, \omega)}{G(r_2, r_o, \omega)} \\ &= \frac{\Delta n_t(r_3, r_o, \omega)}{\Delta n_t(r_2, r_o, \omega)} \end{aligned} \quad (92)$$

the same as Equation (72).

Equation (91) indicates that the transfer function of an unknown system may be accurately determined by the ratio of the cross power spectra between detectors.

If $\Phi_{D1D2}(\tau)$ and $\Phi_{D1D3}(\tau)$ can be measured at the same time, there is no restriction on the source behavior or on the measuring system. In actual practice, it is highly desirable to have the band width of the measuring system wider than the band width of the unknown system, but this is not critical when using the above approach.

If the two cross correlations cannot be performed at the same time, it is necessary to use a pseudo-random source to insure that it repeats the same input for both measurements. The frequency content of the source should be wide enough to insure that the entire band width of the unknown system is excited.

It is interesting to note that if the band width of the measuring system is wider than the band width of the unknown system, and if the source is a white noise over the band width of the unknown system, both $\Phi_{ss}(\omega)$ and $H_{m1}(\omega)$ are effectively constant. Then Equation (88) becomes

$$\begin{aligned}\Phi_{D1D2}(\omega) &= K_{m1} H_1^*(\omega) H_2(\omega) K_{ss} \\ &= K' |H_1(\omega)|^2 H_{21}(\omega)\end{aligned}\quad (93)$$

Any phase shift in $\Phi_{D1D2}(\omega)$ is caused only by $H_{21}(\omega)$, while the attenuation of $\Phi_{D1D2}(\omega)$ depends on $H_1^*(\omega)H_2(\omega)$. Even if the transfer function of the measuring system is not flat, nor the source white, the phase shift in $\Phi_{D1D2}(\omega)$ is still caused only by $H_{21}(\omega)$.

Since the above assumptions about the measuring system and source may not be valid, it is usually better to use Equation (91), even with the requirement of an additional measurement.

Auto power spectrum of one output

The auto power spectrum of Detector 1 is of interest. If $\Phi_{D1D2}(\omega)$ and $\Phi_{D1D3}(\omega)$ are measured at two different times, $\Phi_{D1D1}(\omega)$ may be checked to insure that the fre-

quency content of the source was the same for both measurements. If $\Phi_{ss}(\omega)$ is different, $\Phi_{D1D1}(\omega)$ may be used as a reference in comparing $\Phi_{D1D2}(\omega)$ and $\Phi_{D1D3}(\omega)$.

The relation between $\Phi_{D1D1}(\omega)$ and $\Phi_{ss}(\omega)$ may be obtained using the same procedure as used in the previous section. The definition (from Equation (64)) for the auto correlation is

$$\phi_{D1D1}(\tau) = \lim_{T \rightarrow \infty} \frac{1}{2T} \int_{-T}^T f_{10}(t) f_{10}(t + \tau) dt \quad (94)$$

Substituting Equation (76) for $f_{10}(t)$, or better yet, using Equation (82) and replacing all the 5, 8, and 2 subscripts by 4, 7, and 1, respectively, gives $\phi_{D1D1}(\tau)$. If all the cross correlation functions between the various noise functions and the source are equal to zero (22), then

$$\begin{aligned} \phi_{D1D1}(\tau) = & \phi_{77}(\tau) + \left[\int_{-\infty}^{\infty} h_{m1}(x) dx \int_{-\infty}^{\infty} h_{m1}(y) dy \right. \\ & (\cdot) \phi_{44}(\tau + x - y) + \left[\int_{-\infty}^{\infty} h_{m1}(x) dx \int_{-\infty}^{\infty} h_{m1}(y) dy \right. \\ & (\cdot) \int_{-\infty}^{\infty} h_1(u) du \int_{-\infty}^{\infty} h_1(v) dv \phi_{ss}(\tau + x - y + u - v) \left. \right] \end{aligned} \quad (95)$$

To obtain the auto power spectrum, both sides of Equation (95) are multiplied by $\exp(-j\omega\tau) d\tau/2\pi$ and integrated over τ (Equation (66)). Then, using the same reasoning presented in the previous section (Equations (85, 86, 87, and 88)),

$$\begin{aligned}\Phi_{D1D1}(\omega) &= \Phi_{77}(\omega) + |H_{m1}(\omega)|^2 \Phi_{44}(\omega) \\ &+ |H_{m1}(\omega)|^2 |H_1(\omega)|^2 \Phi_{ss}(\omega) \quad (96)\end{aligned}$$

If the noise inputs are white, their power spectra are constant (22). Thus

$$\begin{aligned}\Phi_{D1D1}(\omega) &= K_{77} + |H_{m1}(\omega)|^2 K_{44} \\ &+ |H_{m1}(\omega)|^2 |H_1(\omega)|^2 \Phi_{ss}(\omega) \quad (97)\end{aligned}$$

So, even if $\Phi_{ss}(\omega)$ cannot be checked directly, $\Phi_{D1D1}(\omega)$ will be the same for each run if $\Phi_{ss}(\omega)$ is also the same.

CHAPTER III

EXPERIMENTAL METHOD AND ANALYSIS

The analysis, procedures, and considerations necessary for the experimental verification of the spatially dependent transfer function equations developed in Chapter II are presented and discussed in this chapter. The method used to obtain the experimental data is discussed first, followed by a description of the data analysis. The experimental equipment is described in Chapter IV.

Experimental Method

The experimental data was obtained using the method outlined in the statistical theory section, in Figure 1 and in the development of Equations (88 and 90).

The flow of information through the experimental system is shown in Figure 2. The shift register generates a pseudo-random binary signal, which is used to turn the neutron generator on and off, producing the input signal. The input signal travels through the nuclear system to the neutron detectors. The neutron detection system is a pulse system which produces an output pulse of constant height for each neutron detected. The pulse rate is measured by a fast response count rate circuit

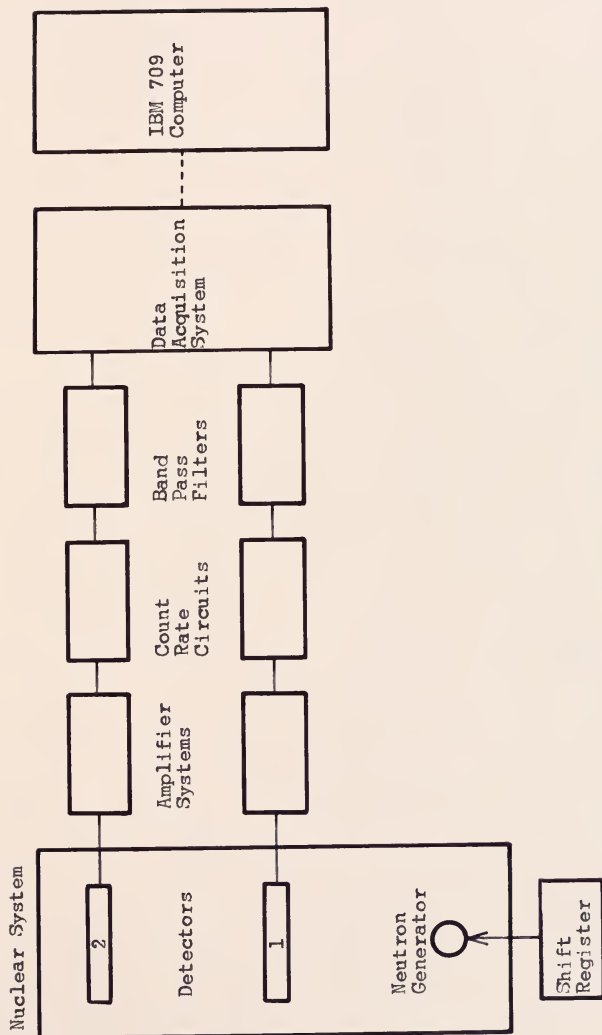


Figure 2. Block diagram of the experimental equipment

which produces an analog voltage proportional to the neutron density at the detector. This signal is conditioned by a wide-band band pass filter to remove the dc component and the components higher in frequency than one half the sampling rate of the data acquisition system. The conditioned signal is sampled by the data acquisition system, and the samples are stored on magnetic tape in digital form. The data is processed by an IBM 709 computer at the University of Florida Computing Center, using the procedure discussed in the second section of this chapter.

Input signal

Equations (89 and 90) show that almost any input signal may be used to measure the experimental transfer function, as long as it has the desired band width. The input actually used is discussed below.

The input to the nuclear system is controlled by a predetermined pseudo-random binary signal which turns the neutron source on and off. The signal is generated by an eight stage shift register, with the correct feedback circuitry for producing a maximum length sequence of $255 \Delta t$ intervals.

The maximum length sequence generated by a shift register has a special auto correlation function, which is shown in Figure 3. The integration required to calculate the auto correlation function (Equation (64)) is performed over an integral number of periods, T_1 , of the shift register. The function $\phi_{ss}(\tau)$ has a constant

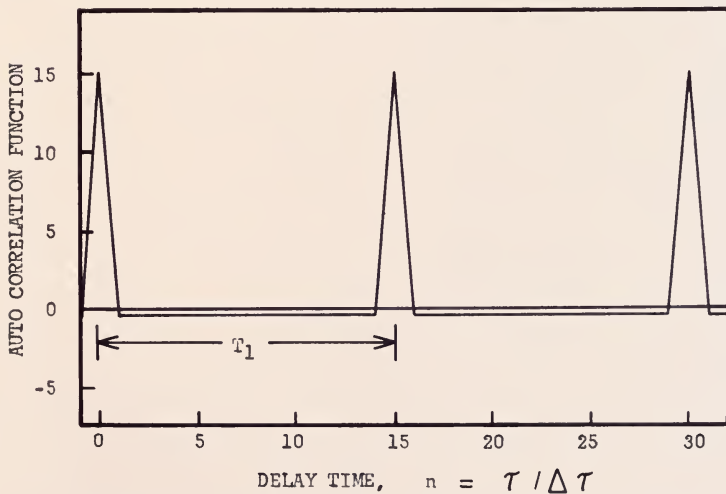
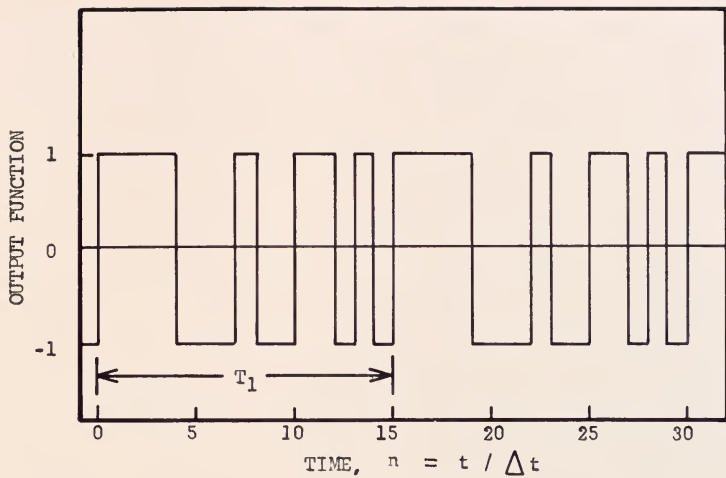


Figure 3. Typical maximum length sequence and its auto correlation function

negative component of $-1/N$ magnitude, N being the number of intervals in the sequence. With every T_1 , the period of the sequence, the shape of $\phi_{ss}(\tau)$ approaches a delta function. This characteristic of $\phi_{ss}(\tau)$ has been used (16) to measure the impulse response of a reactor by cross correlation of the input and the output. If $\phi_{ss}(\tau - \nu)$ in Equation (70) is replaced by a delta function, the cross correlation becomes

$$\begin{aligned}\phi_{10}(\tau) &= \int_{-\infty}^{\infty} h(t) \delta(\tau - t) dt \\ &\cong h(\tau) \Delta t\end{aligned}\quad (98)$$

if the settling time of $h(\tau)$ is less than T_1 . The impulse response is obtained as a function of the delay time.

This particular property of the input signal is not used directly in this study for several reasons. First, the determination of the spatially dependent transfer function requires accurate measurements to show the phase shift and attenuation of the neutron disturbance as it passes the detectors. Thus, the approximation of $\phi_{ss}(\tau)$ by a delta function is not an accurate one for this work.

Second, the system being measured, represented by $h(\tau)$, must have a band width narrower than $\phi_{ss}(\tau)$ if Equation (98) is to be a good approximation of Equation (70). Another way of stating this is that the time constant of the system must be less than the period of the input sequence, usually at least five times less.

Third, $h(\tau)$ should not change significantly over one Δt interval, the average width of the triangle on the $\phi_{ss}(\tau)$ curve. This means that the time constant of the system must be several times larger than Δt .

The auto power spectrum of the source, $\Phi_{ss}(\omega)$ (Figure 4), has several interesting features. If $\phi_{ss}(\tau)$ is treated as an aperiodic function, which is valid if the settling time of the system is less than the period of the input sequence T_1 , the spectrum is continuous and is (using Equation (66))

$$\Phi_{ss}(\omega) = \frac{\Delta t}{2\pi} \left\{ \frac{\sin\left(\frac{\omega \Delta t}{2}\right)}{\frac{\omega \Delta t}{2}} \right\}^2 \quad (99)$$

However, if the settling time of the system is greater than T_1 , $\phi_{ss}(\tau)$ is periodic, and the auto power spectrum is discrete (using the periodic Fourier expansion, Equation (A2))

$$\Phi_{ss}(n\omega_1) = \frac{1}{N} \left\{ \frac{\sin\left(\frac{n\omega_1 \Delta t}{2}\right)}{\frac{n\omega_1 \Delta t}{2}} \right\}^2 \quad (100)$$

The fundamental frequency, ω_1 , corresponds to T_1 . The locus of the discrete spectrum components has the same shape as Equation (99), the continuous case. The half power frequency is approximately $0.44/\Delta t$ for both cases. It is clear that the period of the input sequence T_1 should be larger than the settling time of the system if at all

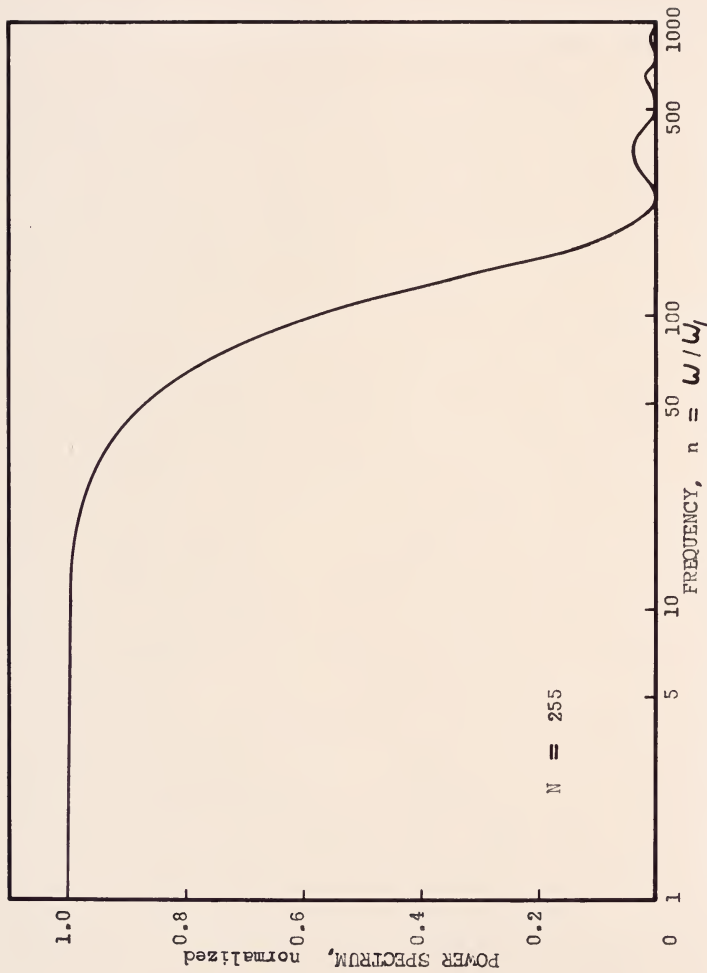


Figure 4. Auto power spectrum of the maximum length input sequence

possible, so that the input spectrum will appear continuous to the system being investigated.

Sampling theory

The perturbations in the neutron density caused by the input signal and uncorrelated noise are presented in analog form by the measuring system and sampled at a high rate by the data acquisition system.

Since the analog signal is sampled a finite number of times, it cannot be completely reconstructed. In terms of frequency, the reconstructed signal cannot have a frequency content higher than one half the sampling rate. On the other hand, if the analog signal has frequencies greater than one half the sampling rate, they will contribute false information on the amplitudes of lower frequencies through the process known as aliasing (28). Thus, the sampling rate should be at least twice as high as the band-pass of the unknown system to obtain the maximum amount of information. If this condition is not met, because of limitations in the sampling rate or lack of interest concerning the high frequency response, the input to the sampling equipment must be filtered to eliminate the frequency components above one half the sampling rate.

If it is desired to process data already recorded, but only the low frequency components are of interest, it is possible to skip samples, using only every n^{th} sample. Now, however, it might be necessary to numerically filter the

data to remove any high frequency components present above one half the new, or effective, sampling rate.

The variance of the sample mean can be used to estimate the minimum number of samples needed to have the correct function average. Lee (22) shows

$$\sigma_{\bar{x}}^2 = \frac{1}{n} \sigma_f^2 \quad (101)$$

where $\sigma_{\bar{x}}^2$ is the variance of the sample mean, σ_f^2 is the variance of the function being sampled, and n is the number of samples. Thus, as a large number of samples is taken, $\sigma_{\bar{x}}^2$ approaches zero. The error in \bar{x} may be taken as $\sqrt{1/n}$.

Data Analysis

The data stored on magnetic tape by the data acquisition system corresponds to $f_1(t)$ and $f_2(t)$, the two output functions, in Equation (64). The equations used to numerically process this data and compare the experimental and theoretical spatially dependent transfer functions are discussed in this section.

Experimental correlation functions

The equations developed in the statistical theory section cannot be used directly in a practical experiment, since the data is processed digitally, and the integration times must be finite.

Integration time errors. Equation (79) may be approximated by

$$\phi_{D1D2}(\tau) \cong \frac{1}{T} \int_0^T f_{10}(t) f_{11}(t + \tau) dt \quad (102)$$

for a finite integration time T .

The integration time necessary to obtain a reasonably accurate answer for $\phi_{D1D2}(\tau)$ has been investigated by others. Balcomb (16) treated the cross correlator as a band pass filter, and showed that the "improvement factor" is at least

$$IF = \frac{(S/N)_{out}}{(S/N)_{in}} = \sqrt{\frac{T}{L}} \quad (103)$$

IF is defined as the ratio of the signal to noise ratio at the input to the same ratio at the output of the cross correlator, T is the integration time, and L is the settling time of the system. The above derivation is based on a cross correlator designed to utilize Equation (98). By making $T > L$, the uncorrelated noise is averaged over a longer period than the correlated signal. Since the uncorrelated noise is assumed to satisfy Equation (83), its contribution to the answer is decreased with greater T . While Equation (103) defines an improvement factor, it gives no information on the amount of noise present before the signal enters the cross correlator.

Since the input signal discussed earlier is a periodic pseudo-random function, no additional information is gained about the system by integrating for times longer than one period of the input. However, the S/N ratio may be sub-

stantially improved by averaging the uncorrelated noise over several periods.

Rajagopal (17) approached the error problem by considering the ratio of the cross correlation function for an infinite T to the square root of its variance for a finite T. Considering a simple lag filter as the unknown system with a white noise input, the signal to noise ratio from the cross correlator, as defined in Reference (17), is

$$\frac{S}{N} \equiv \frac{\phi_{io}(\tau)}{\sigma[\phi_{io}(\tau, T)]} \cong \frac{\exp(-a\tau)}{\sqrt{\frac{2}{\pi}[1 + \exp(-a\tau)]}} \quad (104)$$

for $T \gg \tau$. Thus, as in Equation (103), the S/N is proportional to the square root of the integration time T.

As the delay time τ approaches the time constant of the lag system, $1/a$, the integration time T becomes very large for what seems to be a reasonable error limit. For example, for S/N equal to 100, T equals 10^5 seconds for a $\tau = 0.625$. For S/N equal to 2, T becomes a reasonable 43 seconds. Thus, even though the cross correlation function is still quite large ($\exp(-0.625) = 0.535$), the error, as defined in Equation (104), can also be quite large for reasonable integration times. Equation (104) is specialized, however. For inputs that have a finite band width, the error will be much less than that calculated by Equation (104).

Stern (23) presents a detailed analysis of three sources of error for the cross correlation function as represented by Equation (70). This analysis is applicable to the cross correlation calculations performed herein.

Defining the relative error as (23)

$$R = \frac{\sigma[\phi_{io}(\tau_o)]}{\phi_{io}(\tau_o)} \quad (105)$$

Stern (23) shows that, for $T_1/N \ll \tau_o \ll T_R$,

$$R^2 = \frac{T_R}{2T} + \left[\frac{T_R^N}{2T_1 \eta} \right]^2 \frac{1}{\bar{T}T} + \frac{T_R^2 N}{2TT_1 \eta^2} \left[1 + \frac{A}{S_o T_R} \right] \quad (106)$$

T_R is the time constant of the unknown system, and T_1 is the period of the pseudo-random input signal. The number of Δt intervals in the input signal is N , η is the duty cycle of the input (~ 0.5), and \bar{T} is the average counting rate. The average source strength is S_o , and

$$A = \left[\frac{\overline{\nu^2} - \bar{\nu}}{-2\bar{\nu}\rho} + 1 \right] \quad (107)$$

where ν is the number of neutrons emitted per fission and ρ is the reactivity of the nuclear system.

The terms on the right in Equation (106) are due to the finite integration time T , the finite counting rate, and the natural neutron population fluctuation, or the uncorrelated noise (23). Equation (106) may be used to estimate the required integration time T for any value of R .

As an example a medium of light water with the following typical values may be considered.

$$\begin{aligned} T_R &= 2 \times 10^{-4} \text{ sec} & \eta &= 0.5 & \rho &= 0 \\ \bar{T} &= 5 \times 10^3 \text{ counts/sec} & S_o &= 5 \times 10^7 \text{ neu/sec} \\ T_1 &= 0.1 \text{ sec} & N &= 255 \end{aligned}$$

Then

$$R^2 = \frac{10^{-4}}{T} + \frac{5.2 \times 10^{-5}}{T} + \frac{2.04 \times 10^{-4}}{T}$$

$$\cong 3.56 \times 10^{-4}/T \quad (108)$$

Therefore, for an error of one per cent, the integration time T is 3.56 seconds.

This is in sharp contrast to the 10^5 seconds obtained from Equation (104) for \mathcal{T}/T_R equal to 0.625. However, there are several differences between the two approaches, preventing them from being compared directly. Rajagopal (17) used an input having an infinitely wide spectrum, while Stern (23) used an input having a finite band width. Rajagopal considered only the finite integration time error, for variable \mathcal{T} , with a simple lag system. Stern considered three error sources, but for a fixed \mathcal{T}_0 .

Probably the greatest difference is that Stern considered a periodic pseudo-random source. As shown in Reference (25), the variance of the correlator output is smaller if a periodic pseudo-random binary input signal is used, rather than a purely random input. The variance is reduced even more if the integration time is equal to an integral number of periods of the input. Thus it would appear that the purely random input is not the best input signal for experimental work. The infinitely wide band width adds unnecessary noise, requiring greater integration times to reduce the error.

It is clear that the error analysis of cross correlation functions is not an exact procedure. However, consideration of the discussion presented above, particularly that of Stern (23), enables a reasonable estimate of the error to be made.

Digital analysis. The actual calculation of the cross correlation function was done numerically, using the University of Florida IBM 709 computer. The sampled output functions from the unknown system were read into the computer and the cross correlation function calculated at discrete delay times by (from Equation (102)) (31)

$$\begin{aligned}\phi_{D1D2}(n\Delta\tau) &\cong A \sum_{i=1}^I f_{10}(i\Delta t) f_{11}(i\Delta t + n\Delta\tau) \\ &\qquad\qquad\qquad n = 0 \text{ to } N \\ &\cong A \sum_{i=1}^I f_{11}(i\Delta t) f_{10}(i\Delta t + n\Delta\tau) \\ &\qquad\qquad\qquad n = 0 \text{ to } -N \quad (109)\end{aligned}$$

The integration time T is $I\Delta t$, the delay time is $n\Delta\tau$, and A is a normalizing factor. The delay time interval, $\Delta\tau$, is equal to Δt and is determined by the sampling rate of the data acquisition system. N is usually much less than I . The functions $\phi_{D1D2}(\tau)$ and $\phi_{D1D3}(\tau)$ are calculated the same way, using the appropriate output functions in Equation (109).

Experimental Power Spectra

The power spectra are calculated by performing a numerical Fourier transformation of the correlation

functions (from Equation (66)). Balcomb (16) investigated the effects of several interpolation schemes on the Laplace transform of a function having the form $f(n\Delta x) = \exp(-an\Delta x)$. The result was compared with the known transform of $\exp(-ax)$. His conclusion was that a linear interpolation was as accurate as higher order polynomial interpolations, and was much superior to no interpolation of $f(n\Delta x)$ at all.

Since $\Phi_{D1D2}(\tau)$ was expected to have a functional form

$$f(\tau) = \sum_{i=1}^{\infty} A_i \exp(-a_i \tau) \quad (110)$$

it was decided to use a linear interpolation of $\Phi(\tau)$. Therefore, the numerical form of the Fourier transform becomes

$$\Phi_{D1D2}(\omega) \cong \sum_{n=-N}^{N-1} \int_{\tau_n}^{\tau_{n+1}} \left[\phi_n + \left(\frac{\phi_{n+1} - \phi_n}{\Delta \tau} \right) (\tau - \tau_n) \right] \exp(-j\omega \tau) d\tau \quad (111)$$

where $\phi_n = \Phi_{D1D2}(\tau_n)$ and $\Delta \tau = \tau_{n+1} - \tau_n = \text{constant}$. Performing the integration and simplifying the sum results in

$$\Phi_{D1D2}(\omega) \cong \exp(-j\omega \tau_{-N}) \left[\frac{-j\phi_{-N}}{\omega} - \frac{\phi_{-N+1} - \phi_{-N}}{\Delta \tau} \frac{1}{\omega^2} \right]$$

$$\begin{aligned}
& + \sum_{n=-N+1}^{N-1} \exp(-j\omega\tau_n) \left[\frac{-\phi_{n+1} + 2\phi_n - \phi_{n-1}}{\Delta\tau\omega^2} \right] \\
& + \exp(-j\omega\tau_N) \left[\frac{j\phi_N}{\omega} + \frac{\phi_N - \phi_{N-1}}{\Delta\tau} \frac{1}{\omega^2} \right] \quad (112)
\end{aligned}$$

$\Phi_{D1D3}(\omega)$ and $\Phi_{D1D1}(\omega)$ are calculated by substituting the appropriate $\phi(\tau)$ in Equation (112). A Fortran subroutine TRNS was programmed to calculate the power spectrum using Equation (112). It was included as part of the general program (31) for processing the experimental data. See Appendix D for a description of TRNS.

Experimental transfer function

The transfer function is calculated using a modified form of Equation (91). Although Equation (91) is derived using three outputs from the system (Figure 1), the actual experimental setup (Figure 2) contains only two detection systems. By making two separate recordings, with a detector first in the D2 position and then in the D3 position, $H_{23}(\omega)$ may be calculated using $\Phi_{D1D1}(\omega)$ as a normalizing factor.

$$H_{23}(\omega) = \frac{\left[\frac{\Phi_{D1D3}(\omega)}{\Phi_{D1D1}(\omega)} \right]_{\text{Run 2}}}{\left[\frac{\Phi_{D1D2}(\omega)}{\Phi_{D1D1}(\omega)} \right]_{\text{Run 1}}} \quad (91a)$$

The numerical errors that accumulate as the data is processed cause $H_{23}(\omega)$ to become less accurate as the

power spectra are attenuated at the higher frequencies. However, as noted with Equation (93), the phase shift of the system's transfer function can be found directly from $\Phi_{D1D2}(\omega)$ or $\Phi_{D1D3}(\omega)$.

Calculation of dynamic parameters

The determination of the dynamic reactor parameters was aided by the use of a Fortran code, "General Least Squares Program", originally written at Oak Ridge National Laboratory by Bussing and extensively modified since by Cockrell (24) for use by the Nuclear Engineering Department, University of Florida.

Input to the program is the experimental data and the theoretical function that is to be fitted. The program is informed which parameters in the theoretical function are to be varied to minimize the variance between the data and the function.

As the theoretical function, Equation (57) was incorporated into a main subroutine CALC, and several minor subroutines, CRT, GUEST, GUESS, TERM, ERROR, and FINAL. The computer codes are discussed in detail in Appendix D.

It is not possible to determine the five parameters l_s , l_T , L^2 , T , and k_∞ simultaneously. The dependence of the transfer function on them is such that no single combination of l_s , l_T , L^2 , T , and k_∞ exists for minimizing the variance. However, if two or three of the parameters are known from other sources, the remaining ones may be estimated using the General Least Squares program.

CHAPTER IV

EXPERIMENTAL EQUIPMENT

The equipment used to generate the input signal and to measure the output of the subcritical assembly is described in this chapter. A schematic of the measuring system is shown in Figure 2.

The experiments using the light water subcritical assembly were conducted at a different location than the experiments using the heavy water subcritical assembly. Thus, some items of equipment were different for the two experiments.

Input System

The input system contains two major components: the shift register and the neutron generator.

Shift Register

The pseudo-random binary input signal is generated by a shift register with "modulo 2" feedback. By using the proper feedback logic, the maximum length sequence can be obtained. This sequence has the special autocorrelation function described in Chapter III. Peterson (26) discusses the correct feedback circuitry for obtaining the maximum length sequence for shift registers

containing up to 34 stages. The number of intervals, N , contained in a maximum length sequence generated by a shift register having m stages is

$$N = 2^m - 1 \quad (113)$$

References (23, 25) describe in some detail the characteristics of a shift register used to generate a pseudo-random signal.

The shift register used in the present study has eight stages, producing a sequence having 255 intervals before repeating. A schematic of the shift register is shown in Figure 5. The Δt time interval is controlled by a free running multivibrator, whose speed may be varied from 1 cps to 10 KC.

Neutron Generator

A Norelco neutron generator was used for the experiments with light water, and a Texas Nuclear Corporation neutron generator was used for the heavy water experiments.

Norelco neutron generator. The Norelco neutron generator (32) produces neutrons of 14 MEV energy by the d-t reaction, with an average source strength of 10^8 neutrons per second.

The neutron source tube contains a replenisher system which emits hydrogen isotopes when it is heated by an electric current. The isotopes are ionized in a Penning ion source and moved to the one stage accelerating system

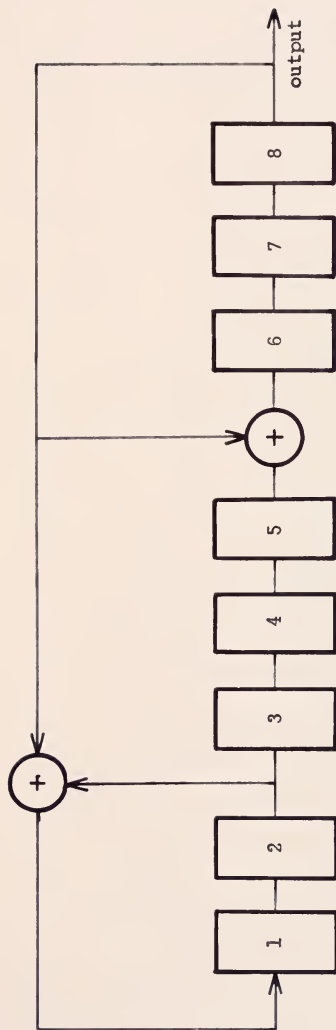


Figure 5. An eight-stage, maximum length sequence, pseudo-random binary signal generator

by the ion source voltage. The accelerating system imparts enough energy to the ions (125 KV) to overcome the electrostatic potential of the deuterium and tritium nuclei already embedded in the titanium target, thus causing the nuclear reaction. The size of the source tube is 3" x 20".

The neutron generator may be pulsed by controlling the ion source voltage, with a maximum pulsing rate of about 3 KC at a 50 per cent duty cycle. The signal generated by the shift register is used to control the ion source voltage through an intermediate voltage matching amplifier.

A high voltage transformer that supplies the accelerating voltage is located close to the source tube. A control rack, containing the electronic equipment and ion source voltage transformers, is connected to the source tube by a 30-foot cable. This length allows the rack and operator to be located a safe distance from the neutron generator.

Texas Nuclear Corporation neutron generator. The TNC neutron generator produces neutrons by either the d-t or d-d reactions. The d-d reaction was used for the heavy water experiments.

While the TNC neutron generator is physically different from the Norelco neutron generator, the sequence of events required to produce neutrons is the same.

The replenisher system is a pressurized tank containing deuterium gas. The deuterium is ionizing in a

Penning ion source and is moved to the acceleration system by the ion source voltage. The high energy ions leave the acceleration system and strike the deuterium, titanium target, producing neutrons.

The shift register controls the pulsing of the neutron generator through an intermediate circuit. The random width pulse from the shift register is differentiated, and on and off pulses are supplied to the neutron generator to control the beam deflection plates. The plates are located between the ion source and the acceleration system. A higher pulsing rate is possible with this generator than with the Norelco generator.

Nuclear Systems

A light water subcritical assembly and a heavy water subcritical assembly, each containing various amounts of natural uranium, were used as the test media.

Light Water Subcritical Assembly

The light water subcritical assembly consists of a right cylinder tank containing water, an aluminum support grid, and natural uranium fuel rods. The main features of the tank are shown in Figure 6.

The neutron generator was installed inside a 3 1/4 inch horizontal pipe in the bottom of the tank, such that the neutron source was on the longitudinal axis of the assembly. With no fuel elements, the effective radius of the tank is 52 cm. When the uranium is added, the core is

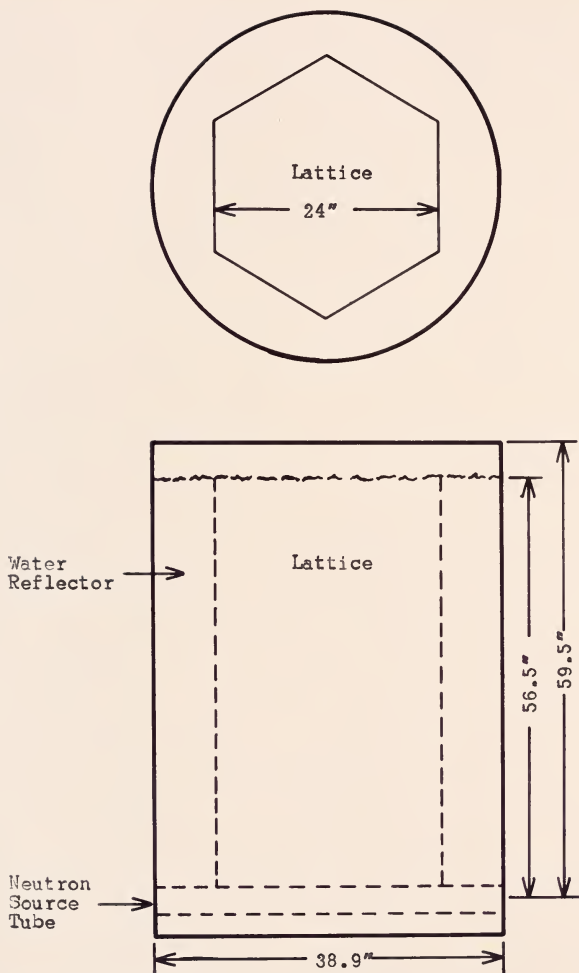


Figure 6. Light water subcritical assembly

surrounded by a water reflector. For a full loading of fuel, the effective radius of the core is 37 cm. The core is immediately above the neutron generator and extends to the surface of the water, 142.9 cm from the source.

The support grid holds the uranium in a triangular lattice 4 cm on a side. Two hundred four fuel elements make up a full load, with one diagonal row of elements missing to leave room for the neutron detectors. The natural uranium slugs are housed inside 1 inch aluminum tubing, which is held upright by the grid.

The volume fractions for the full load are: $F_{H_2O} = 0.42133$, $F_{AL} = 0.16058$, and $F_{UR} = 0.41809$.

Heavy Water Subcritical Assembly

The heavy water subcritical assembly (Figure 7) is essentially the same as the light water subcritical assembly. The main differences are: a. The target of the neutron generator is placed inside a 2 1/2 inch pipe through the center of the tank. b. The lattice spacing is 12 cm, resulting in volume fractions of: $F_{D_2O} = 0.9357$, $F_{AL} = 0.01784$, and $F_{UR} = 0.04646$, for a full loading of 55 fuel elements. c. The lattice occupies the entire volume of the D_2O tank. Thus, the effective radius is 59 cm for both the non-multiplying and multiplying cases. d. The water level is maintained at 60.8 cm above the source.

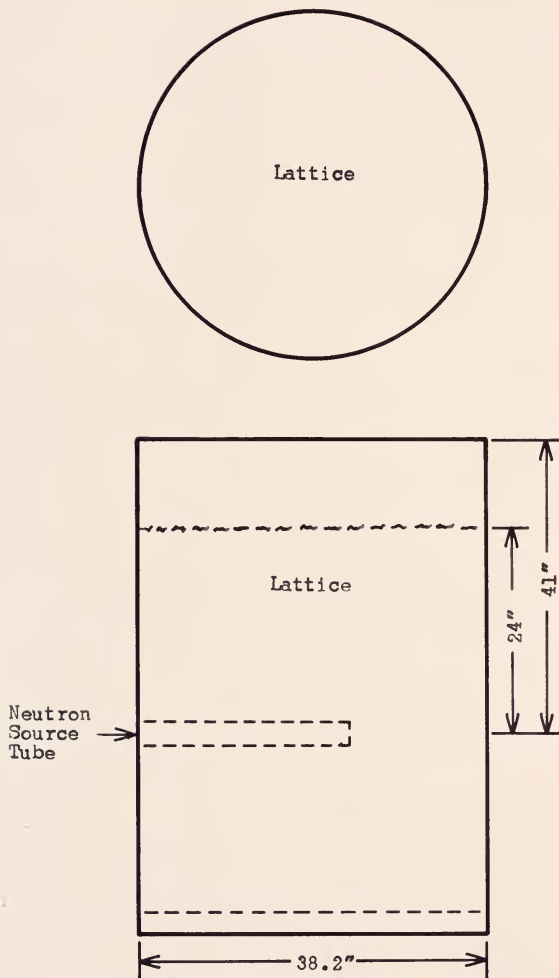


Figure 7. Heavy water subcritical assembly

Output System

The variation of the neutron density is sensed by the output system. The major components in this system are the detection and amplification equipment, the count rate circuits, the band pass filters, and the data acquisition system.

Neutron Detectors

The neutron detectors were placed inside aluminum conduit to protect them from the water. The conduit was L-shaped, supporting the detectors in a horizontal position above the neutron generator. The height of the individual detectors could be easily changed by vertical adjustment of the conduit.

The detectors have a 12 inch active length, filled with He^3 to 4 atmospheres of pressure.

Pulse Amplifiers

For the light water experiment, preamplifiers and linear amplifiers manufactured by Hamner Electronics Inc. were used. Preamplifiers and linear amplifiers made by Nuclear Chicago were used for the heavy water experiment. Both systems supplied constant height, one microsecond long voltage pulses to the count rate circuits at a rate proportional to the neutron density at the detectors.

Count Rate Circuit

The count rate circuit was specially designed for this study. The specifications were: a. a fast response circuit, whose output would duplicate the neutron density variation as closely as possible; b. little ripple, or decay of the output voltage between input pulses; and c. adequate output voltage (2 to 10 volts).

The count rate circuit has five counting ranges, which are shown with their measured break frequencies in Table 1. Appendix E contains detailed information on the count rate circuit, including the design criteria, a circuit diagram, and a plot of the transfer function of the circuit.

TABLE 1
Count Rate Meter

<u>Range</u>	<u>Counts/sec.</u>	<u>-3 db point</u>
1	100K to 250K	5400 cps
2	40K to 100K	2000 cps
3	20K to 50K	1000 cps
4	10K to 25K	600 cps
5	4K to 10K	350 cps

FM Tape Recorder

A Minneapolis-Honeywell four-channel tape recorder was used for storing the output from the count rate circuits during the heavy water experiments and for transporting the information to the data acquisition system.

The tape recorder has a band width of 0 to 10 KC at a recording speed of 30 inches per second; a speed of $1 \frac{7}{8}$ inches per second is also available. An internal calibration circuit and compensation channel allows the original signal to be reproduced with less than one per cent error.

Band Pass Filters

Krohn-Hite ultra-low frequency band pass filters were used to condition the analog signal from the count rate circuit. The high pass filter was set at .02 cps to remove the low frequency components from the signal. The low pass filter was set to remove the frequencies higher than one half the sampling rate of the data acquisition system.

Data Acquisition System

The main components of the data acquisition system are shown in Figure 8. The multiplexer samples two, four, six, or eight input analog signals at a rate of 15,000 samples per second in the low density tape mode. The twelve-bit binary analog to digital converter accepts an input from each channel in turn of -4.096 to 4.096 volts. The format unit calculates and includes in the final binary word a lateral odd parity bit. The unit also calculates the longitudinal parity check sum for inclusion at the end of each record, and performs other control functions.

The resultant computer words are written on tape by the recorder unit, in a form compatible with the IBM 709 computer. The system can also produce a high density tape for the IBM 7090 computer, at a sampling rate of 28,571 samples per second.

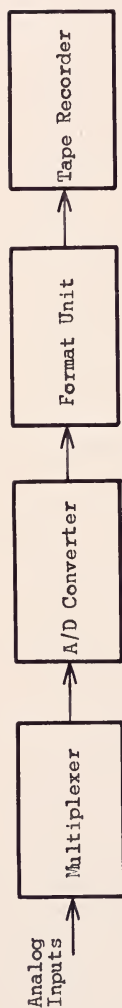


Figure 8. Block diagram of the data acquisition system

CHAPTER V

RESULTS

The results from the theoretical and experimental study of the spatially dependent transfer function of a nuclear system are presented in this chapter.

Theoretical Results

The computer code SPAT, described in Appendix D, was used to calculate the transfer function between a thermal neutron detector and a point source of fast neutrons (Equation (57)) for four cases, presented in Figures 9 through 13. The same geometry described in Chapter II was used, with values of $c = 150$ cm, and $R = 50$ cm. The values of the nuclear parameters used in the calculations are listed in Table 2.

The series in Equation (57) were terminated when the magnitude of additional terms was less than one tenth per cent of the sum of the absolute values of the preceeding terms. The curves labeled L in the figures represent the lumped parameter transfer function for the nuclear systems.

TABLE 2

Nuclear Parameters Used for the Theoretical Results

Figure	L^2, cm^2	T, cm^2	$l_s, \mu\text{sec}$	$l_T, \mu\text{sec}$	k_∞
9, H_2O^a	8.12	30	200	10	0
10, H_2O^a	8.12	30	200	10	0
11, D_2O^a	13,700	110	40,000	46	0
12, $\text{H}_2\text{O} + \text{Ur}^b$	1.61	40	200	10	0.923
13, $\text{D}_2\text{O} + \text{Ur}^c$	87.2	133	300	40	1.15

a. References (2, 18)

b. References (18, 29)

c. References (30, 33, 39)

The variation of the phase shift with frequency and with distance from the source is of interest. At 100 cm from the source, the phase shift in light water (Figure 9, Part D, and Figure 10) is -720 degrees at 800 cps and is -1440 degrees at 2400 cps. In other words, four complete cycles of the 2400 cps neutron wave are located between the source and the detector. As the detector is moved closer to the source, the transfer function experiences a maximum negative phase shift (Figure 9, Part C). A point is reached where the phase shift is always positive (Figure 9, Part B). The data for heavy water, Figure 11, also shows a positive phase shift. The multiplying media data, Figures 12 and 13, shows a great reduction with frequency in the amount of the phase shift.

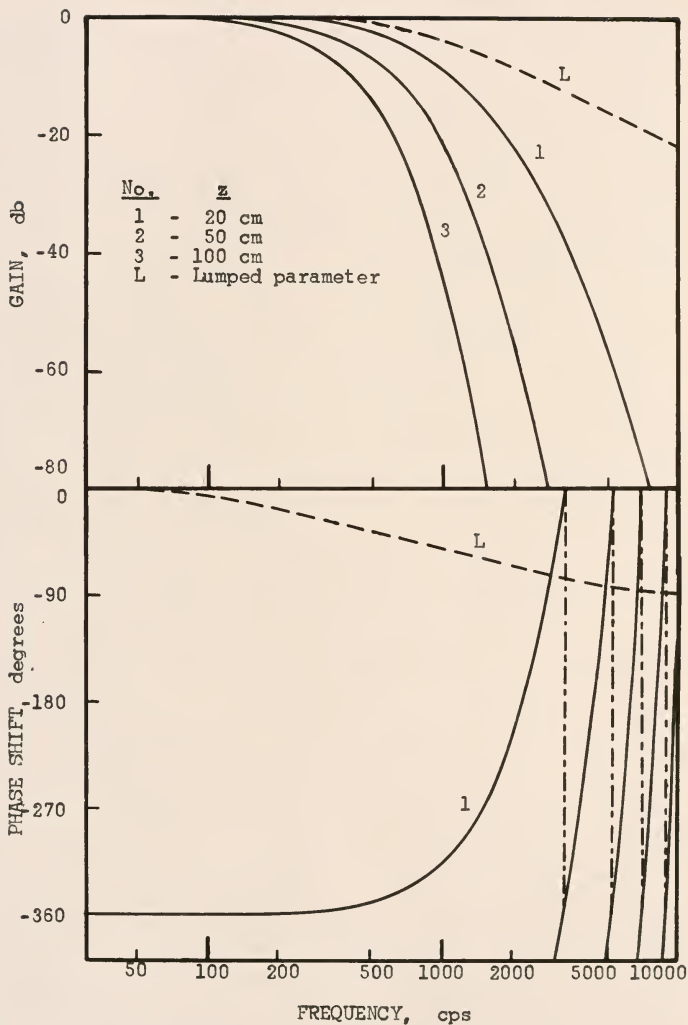


Figure 9, a and b. Theoretical transfer function for light water

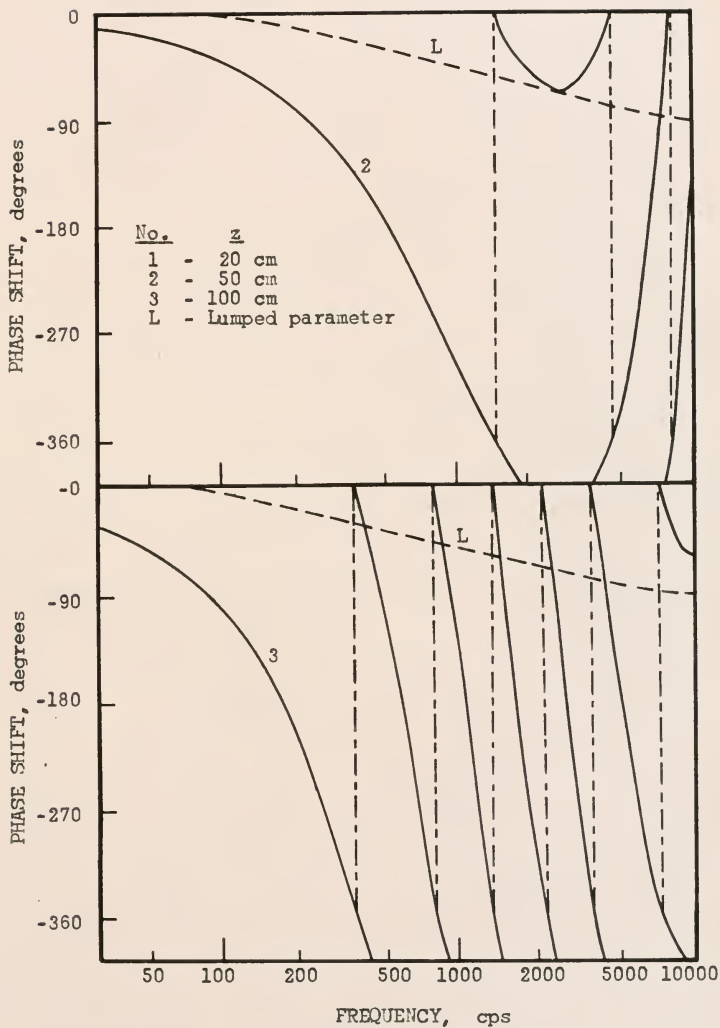


Figure 9, c and d. Theoretical transfer function for light water

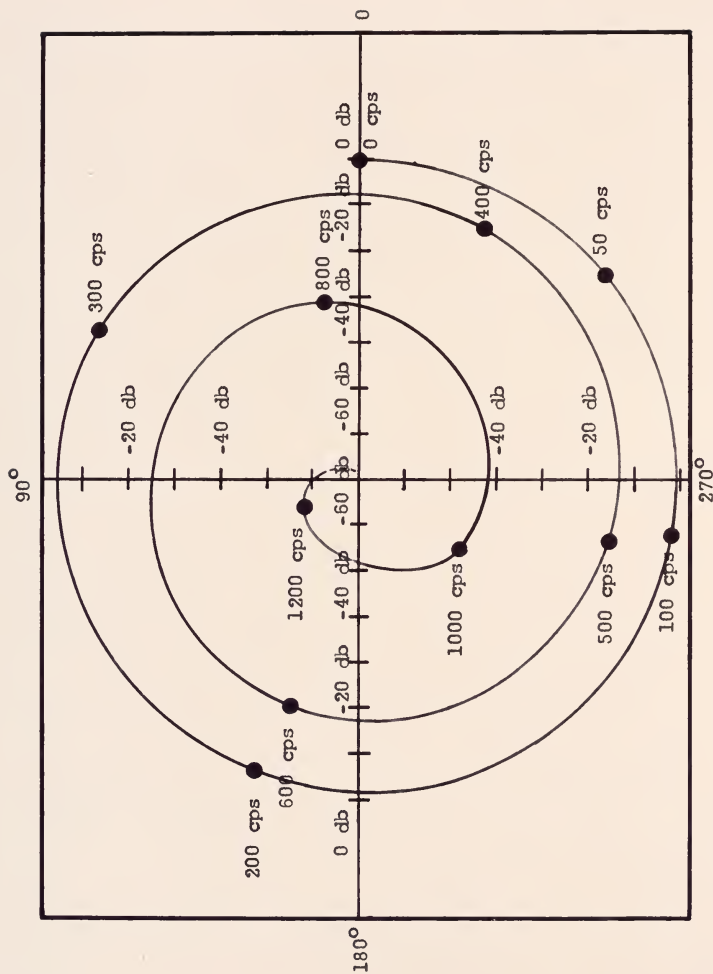


Figure 10. Theoretical transfer function for light water, $z = 100$ cm

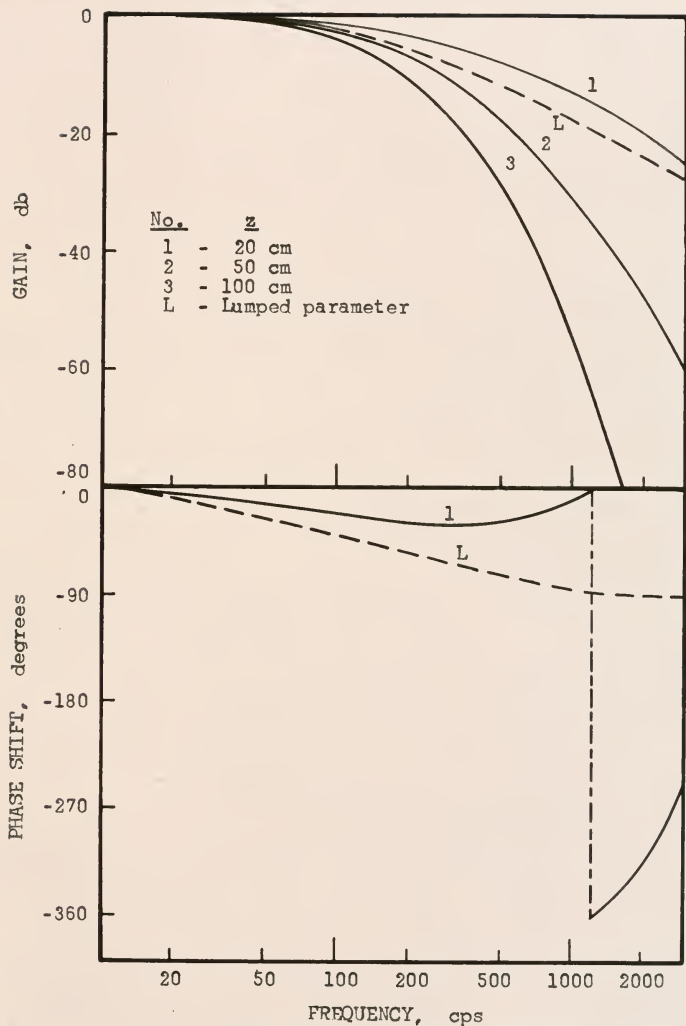


Figure 11, a and b. Theoretical transfer function for heavy water

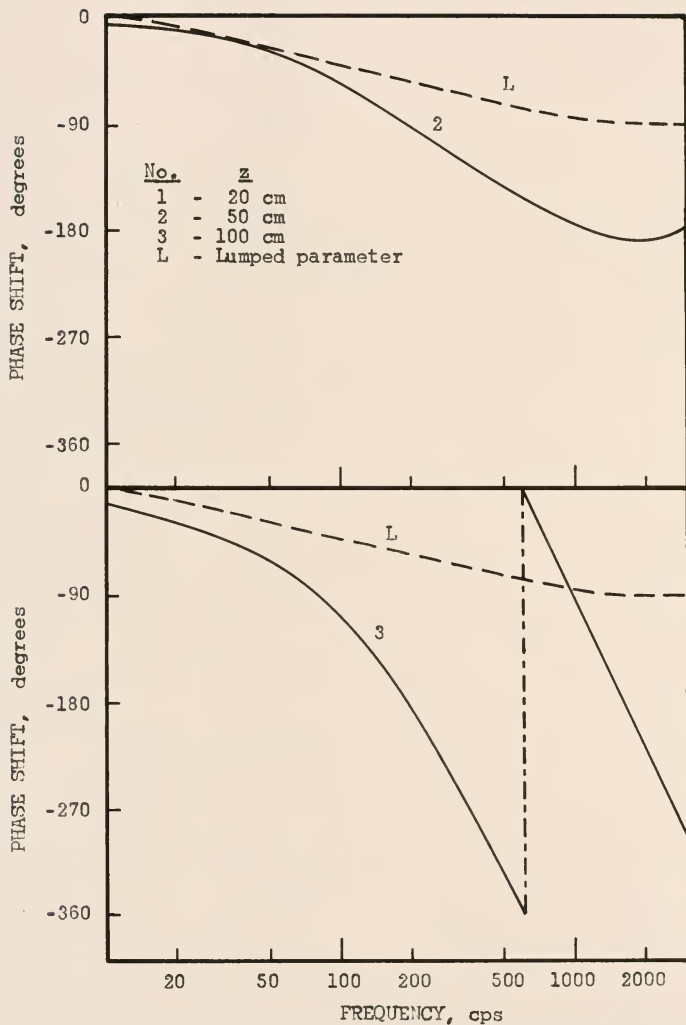


Figure 11, c and d. Theoretical transfer function for heavy water

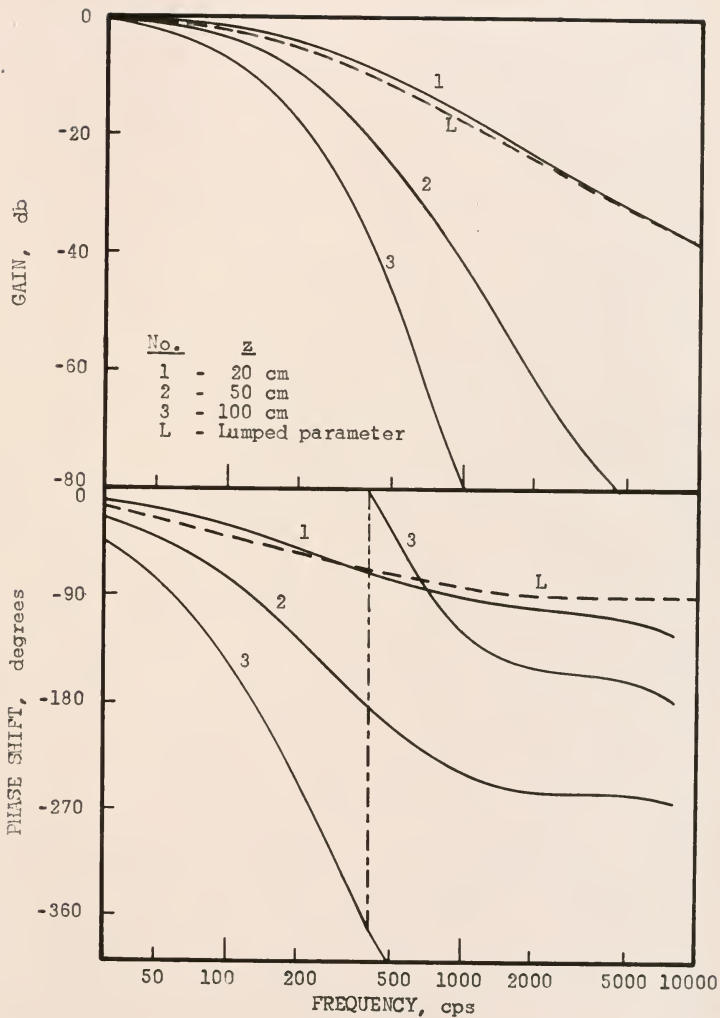


Figure 12, a and b. Theoretical transfer function for a light water subcritical assembly

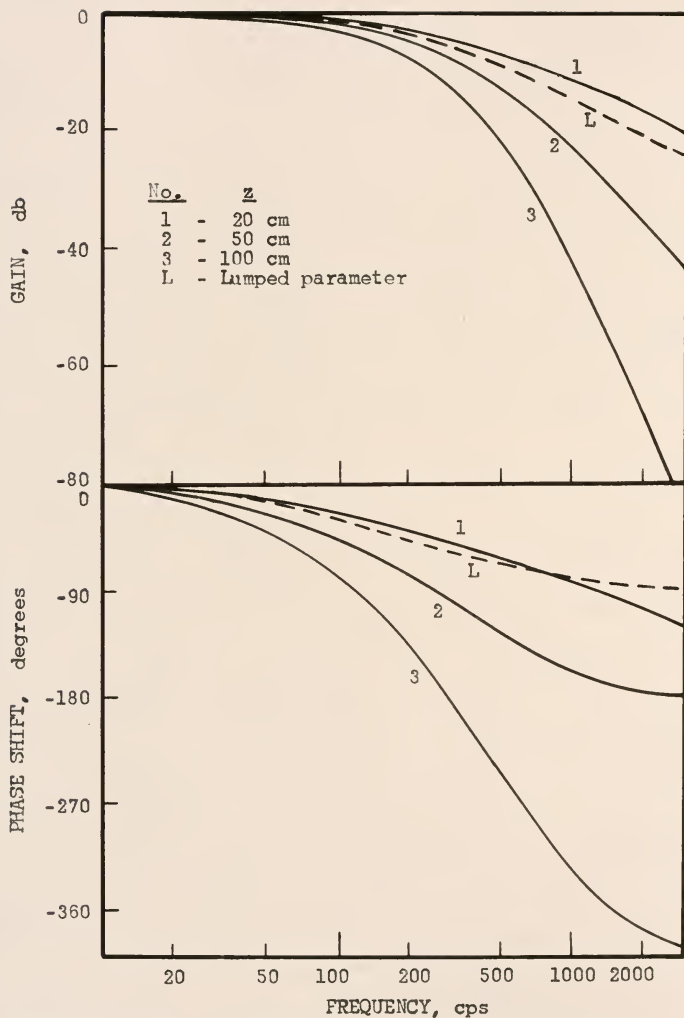


Figure 13, a and b. Theoretical transfer function for a heavy water subcritical assembly

The behavior of the phase shift clearly illustrates the effect of frequency on the wave length and wave velocity. A discussion of the dependence of the wave velocity and wave length of a thermal neutron disturbance on frequency may be found in References (5, 6).

A comparison of the spatially dependent transfer function, SDTF, and the lumped parameter transfer function, LPTF, shows, in general, that the lumped parameter model is not an adequate representation of the nuclear system (see Figures 9 through 13). However, it appears that the two models can give similar results if the output detector is located at a specific distance from the source.

As the multiplication factor approaches one, the two models give essentially the same attenuation and phase shift for $z \gtrsim 20$ cm. As k_{∞} approaches zero, the heavy water case can still be represented by the LPTF for $z = 20$ to 30 cm and for frequencies less than 1000 cps, but there is a significant difference between the SDTF and the LPTF for the light water case.

McInerney (40) has shown that diffusion theory gives the correct spatial dependence for fast neutrons when the reciprocal diffusion length, $1/L$, is approximately equal to the total cross section, Σ_t . McInerney's development helps explain why the LPTF, which is derived from diffusion theory, cannot be used with light water but can be used in a light water moderated reactor at specific distances from the source. As uranium is added to the water, $1/L$ approaches Σ_t , fulfilling the requirement stated above.

In using Equation (57) to determine the parameters of a nuclear system from experimental data, it is of interest to know the number of terms that must be used to adequately fit the data. An indication of the effects of changes in z , media, and frequency on the number of terms was obtained by considering the four cases listed in Table 2. The results presented in Table 3 were obtained by assuming the average experimental error to be four per cent and using this percentage as the accuracy criterion in SPAT.

As expected, only the first term of Equation (57) is needed when the detector is at a sufficient distance from the source. The higher spatial modes are attenuated more than the fundamental mode and can be neglected at low frequencies. At higher frequencies, though, the higher spatial harmonics are not attenuated much faster than the fundamental mode. They must be included in the equation even for large z . Figure 31 illustrates part of the reason for this effect.

The fundamental root, ζ_0 , which is much smaller than the other roots at a frequency of 0 cps, is only slightly smaller at 2000 cps. At higher frequencies, at least three terms in the i series must be included in the equation, and possibly several terms from the n series (see Equation (57)). The spatial modes contributed by the m series are usually quickly attenuated, so that only the fundamental m term need be included.

TABLE 3
Number of Terms Required for Four Per Cent Error
in Equation (57)

<u>Case</u>	<u>Frequency, cps</u>			
	<u>0</u>	<u>10</u>	<u>100</u>	<u>1000</u>
Figure 9, H_2O				
z = 20 cm	6	7	7	7
z = 50 cm	4	4	4	5
z = 100 cm	2	3	3	3
Figure 11, D_2O				
z = 20 cm	3	3	3	5
z = 50 cm	2	2	2	3
z = 100 cm	1	1	1	2
Figure 12, $H_2O + Ur$				
z = 20 cm	3	3	3	7
z = 50 cm	2	2	2	3
z = 100 cm	1	1	1	2
Figure 13, $D_2O + Ur$				
z = 20 cm	3	3	6	9
z = 50 cm	1	1	2	2
z = 100 cm	1	1	1	2

As the multiplication factor approaches one, the fundamental mode becomes dominant, making fewer terms necessary for most systems, even close to the source.

Unfortunately, it is more difficult to make measurements in that portion of the system which can be represented by only one term of the equation, since there are fewer neutrons present and the counting rate is lower.

Experimental Results

The methods used to check the accuracy of the equipment and the computer calculations are discussed first. The experimental data follows.

Calibration

Equation (90) shows that the effects of the measuring system on the input signals are cancelled when the ratio of the cross power spectra between two detectors is calculated. Thus a calibration of the measuring system is not necessary in the usual sense of the word. However, it is important to know the amount of noise that is added to the input signal by the equipment and to determine the extent of the numerical errors accumulated in the data during the computer processing.

The computer code was checked by correlating and transforming known mathematical functions. Once the program was debugged, the error between the calculated and the theoretical results (correlations and power spectra) was less than one per cent.

The next step was to sample the output from the shift register with the data acquisition system, and process the data in the computer. The auto correlation of the recorded function exhibited the characteristic triangular spike at $T = 0$ (see Figure 3), but it did not remain at a constant $-1/N$ (-0.00392) level for the other delay times. Instead, the auto correlation function fluctuated between values of 0.005 and -0.02 . This fluctuation is caused partly by numerical error in the calculation and partly by the discrete sampling interval of the input voltage. The majority of the variation, though, is caused by noise added to the signal by the electronic equipment. The equipment involved in this test was the shift register, an intermediate Schmidt trigger, and the data acquisition system.

Figure 14 shows the auto power spectrum of the shift register and the theoretical curve for the idealized signal. The approximately 1 db gain in the 20 to 200 cps frequency range is caused by the low frequency fluctuations noted in the auto correlation function. If the results presented in Figure 14 are used as a calibration test, it appears that -13 to -15 db is the approximate limit for accurate calculation of the power spectrum.

There are several other items to consider when judging the accuracy of the experimental results. The number of computational steps a particular sampled function has gone through affects the accuracy of the function. As the

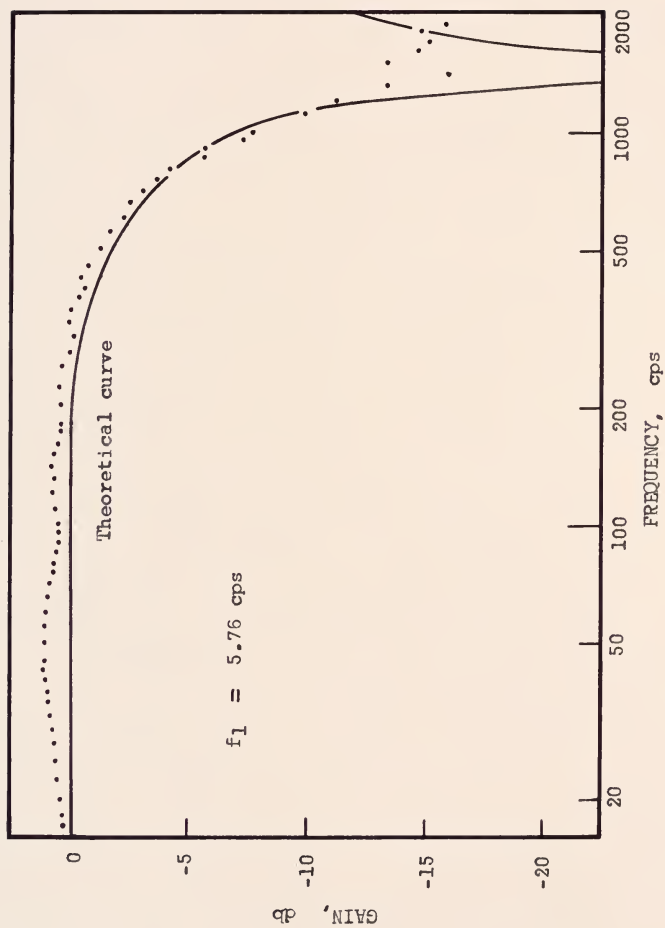


Figure 14. Auto power spectrum of the shift register

power spectra are attenuated at the higher frequencies and the numbers become small, the error is increased. Combining the spectra as in Equation (91a) can produce wildly fluctuating results. Since the functions for calculating $\Phi_{D1D1}(\omega)$ and $\Phi_{D1D2}(\omega)$ are recorded at the same time and then subjected to the same computational procedure, any trends introduced by the process tend to cancel out when $\Phi_{D1D2}(\omega)$ is divided by $\Phi_{D1D1}(\omega)$ in Equation (91a). This process is particularly helpful when the correlation curves are discontinuous at $t=0$ (see, for example, Figure 18), as the discontinuity causes similar bumps on both power spectra curves (see Figures 19 and 20).

Data

The correlation functions presented in this section were calculated using Equation (109). The integration time, $I\Delta t$, was equivalent to ten cycles of the shift register. Equation (112) was used to calculate the power spectra. The time span of the integration, $-N$ to $+N$, was varied to transform only that portion of the correlation data which was of interest.

Runs 1 and 3 were made using the light water subcritical assembly tank, which was filled with water only. The cross correlations (Equations (79, 80, 102, 109)) are shown in Figure 15. When only an "x" appears, it coincides with the dot.

The correlations $\phi_{12}(\tau)$ and $\phi_{13}(\tau)$ are essentially the same, preventing the determination of the spatial

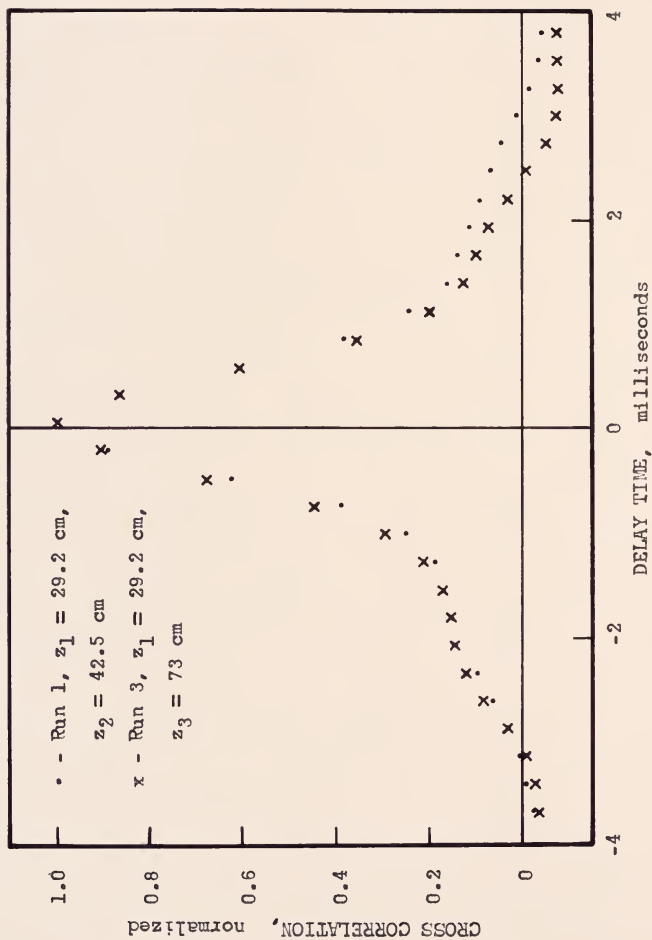


Figure 15. Cross correlation of two detectors, light water

effect on the system's transfer function. The two main reasons for their similarity are: a. the rapid decrease in the counting rate as z increased prevented a sufficient Δz between the detectors, and b. the sampling rate of the data acquisition system is not rapid enough to permit measurement of the travel time of the neutron disturbance between the detectors.

Runs 2 and 6 were made in the heavy water subcritical assembly tank, which contained water only. Figure 16 shows the cross correlation functions. The effect of moving Detector 2 to Position 3 can be observed in the 0.4 millisecond shift of the peak, showing that measurement of the travel time of the neutron disturbance between detectors is possible.

The striking feature of Figure 16 is that the positive correlation peaks appear to be displaced to the right by approximately 10 milliseconds. The reason for this displacement is discussed later with the heavy water subcritical data. The heavy water data was not processed further.

Figure 17 presents the data taken in the light water subcritical assembly with a full load of uranium. The correlation function does not decay to zero within the limits of the figure. Even for much longer delay times, $\phi_{12}(\tau)$ does not go to zero. This strange behavior appears to be caused by the reflection of neutrons from the concrete floor. Other structures were far enough away

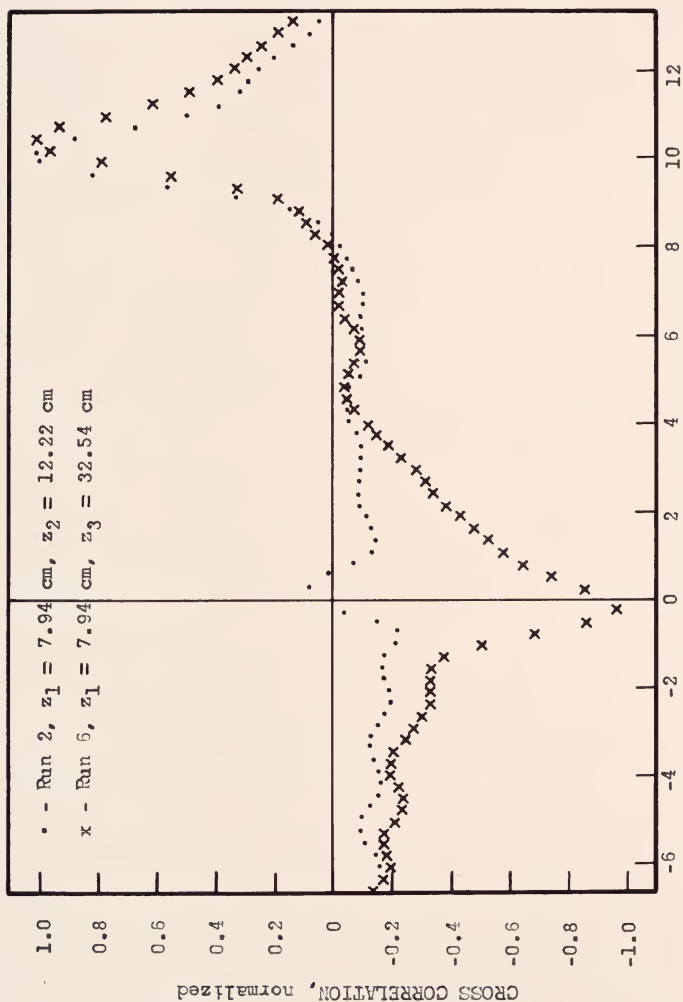


Figure 15. Cross correlation of two detectors, heavy water

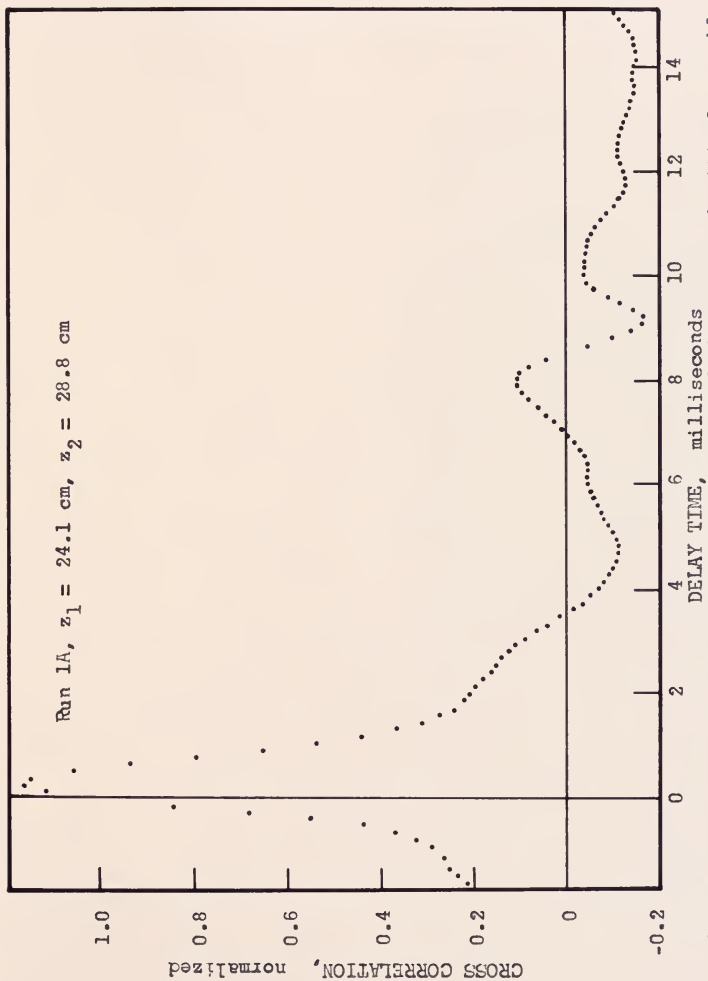


Figure 17. Cross correlation of two detectors, light water subcritical assembly

from the tank to have little effect on the neutron distribution in the tank.

If it is assumed that the actual source variation, $S(t)$, is the intended source variation, $S_i(t)$, plus a reflection of S_i from the floor, the actual source supplying neutrons to the detectors is

$$S(t) = S_i(t) + AS_i(t - T) \quad (114)$$

The intensity of the reflected source relative to the intended source is A , and T is the time lapse before the reflected neutrons re-enter the medium and pass the source position. Using the same procedure as that used in Chapter II to develop Equations (88, 89), the cross power spectrum between two detectors with the source defined by Equation (114) is

$$\begin{aligned} \Phi_{12}(\omega) &= H_{m1}^*(\omega) H_{m2}(\omega) H_1^*(\omega) H_2(\omega) \\ (\cdot) \Phi_{ss}(\omega) &[1 + A^2 + 2A \cos(\omega T)] \end{aligned} \quad (115)$$

The bracketed term shows the effects of the reflection. If A is zero, Equation (115) is the same as Equation (88). The $\cos(\omega T)$ term causes a "beating" of the power spectra. The transform of the correlation function in Figure 17 produces such an effect. Resonance peaks occur approximately every 118 cps, which corresponds to the 8.4 millisecond delay time to the first reflection peak in Figure 17. Figure 17 actually contains other reflection peaks

at multiples of 8.4 milliseconds, for both positive and negative delay times. A single value for A could not be found from the experimental data. A appears to be a function of frequency, varying from 0.2 at 200 cps to 0.4 at 450 cps.

A further check of the assumption that the displaced correlation peaks result from reflections can be made by estimating the average energy of the reflected neutrons.

Using the definition of the group velocity (43)

$$v_g = \frac{\partial \omega}{\partial [\text{Real}(B_p)]} \quad (116)$$

and the solution for the buckling from simple monoenergetic diffusion theory,

$$B_p^2 = \frac{-j\omega}{Dv} - \frac{\sum_R}{D} \quad (117)$$

The average neutron energy is approximately

$$E = \frac{1}{2}mv^2 = \frac{\frac{mv^2}{2}}{8D(DB_n^2 + \sum_R)} \quad (118)$$

the diffusion coefficient is D, B_n^2 is the transverse buckling, \sum_R is the removal cross section, and m is the neutron mass. Since the reflected neutrons must have relatively high energies to survive the trip into the floor and back to the detectors through the water, the values of D and \sum_R used in the calculation are representative of

fast neutrons and are 0.2 cm and 0.1 l/cm (44). The group velocity was estimated to be 1.7×10^5 cm/sec by considering the time delay between the correlation peaks shown in Figure 18 and the distance between Detectors 2 and 3. Using these values in Equation (118) gives an average energy of the neutrons between the two detectors as approximately 0.19 ev. While this energy is low, it is several times greater than thermal energy and it does indicate that the displaced correlations could be due to reflected neutrons. Clearly, further study of the reflections of neutron waves and groups from both the experimental and theoretical standpoint is needed. Clarification of the mechanism involved in the spreading and reflecting of neutron groups should prove most valuable.

Since the development of the spatially dependent transfer function included the assumption that no neutrons re-entered the system, the cross power spectra were obtained by transforming that part of the correlation curves that is close to $\tau = 0$. Unfortunately, since the correlation curves are rarely equal to zero at the $\pm N$ points, a discontinuity is present which adds a small beating effect to the power spectra.

Figures 18 through 23 contain the data obtained from the light water and natural uranium subcritical assembly used to determine the experimental spatially dependent transfer function. Only that portion of the correlation curves between -4 to +4 milliseconds was used to obtain the power spectra curves. In Figures 19 and 20, many of

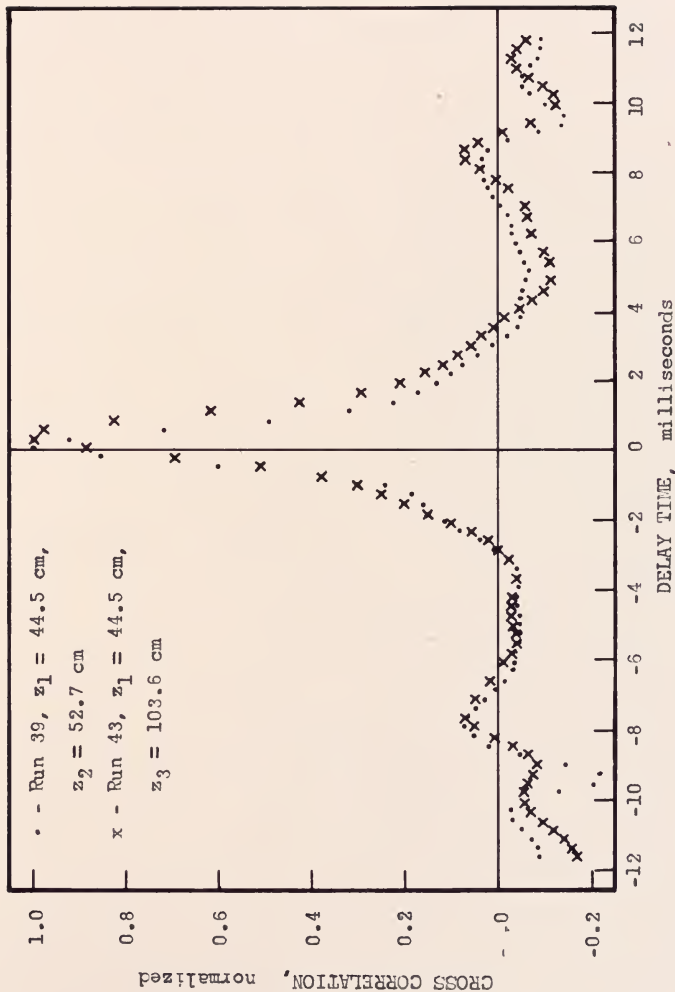


Figure 18. Cross correlation of two detectors, light water subcritical assembly

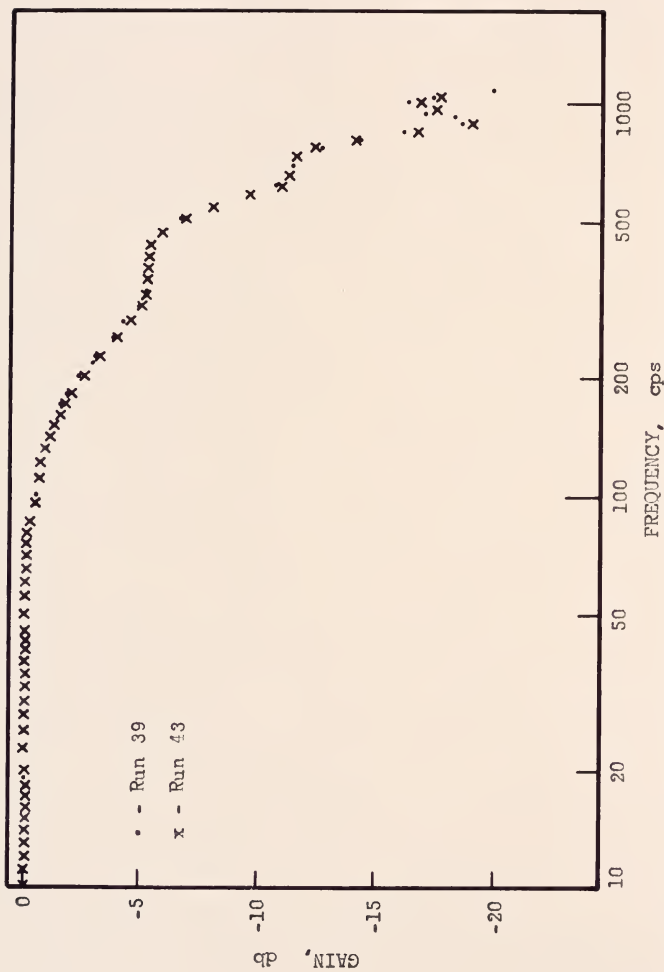


Figure 19. Auto power spectrum of Detector 1, light water subcritical assembly

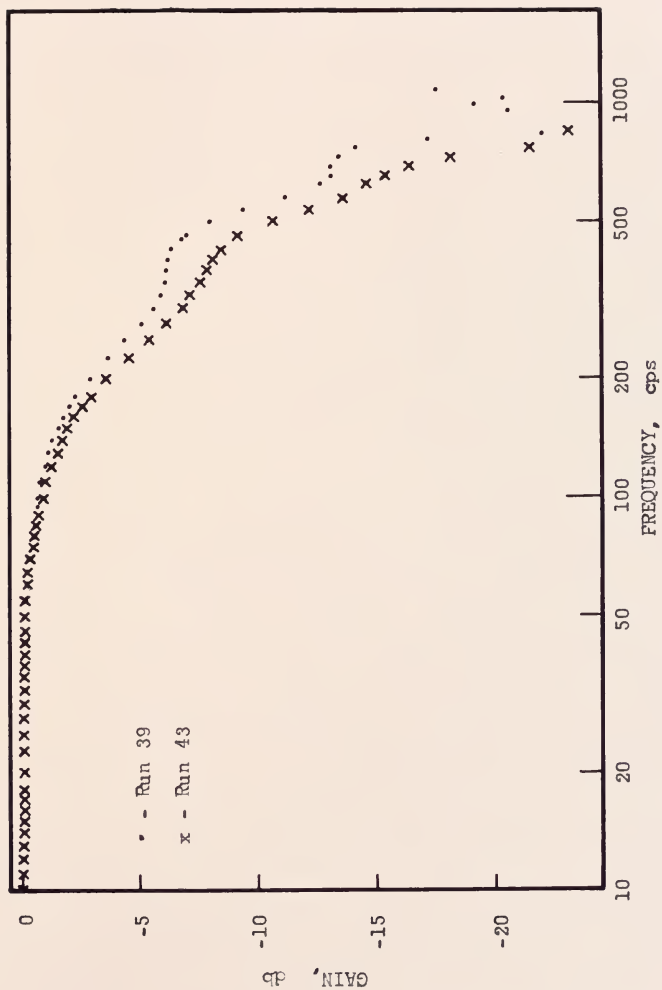


Figure 20. Amplitude of the cross power spectra, light water subcritical assembly

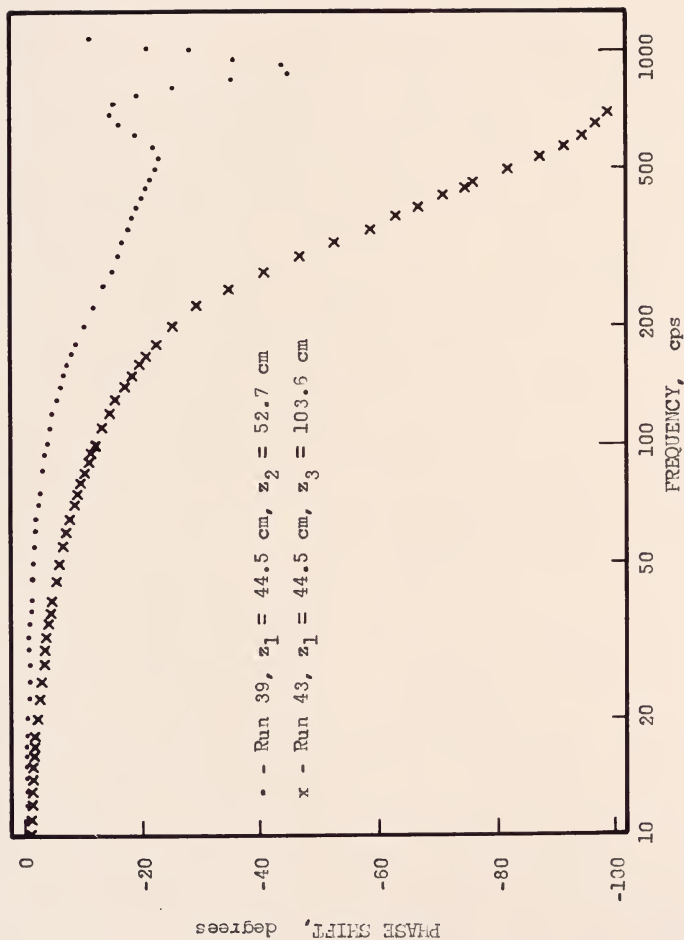


Figure 21. Phase shift of the cross power spectra, light water subcritical assembly.

the dots coincide with the x 's. The points on the two figures begin to become scattered for frequencies greater than 800 cps and for an attenuation greater than 15 db. Also, the discontinuities in the cross correlation function cause bumps on the spectra curves, starting at 300 cps. The correct curve is an average of these bumps. The data beyond 300 cps may be regarded with suspicion and that beyond 800 cps may be disregarded.

The cross power spectrum curve for Run 39, where the detectors are close together, has essentially the same shape as the auto power spectra of Detector 1 (see Figures 19 and 20). Referring to Equations (88, 97), the above fact indicates that there is very little uncorrelated noise in the system; in other words, K_{77} and K_{44} are very small. Thus $\Phi_{D1D1}(\omega)$ may be safely used in Equation (91a) as a substitute for $\Phi_{SS}(\omega)$.

Figures 22 and 23 contain the results from Equation (91a). The attenuation varies smoothly with frequency to 500 cps, where a resonance peak occurs. The peak may be disregarded as being caused by the discontinuities in the correlation functions.

The solid line in Figures 22 and 23 is the theoretical transfer function between two detectors, Equation (92). The values of the nuclear parameters used in SPAT are: $L^2 = 1.61 \text{ cm}^2$, $\tau = 40 \text{ cm}^2$, $l_s = 6 \times 10^{-5} \text{ sec}$, $l_T = 1 \times 10^{-5} \text{ sec}$, and $k_\infty = 0.923$. Only l_s was adjusted to improve the agreement between the theoretical and

experimental data. The other parameters were obtained from Reference (29).

The curves in Figures 22 and 23 were not determined by using the least squares program. It is apparent that the point source transfer function is not adequate for a light water and uranium medium. The large size of τ relative to L^2 makes the first flight collision density very important in determining the thermal neutron distribution. In any future work using Equation (32) with a light water system, the expansion coefficients of the source (Equation (16)) should be determined for a distributed source (see Reference (40) for an excellent example of a source). The point source assumption causes the theoretical transfer function to predict about the right attenuation by selecting an appropriate Fermi age, but it predicts a greater phase shift than actually occurs.

Figures 24 through 30 present the results from the experiments in the heavy water subcritical assembly with a full load of uranium.

It is unfortunate that the heavy water assembly was constructed next to a 4 foot thick concrete wall. The small size of the heavy water tank (relative to L^2 and τ) combined with the nearness of the wall and floor allows both a high neutron leakage rate and a large number of reflected neutrons to re-enter the system. This occurs even though the tank is covered with cadmium. The

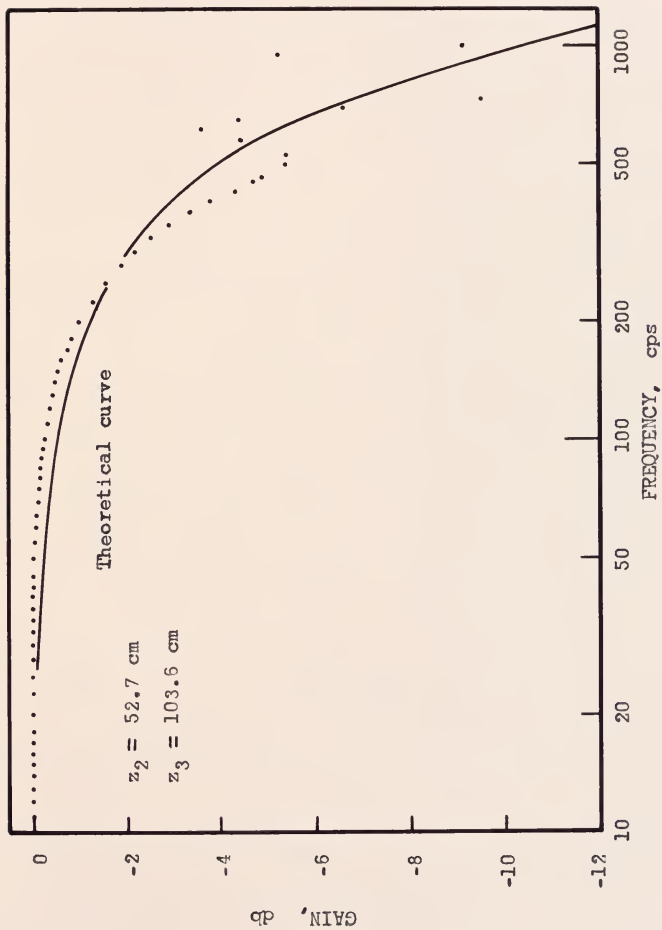


Figure 22. Amplitude of the transfer function between two detectors, light water subcritical assembly

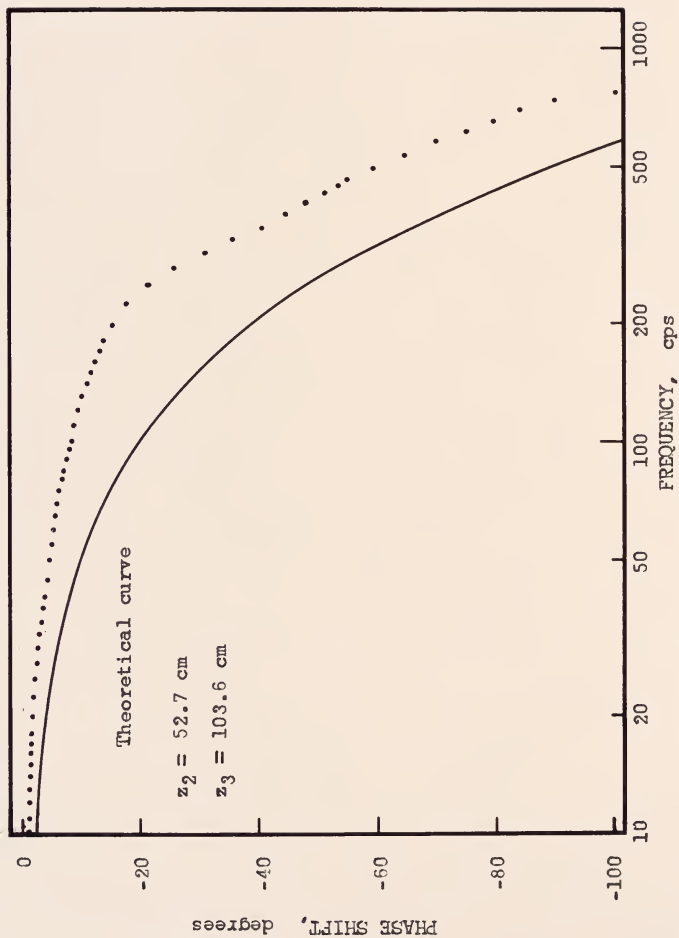


Figure 23. Phase shift of the transfer function between two detectors, light water subcritical assembly

reflection peaks in Figure 24 show the strong correlation between the original source neutrons and the reflected neutrons. The fact that the reflection peaks occur at intervals of approximately 10 milliseconds suggests an explanation for the heavy water data presented in Figure 16.

The Fermi age for the fast neutrons emitted by the source is large enough to permit almost all of the neutrons to leave the system. Very few of the neutrons experience enough collisions to become thermalized within the system. The escaped neutrons are thermalized and reflected back to the tank by the surroundings. Those neutrons having enough energy to avoid being captured by the cadmium re-enter the tank and complete the thermalizing process. The number of returning neutrons that are detected is much larger than the number of original neutrons detected. Thus the strong correlation in Figure 16 at 10 milliseconds in a reflection peak. Run 2 exhibits only a small positive correlation at $\tau = 0$, caused by the detectors being close together. Run 6, where the detectors are farther apart, exhibits a large negative correlation at $\tau = 0$, indicating that the variation of the thermal neutron density is quite different at the two detector locations.

As uranium is added to the system, the artificial source produces a smaller percentage of the fast neutrons, since the fast neutron source is spread throughout the

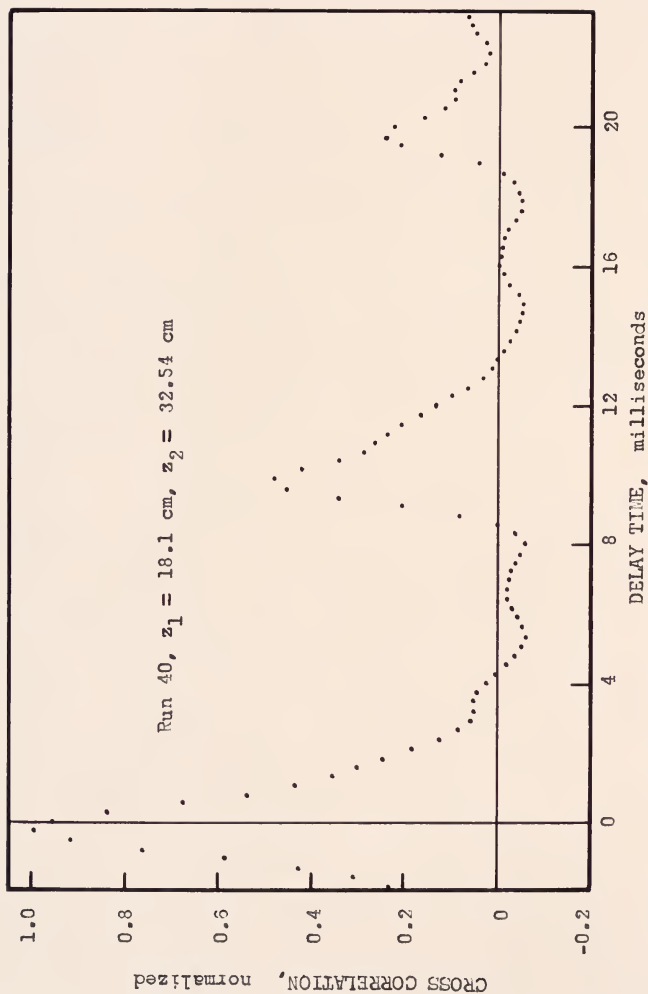


Figure 24. Cross correlation between two detectors, heavy water subcritical assembly

fuel. This spreading of the source reduces the leakage and reflection effect. For Run 40 (Figure 24), the correlation peak at $\tau = 0$ is stronger than the reflection peak at 10 milliseconds. To obtain good data in heavy water only will require at least one of the following items: a. a larger assembly, b. a location far from other structures, and c. a moderating and absorbing structure around the tank so that neutrons are not returned to the tank.

Figures 25 through 30 contain the data used to determine the spatially dependent transfer function in a heavy water subcritical assembly. The portion of the correlation curves between -3.5 and +3.5 milliseconds was transformed. The slight difference in the source behavior for the two runs can be seen in the auto correlation of Detector 1, Figure 26. The power spectra data appears to be correct to 700 cps (Figure 27), with the discontinuity effect first appearing at 250 cps. The positive phase shifts shown in Figure 28 are caused by the peaks of the correlation curves occurring at slightly negative delay times (Figure 25). It is not completely clear why the maximum correlation occurs at this time, but it is expected that the pattern and timing of the neutron reflections and thermalization processes contribute to the effect. Taking the ratio of the power spectra (Equation (91a)) cancels the reflection effects to some extent, as seen in Figures 29 and 30.

The point source model is able to predict reasonably well the attenuation and phase shift of the experimental

transfer function for the heavy water subcritical assembly. The theoretical and experimental data agree fairly well in Figures 29 and 30 for frequencies between 0 and 250 cps. The resonance peak in the attenuation curve and the sudden increase in the phase shift for frequencies greater than 250 cps indicate that effects other than simple slowing down and diffusion have affected the correlations. One of these effects is the discontinuities in the correlation curves, Figures 25 and 26. Another possible effect is the inhomogeneity of the nuclear system.

Investigation of the roots of the characteristic equation for the theoretical heavy water subcritical assembly (Figure 13 and Table 2) shows that the wave length of the fundamental mode approaches the size of the lattice spacing in the actual assembly (12 cm) as the frequency increases (see Figure 31 for the roots at 0 and 2000 cps). The higher order modes have wave lengths that are shorter than the lattice spacing. For example, the wave length of the fundamental mode at 50, 200, and 400 cps is 177, 50, and 30 cm. The wave length of the next higher mode is approximately 8 cm for the above frequencies. As the frequency is increased, the attenuation of the fundamental mode increases faster than for the other modes (see Figure 31), making the higher modes more important relative to the fundamental mode. Thus the nuclear system is being investigated with wave lengths of the same order of magnitude as the lattice spacing.

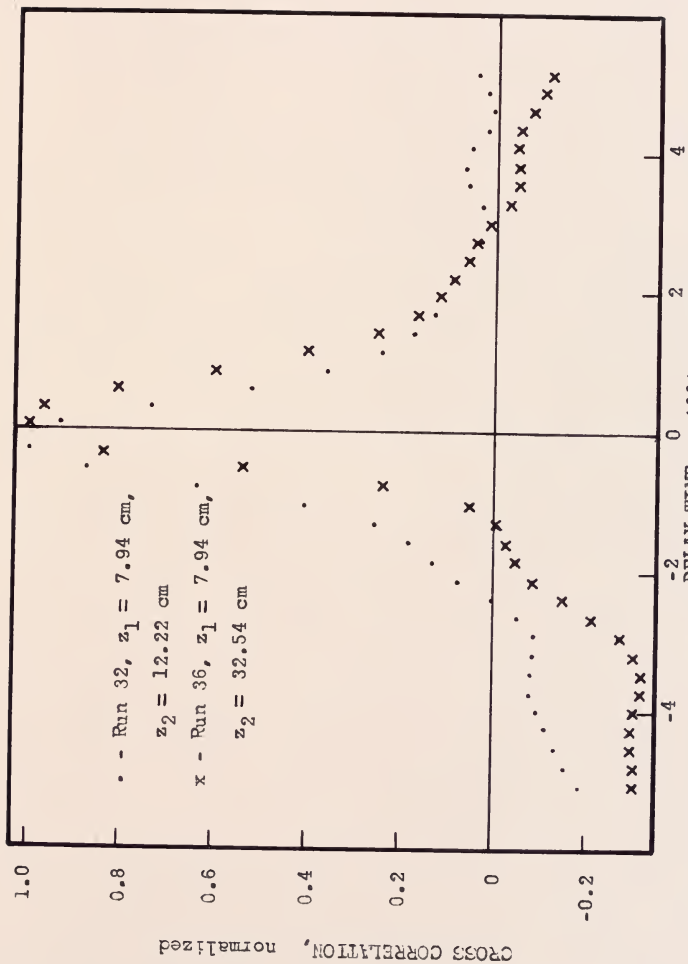


Figure 25. Cross correlation between two detectors, heavy water subcritical assembly

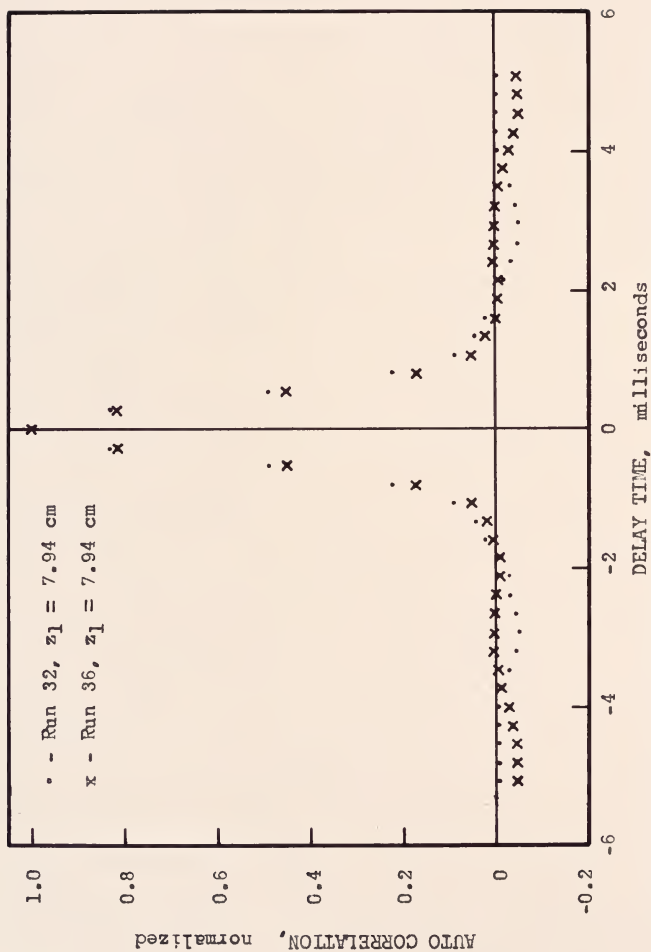


Figure 26. Auto correlation of Detector 1, heavy water subcritical assembly

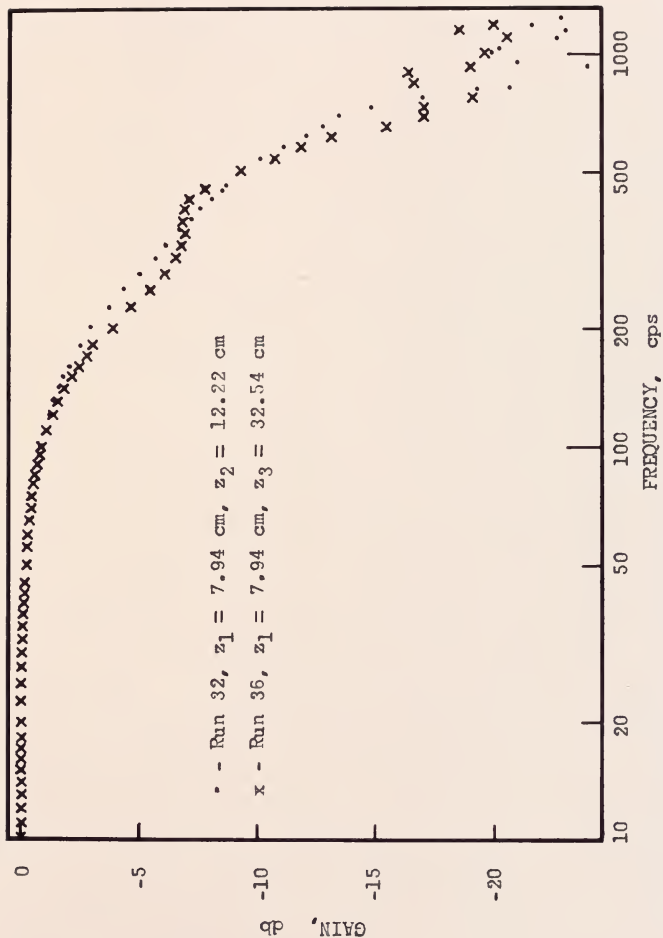


Figure 27. Amplitude of the cross power spectra, heavy water, subcritical assembly

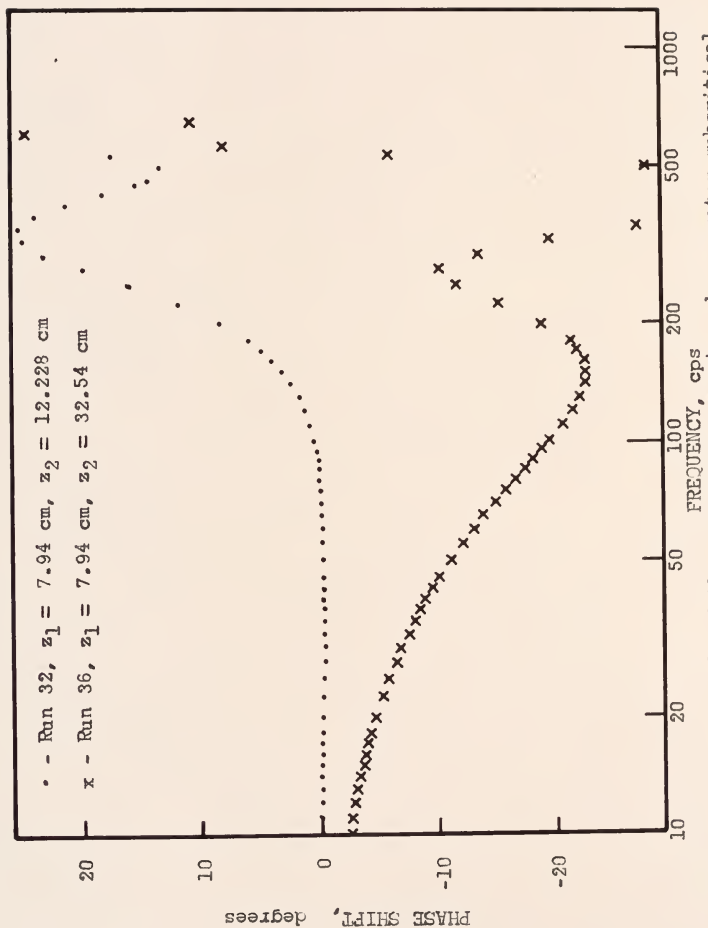


Figure 28. Phase shift of the cross power spectra, heavy water subcritical assembly

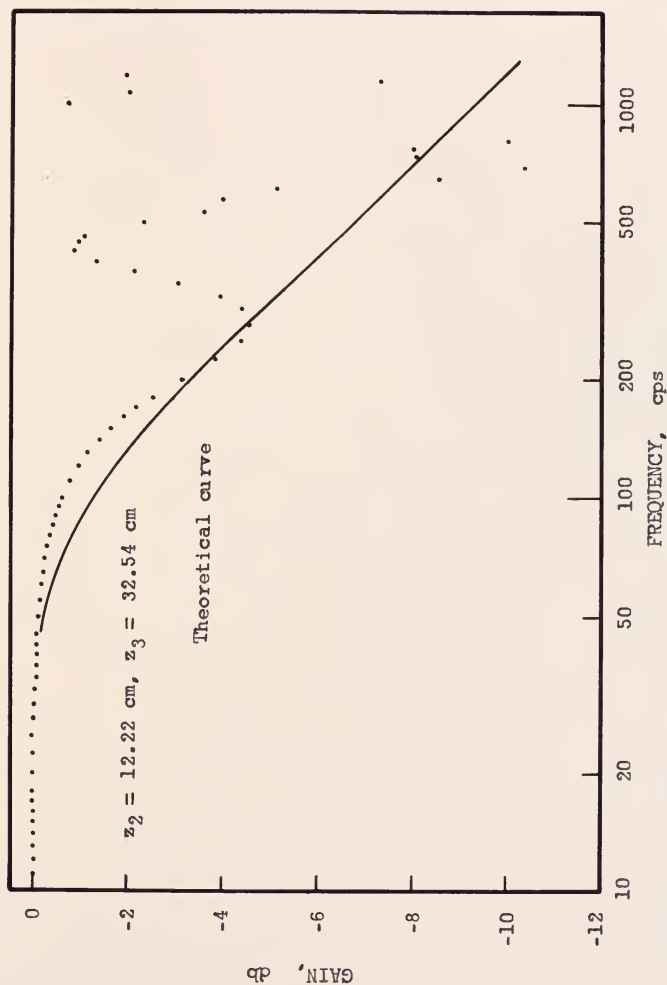


Figure 29. Amplitude of the transfer function between two detectors, heavy water subcritical assembly

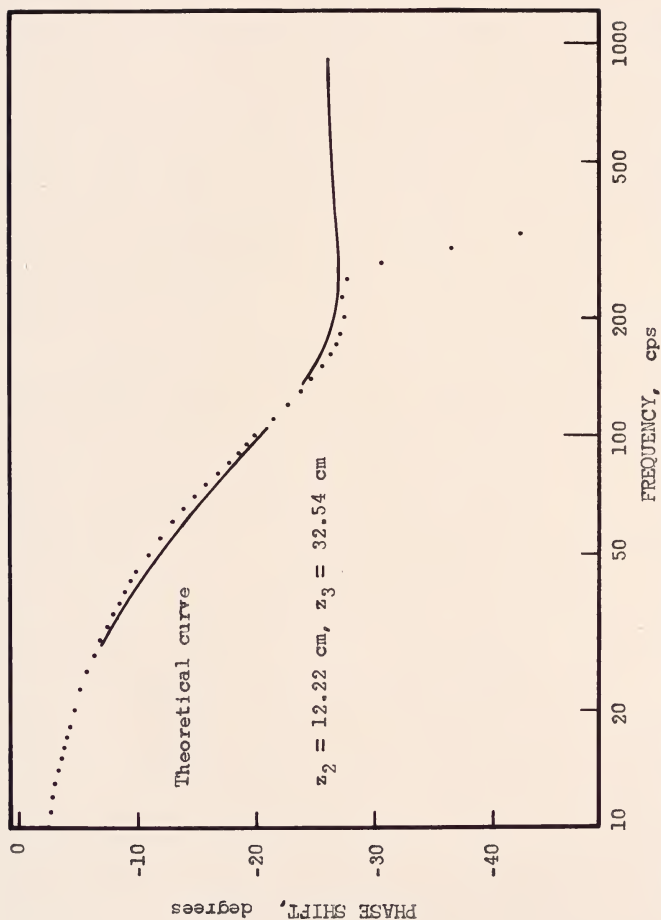


Figure 30. Phase shift of the transfer function between two detectors, heavy water subcritical assembly

The theory contains the assumption that the system is homogeneous. This assumption is not satisfied in the actual experiment at high frequencies. The sudden change in the phase shift and in the attenuation (Figures 29 and 30) could be caused by the lattice acting as a three dimensional diffraction grating (38). This effect is not seen in the light water subcritical assembly for two reasons. The lattice spacing is smaller (4 cm) and the higher frequencies necessary for the shorter wave lengths are not present in the source spectrum.

The values of the nuclear parameters used in SPAT to obtain the theoretical curves in Figures 29 and 30 are: $L^2 = 92.9 \text{ cm}^2$, $\tau = 130 \text{ cm}^2$, $\beta_s = 0.95$ milliseconds, $\beta_\tau = 0.1$ milliseconds, and $k_\infty = 1.15$. L^2 , τ , and k_∞ were obtained from Reference (39). β_s and β_τ were adjusted to obtain a good agreement with the experimental data.

CHAPTER VI

CONCLUSION

The experimental results clearly show a spatial effect that must be included in any theoretical model to correctly describe the transfer function of a nuclear system. Whether the model used to develop the equations in Chapter II is adequate is not definitely known at this time. It does appear that the use of a distributed source, based on the first flight collision density (see, for example, Reference (40)) would give a better representation of the light water system. Whether the additional labor would be worthwhile for other systems is questionable.

The theoretical results show that the lumped parameter model is, in general, not adequate for describing the transfer function of a nuclear system. However, at a specific distance from the source, the lumped parameter model does predict nearly the same results as the spatially dependent transfer function, at least over part of the frequency range. This fact may be used in selecting the location of neutron detectors.

For example, the theoretical spatially dependent transfer function equations (SDTF) developed in Chapter II can be used to determine the locations for which the lumped parameter transfer function is reasonably accurate over a

wide range of k_{eff} values. If the detector for a reactivity instrument designed to utilize Equation (98) is placed at one of the locations determined by SDTF, the measured impulse response function can be easily fitted using the simple lumped parameter impulse response function. Determining the reactivity would then be relatively easy. If the detector is placed elsewhere, a more complicated model which includes the spatial effect must be used.

The use of Equation (91a), which comes from Equation (90), to determine the experimental transfer function of a system has several advantages over other statistical methods (9, 10, 16). The major one is the ability to cancel the effects of the source and the effects of the measuring system from the final result by taking the ratio of the cross power spectra. Another advantage is the ability to eliminate the effects of uncorrelated noise. The main problem in using the cross correlation of two outputs to measure the characteristics of a system comes from its accuracy. Every unwanted effect, such as the reflection of the source from the floor, is detected and added to the correlation function. The correlation function cannot be adequately corrected by using just part of it or by shifting it vertically to make the function equal to zero at $\pm N$. The unwanted effects should be subtracted from the recorded signals before correlating them, which requires knowledge of the undesired signal. It would be better to conduct the experiment on a facility specially designed to minimize the undesired effects.

The FM tape recorder, which was acquired after the experiments on the light water system were finished, could be used in future work with that system. By recording data at 30 inches per second, and then reproducing the signal at $1 \frac{7}{8}$ inches per second for the data acquisition system, a time expansion of sixteen would occur, permitting the fast response of the light water system to be seen.

The use of a pulse detection system for neutrons seems to be much superior to an ion chamber and current amplifier, because the problems of 60 cycle per second interference are greatly reduced. Other noise may be removed from the signal by use of a discriminator in the linear amplifier. The signal supplied to the count rate circuit is essentially noise free. Unfortunately, further processing of the signal by other electronic equipment soon increases the noise content of the signal.

Some suggestions for further work, such as using a distributed source to find the source expansion coefficients (Equation (16)), have been discussed elsewhere when applicable. Another possibility for further work is to expand the theory to include two or more region systems, using the approach of Foderaro and Garabedian (41). Also, the transfer function (Equation (46)) could be transformed on the ω variable, rather than the axial buckling variable, to obtain the Fermi age, diffusion theory impulse response function. This function could be used directly with Equation (98). Further study of

the neutron reflection phenomenon and its effect on the correlation function could prove to be beneficial and should be investigated more completely.

APPENDICES

APPENDIX A

FOURIER TRANSFORM OF A PERIODIC DELTA FUNCTION

The Fourier transform of a periodic delta function may be obtained in a limiting process, starting with periodic pulses of width b and height a , and area ab equal to one. The first pulse is symmetrical about $t = 0$ while the rest are repeated every T_1 seconds. In integral form, the Fourier series expansion is (10, 12)

$$f(t) = \sum_{n=-\infty}^{\infty} F(n) \exp(j 2\pi n t / T_1) \quad (A1)$$

where T_1 is the period of the function $f(t)$, and $F(n)$, the expansion coefficients, are

$$F(n) = \frac{1}{T_1} \int_{-T_1/2}^{T_1/2} f(t) \exp(-j 2\pi n t / T_1) dt \quad (A2)$$

For the periodic pulses, $F(n)$ is found by

$$F(n) = \frac{1}{T_1} \int_{-b/2}^{b/2} a \exp(-j 2\pi n t / T_1) dt \quad (A3)$$

Since $f(t)$ is even, Equation (A3) may be reduced to the cosine transform of a , which is (37)

$$F(n) = \frac{ab}{T_1} \left\{ \frac{\sin \frac{n\pi b}{T_1}}{\frac{n\pi b}{T_1}} \right\} \quad (A4)$$

In the limit, as a goes to infinity, b goes to zero, and ab goes to 1, Equation (A4) becomes

$$F(n) = \frac{1}{T_1} \quad (A5)$$

Using this result in Equation (A1) gives for the periodic delta function

$$\begin{aligned} f(t) &= \sum_{m=-\infty}^{\infty} \delta(t - mT_1) \\ &= \frac{1}{T_1} \sum_{n=-\infty}^{\infty} \exp(j2\pi nt/T_1) \end{aligned} \quad (A6)$$

APPENDIX B
COMBINATION OF TRIGONOMETRY FUNCTIONS,
EQUATION (50)

The function in Equation (50), repeated below, may be simplified by using standard trigonometry functions as given in Reference (37).

$$f(\xi) = \sum_{m=-\infty}^{\infty} \cos \xi z \sin^2 \xi c \cos 4mc\xi \quad (B1)$$

Using

$$\sin^2 \xi c = \frac{1}{2} - \frac{1}{2} \cos 2 \xi c \quad (B2)$$

and

$$\cos \xi z \cos 4mc\xi = \frac{1}{2} \cos \xi (z + 4cm) + \frac{1}{2} \cos \xi (z - 4cm) \quad (B3)$$

in Equation (B1) and then using Equation (B3) again in the result, $f(\xi)$ becomes

$$\begin{aligned} f(\xi) = \sum_{m=-\infty}^{\infty} \frac{1}{8} [& 2 \cos \xi (z + 4cm) + 2 \cos \xi (z - 4cm) \\ & - \cos \xi (z + 4cm + 2c) - \cos \xi (z + 4cm - 2c) \\ & - \cos \xi (z - 4cm + 2c) - \cos \xi (z - 4cm - 2c)] \quad (B4) \end{aligned}$$

Consolidating the terms, Equation (B4) is

$$\begin{aligned}
 f(\xi) &= \frac{1}{2} \sum_{m=-\infty}^{\infty} (-1)^m \cos \xi (z + 2cm) \\
 &= \frac{1}{2} \sum_{m=-\infty}^{\infty} (-1)^m \exp [j \xi (z + 2cm)] \quad (B5)
 \end{aligned}$$

Either form may be used in Equation (50).

APPENDIX C ROOTS OF THE CHARACTERISTIC EQUATION

The characteristic equation for the Fermi age theory, diffusion theory model used in this thesis is a complex, transcendental equation. It is (see Equation (32))

$$DF = (1 + L^2 B_n^2 + L^2 \xi^2 + j\omega l_s) \exp(j\omega l\tau) + \tau B_n^2 + \tau \xi^2 - k_\infty \beta_c = 0 \quad (C1)$$

with the eigenvalue, or buckling, separated into the radial buckling and the axial buckling. Solving Equation (C1) for the axial buckling in terms of the frequency and system characteristics allows the numerical calculation of Equation (57), the inverted transfer function.

Investigation of this equation for the steady state case has been done by others (20). Taking the roots of Equation (C1) as

$$\zeta_1 = \pm jR_1 = \pm j(A_1 + jB_1) \quad (C2)$$

with $i=0$ corresponding to the smallest value of R_1 , it is found, for $\omega=0$, that (20)

$$\begin{aligned} A_{-1} &= A_1 \\ B_{-1} &= -B_1 \\ B_0 &= 0 \end{aligned} \quad (C3)$$

or the roots are symmetrical about the imaginary axis, with the locus of the roots crossing the imaginary axis. For $\omega \neq 0$, the locus of the roots is not symmetrical. As an example, Figure 31 shows a plot of the roots for a frequency of 0 and 2000 cps. The parameters used in Equation (C1) were the same as those used in calculating the transfer function presented in Figure 13.

Defining ζ_1^2 as

$$\begin{aligned}\zeta_1^2 &= -(a_i + jb_i) \\ &= -[A_i^2 - B_i^2] + j2A_iB_i\end{aligned}\quad (C4)$$

Equation (C2) may now be written in terms of ζ_1^2 .

$$\zeta_1 = \pm j \left[\left\{ \frac{(a_i^2 + b_i^2)^{\frac{1}{2}} + a_i}{2} \right\}^{\frac{1}{2}} + j \left\{ \frac{(a_i^2 + b_i^2)^{\frac{1}{2}} - a_i}{2} \right\}^{\frac{1}{2}} \right] \quad (C5)$$

Equation (C1) is used to solve for ζ_1^2 , and Equation (C5) is then used to find ζ_1 .

The real and imaginary parts of Equation (C1) may be separated. Substituting Equation (C4) in Equation (C1), the real part is

$$\begin{aligned}& \left[(1 + L^2B_n^2 - L^2a_i) \cos(\omega l_\tau - \tau b_i) - (\omega l_s \right. \\ & \quad \left. - L^2b_i) \sin(\omega l_\tau - \tau b_i) \right] \exp(\tau B_n^2 - \tau a_i) \\ & \quad - \frac{k_\infty [1 + \omega^2 \tau_i^2 (1 - \beta)]}{1 + \omega^2 \tau_i^2} = 0\end{aligned}\quad (C6)$$

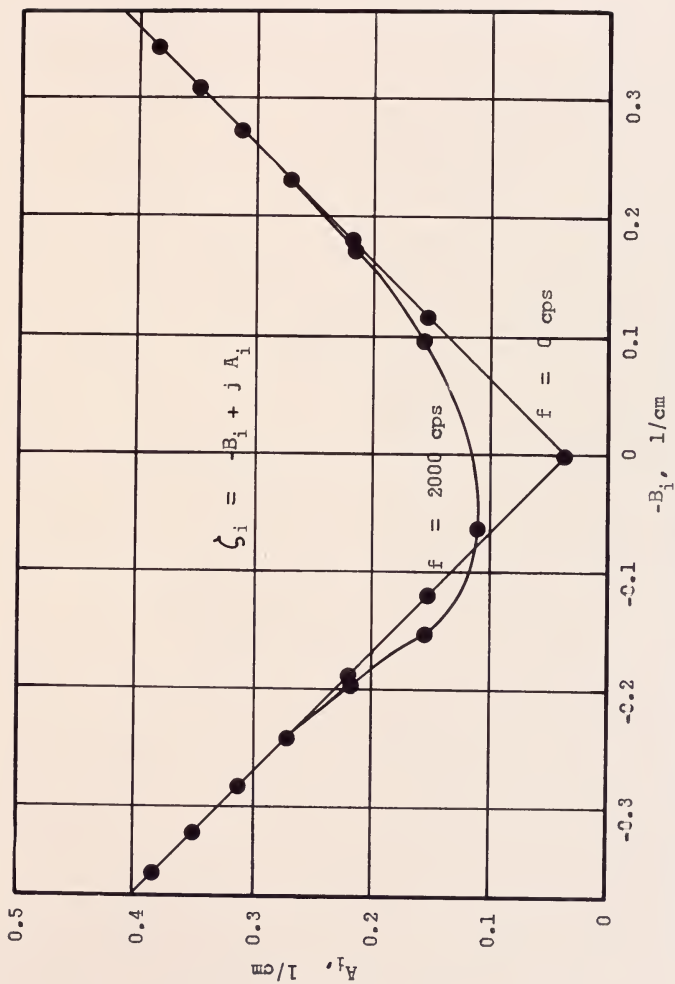


Figure 31. Typical roots of the characteristic equation

and the imaginary part is

$$\begin{aligned} & \left[(1 + L^2 B_n^2 - L^2 a_1) \sin(\omega l_T - \tau b_1) + (\omega l_s \right. \\ & \quad \left. - L^2 b_1) \cos(\omega l_T - \tau b_1) \right] \exp(\tau B_n^2 - \tau a_1) \\ & \quad + \frac{k_\infty \omega \tau_1 \beta}{1 + \omega^2 \tau_1^2} = 0 \quad (C7) \end{aligned}$$

where β_c (Equation (28)) has been simplified by considering only one group of delayed neutrons, represented by τ_1 .

Equations (C6 and C7) may be solved numerically for a_1 and b_1 , using standard iterative techniques.

Newton's method, as applied to complex equations, is used in the computer code described in Appendix D. Once an estimate of the value of a root is obtained,

$$\Delta \zeta^2 = - \frac{\frac{\partial DF}{\partial \zeta^2}}{DF} \quad (C8)$$

may be used to converge on the correct value of a root.

The major problems are insuring that R_0 is found, and that no roots are skipped. For most systems, only the first few roots will be needed in the calculation of the transfer function, Equation (57).

A good first guess for ζ_0^2 may be obtained one of two ways, depending on the values of the parameters. If ωl_T and τB_n^2 are greater than ωl_s and $L^2 B_n^2$, it may be assumed that

$$1 + L^2 B_n^2 + L^2 \zeta^2 + j \omega l_s \cong \exp(L^2 B_n^2 + L^2 \zeta^2 + j \omega l_s) \quad (C9)$$

Using the definitions (18)

$$\begin{aligned} M^2 &= L^2 + \tau \\ l_t &= l_s + l_\tau \end{aligned} \quad (C10)$$

Equation (C1) becomes

$$\exp(M^2 B_n^2 + M^2 \zeta^2 + j\omega l_t) - k_\infty \beta_c = 0 \quad (C11)$$

and the solution for ζ^2 is

$$\zeta^2 = \frac{1}{M^2} \left[\ln \left(\frac{1}{k_\infty \beta_c} \right) + M^2 B_n^2 + j\omega l_t \right] \quad (C12)$$

Substituting Equation (C12) in Equation (C1), it is seen that Equation (C12) is an exact solution if

$$\frac{l_s}{l_\tau} = \frac{L^2}{\tau}$$

and

$$k_\infty \beta_c = 1 \quad (C13)$$

When ωl_τ and τB_n^2 are smaller than ωl_s and $L^2 B_n^2$, it may be assumed that

$$\exp(\tau \zeta^2) = 1 + \tau \zeta^2 \quad (C14)$$

Equation (C1) becomes

$$\begin{aligned} L^2 \tau \zeta^4 + [\tau(1 + L^2 B_n^2) + L^2 + j\omega l_s \tau] \zeta^2 \\ + [1 + L^2 B_n^2 + j\omega l_s - k_\infty \beta_c \exp(-\tau B_n^2 - j\omega l_\tau)] = 0 \end{aligned} \quad (C15)$$

Equation (C15) is a second order equation in ζ^2 and may be solved using the quadratic formula.

Both Equations (C12 and C15) are available in the computer code for calculating the first guess for ζ_0^2 . As k_∞ approaches zero, the roots of the non-multiplying medium case (Equation (59)) may be used for the first guess of the value of ζ_0^2 . Since the other ζ_i^2 are nearly periodic in the b_i direction, the first guess for them may be based on ζ_0^2 .

APPENDIX D

COMPUTER CODES

The programs used to calculate the spatially dependent transfer function (Equations (57 and 63)) are presented in the first section of this appendix. The second section contains two programs used in the general data processing code to calculate the Fourier transform of the correlation function (Equation (112)), and to obtain the transfer function (Equation (91)).

Transfer Function

Equations (57 and 63) are evaluated by a Fortran II code named SPAT. The code may be used for a straight-forward calculation of the transfer function as a function of frequency or with the "General Least Squares Program" (24). If two distances are specified in the input, the ratio of the transfer functions (Equation (92)) is calculated.

The main program, MAIN, is used as an input and output program when the least squares program is not being used in that capacity. Subroutine CALC has an argument list that is compatible with the least squares program. All input is supplied to CALC by the P array, which is defined by the first nineteen instructions in CALC. The output from CALC

is controlled by $P(4)$, which is defined in the FINAL subroutine. Either the real and imaginary part of the transfer function, or the phase shift and the attenuation in db, is available. Subroutine GUEST calculates a normalizing factor used in each term of the series to avoid exceeding the numerical capacity of the computer. Subroutine CRT finds the roots of DF (Equation (54)), which are needed for the sum over i in Equation (57). The guess for the first root is made by GUESS, using the approximate equations developed in Appendix C. Subroutine TERM evaluates the real and imaginary parts of each term. Subroutine ERROR calculates the magnitude of the last term computed, relative to the sum of the absolute values of all the previous terms. Both the real and imaginary parts must be less than a specified value before the series is terminated. The first frequency should always be zero, as the results for the other frequencies are normalized to the results for $f = 0$.

The programs are listed on the following pages.

```

C      MAIN PROGRAM FOR CALLING CALC, KYLSTRA
      DIMENSION F(100), P(40), DD(40)
C      HAVE P(4) = 1. FOR THIS PROGRAM
      CALL BCDCON ( 50H NF, F(100), P(40), NC
1          ,NF, F, P, NC )
C
      CL = 8.68588964
      CT = 57.29578
      P(20) = 0.
      P(21) = 0.
1  CALL SYMBOL ( IN, 10)
C      SYMBOL IS A NON-FIXED FORMAT INPUT SUBROUTINE
C      SYMBOL AND BCDCON MAY BE REPLACED BY REGULAR INPUT
      E = P(3)
      CK = P(4)
      NP = P(8)
      FN = P(16)
      CFAC = P(17)
      EF = P(18)
      DFAC = P(19)
5  WRITEOUTPUTTAPE 6, 1001
1001 FORMAT (1H1/ 37X 28HRESULTS FOR MULTIPING MEDIUM
1      1 18H TRANSFER FUNCTION )
      WRITEOUTPUTTAPE 6, 1003, P(1), P(2), P(7), P(9), P(10)
1003 FORMAT ( 1H0 14X 26HVALUES OF PARAMETERS ARE,
1      1 9H RADIUS =
1          F8.1, 18H CM. AND LENGTH = F6.1,
2      15H CM. FOR TANK, / 15X 9H RADIUS = F6.1,
3      19H CM. AND LENGTHS = 2F6.1,
4      28H CM. FOR DETECTORS 2 AND 3. / )
      WRITEOUTPUTTAPE 6, 1005, P(15), P(11), P(12), P(14)
1      1, P(13), P(5), P(6)
1005 FORMAT ( 1H 14X 20H MULTIPLYING FACTOR = F7.4,
1      1 21H, DIFFUSION LENGTH = F6.1, 18H CM., FERMI AGE =
2      2 F6.1, 6H CM2. / 15X 29H THERMAL AND FAST LIFETIMES =
3      32F9.6, 27H SECS., AND BETA AND TAU = F9.6, F8.2,
4      4//7X 4HFREQ 12X 4HREAL 12X 4HIMAG 13X 3HAMP 14X 2HDB
5      5 12X 5H THETA 11X 5H THETA 6X 5H TERMS )
      DO 40 I = 1, NF
      W = F(I)
      CALL CALC ( W, X1, X2, A, P, DD, XK )
      A1 = SQRTF ( A*A + XK*XK )
      A2 = CL * LOGF (A1)
      THE = CT * ATANF ( XK / A )
      TH2 = 180. - THE
      WRITEOUTPUTTAPE 6, 1004, W, A, XK, A1, A2, THE, TH2, DD(1)
1004 FORMAT ( 1H 7E16.7 , F7.0 )
40  CONTINUE
      GO TO 1
      END

```

```

C      SPATIALLY DEPENDENT TRANSFER FUNCTION, KYLSTRA
C      FOR A MULTIPLYING MEDIUM, POINT SOURCE
C      FOR A NON - MULTIPLYING MEDIUM, POINT SOURCE
C      P VECTOR DEFINED BY FIRST 19 INSTRUCTIONS
C      XK CONTAINS UNWANT PART OF H, REAL OR IMAG
C      OR DB AND THETA
C

```

```

      SUBROUTINE CALC ( F, X1, X2, H, P, DD, XK )
      DIMENSION P(40), BE(20), BZ(20), DD(40)

```

```

      R  = P(1)
      C  = P(2)
      E  = P(3)
      NCK = P(4)
      B  = P(5)
      T1 = P(6)
      RO = P(7)
      NP = P(8)
      Z2 = P(9)
      Z3 = P(10)
      DL = P(11)
      T  = P(12)
      SL = P(13)
      TL = P(14)
      RKF = P(15)
      FNN = P(16)
      CFAC = P(17)
      EE  = P(18)
      DFAC = P(19)

```

```

C      CFAC FOR DELTA B, DFAC FOR DELTA R AND S
      IF(P(20)) 550, 550, 555

```

```

550  CONTINUE

```

```

C      20 BESSEL FUNCTION VALUES

```

```

      BE(1) = .269465
      BE(2) = .115804
      BE(3) = .073712
      BE(4) = .054056
      BE(5) = .042642
      BE(6) = .035231
      BE(7) = .030033
      BE(8) = .026169
      BE(9) = .023165
      BE(10) = .020794
      BE(11) = .018851290
      BE(12) = .017241414
      BE(13) = .015901210
      BE(14) = .014737960
      BE(15) = .013735840
      BE(16) = .012859560
      BE(17) = .012100000
      BE(18) = .011406240
      BE(19) = .010816000

```

```

BE(20) = .010261690
BZ(1) = 2.4048
BZ(2) = 5.5201
BZ(3) = 8.6537
BZ(4) = 11.7915
BZ(5) = 14.9309
BZ(6) = 18.0711
BZ(7) = 21.2116
BZ(8) = 24.3525
BZ(9) = 27.4935
BZ(10) = 30.6346
BZ(11) = 33.7758
BZ(12) = 36.9171
BZ(13) = 40.0584
BZ(14) = 43.1998
BZ(15) = 46.3412
BZ(16) = 49.4826
BZ(17) = 52.6241
BZ(18) = 55.7655
BZ(19) = 58.9070
BZ(20) = 62.0485
AN = BN
RC2 = SC2
RC4 = SC4
PI2 = 6.28318531
P(20) = 1.
NX = P(21)
NY = P(21)
NP1 = 0
555 CONTINUE
DL2 = DL ** 2
W = PI2 * F
WS = W * SL
WT = W * TL
S3 = 0.
R3 = 0.
S2 = 0.
R2 = 0.
S6 = 0.
R6 = 0.
AR3 = 0.
AS3 = 0.
AR2 = 0.
AS2 = 0.
CL = 2.*C
DB = 1. - B
T1W = W * T1
T1W2 = T1W ** 2
RKD = RKF / ( 1. + T1W2)
RK = RKD * ( 1. + T1W2 * DB)
SK = RKD * T1W * B

```

```

      COU = -1.
      IF ( F ) 600, 600, 625
600  IF( NY ) 605, 605, 300
605  NY = 1
      IF(RKF-.05) 510, 510, 500
500  CONTINUE
      B2S = ( 2.4 / R ) **2
      CALL GUEST ( B2S, DL2, T,RKF, RC2, SC2 )
      CRR = Z3 * SQRTF( RC2)
C    CONSTANT FACTOR IN EACH TERM
      GO TO 300
510  CRR = Z3 / DL
      GO TO 300
625  NY = 0
300  CONTINUE
      DO 70 N = 1, 20
      B2N = ( BZ(N)/ R ) ** 2
      DLBN = DL2 * B2N
      TB1 = T*B2N
      AA = 1.
301  CONTINUE
      IF( RO ) 3, 3, 2
      2 AA = BJO( BZ(N)* RO )
C    BJO CALCULATES THE JO BESSEL FUNCTION
      3 CONTINUE
      CO1 = 1. + DLBN
      CO2 = AA / BE(N)
      NR = 0
      4 CONTINUE
      EF = EE
      CALL CRT (CO1,DL2,TB1,T,WS,WT,RK,SK,NP1,NR,AD2,BD2,
      IAN,BN,EF,CFAC,DFAC)
      IF(EF - 9.5) 302, 302, 2001
2001 H = 0.
      XK = 0.
      GO TO 101
302  CONTINUE
      RC1 = T * AD2 - TB1
      SC1 = T * BD2
      CALL CEX (RC1, SC1, RC2, SC2)
      IF(RK) 303,413,303
413  RC3 = 1.
      SC3 = 0.
      GO TO 415
303  CONTINUE
      RC3 = DL2 + T * ( CO1 - DL2* AD2)
      SC3 = T * ( WT - DL2 * BD2 )
415  CONTINUE
      CALL CMUL (AN, BN, RC3, SC3, RC4, SC4 )
      CALL CDIV ( RC2, SC2, RC4, SC4, RC5, SC5)
      RN = RC5 * CQ2

```

```

      SN = SC5 * C02
C      THESE ARE CONSTANTS FOR M INDEX
      M = 0
      FM = 0.
      NCT = 0
      NCT1 = 0
      GT = 0.
505 CONTINUE
      CALL TERM (Z3,GT,M,AN,BN,RN,SN,DR,DI,CRR)
      S3 = S3 + DI
      R3 = R3 + DR
      CALL ERROR( DR , DI , AR3, AS3, RAR3, RAI3 , NR)
      IF(Z2) 405,405,5
      5 CONTINUE
      CALL TERM (Z2,GT,M,AN,BN,RN,SN,DR,DI,CRR)
      R2 = R2 + DR
      S2 = S2 + DI
      CALL ERROR( DR , DI , AR2, AS2, RAR2, RAI2 , NR)
405 CONTINUE
      COU = COU + 1.
      6 IF( COU) 30, 30, 9
      9 CONTINUE
      IF( NCT - 100) 55, 55, 50
      50 NCT = 2
      NCT1 = NCT1 + 1
      WRITEOUTPUTTAPE 6, 1001,NCT1,NR,N,R3,S3,R2,S2,F,
      1 RAR3,RAI3,RAR2,RAI2
1001 FORMAT( 41H0 VALUES OF NCT1, NR, N, R3, S3, R2, S2,
      1 31HF, RAR3, RAI3, RAR2, RAI2, ARE /315, 4E20-8,
      2 / 5E20-8 )
      IF (NCT1 - 5) 55, 55, 75
      55 IF ( RAR3 - E) 56,56, 30
      56 IF ( RAI3 - E) 57,57, 30
      57 IF( Z2) 65, 65, 60
      60 IF ( RAR2 - E) 61, 61, 30
      61 IF ( RAI2 - E) 65, 65, 30
      30 FM = FM + 1.
      M = M + 1
      NCT = NCT + 1
      GT = CL * FM
C      SKIP NEXT M IF
      IF ( ( GT- 2.*Z3)*AN - 10. ) 505, 65, 65
      65 IF(RK) 201, 201, 250
      201 IF (FM) 75, 75, 70
      250 IF( FM ) 260, 260, 4
      260 IF ( NP ) 262, 262, 261
C      NP = 1, CRT PRINTS OUT ROOTS
      261 CALL CRT (C01,DL2,TB1,T,WS,WT,RK,SK,NP,NR,AD2,BD2,
      1AN,BN,EF,CFAC,DFAC)
      262 CONTINUE
      IF(NR - 1 ) 75, 75, 70

```

```

70 CONTINUE
C   END OF N DO LOOP
75 CONTINUE
   IF( Z2 ) 80, 80, 85
80 CONTINUE
   RR5 = COSF( WS)
   SR5 = -SINF( WS)
   CALL CMUL ( RR5, SR5, R3, S3, R6, S6 )
   GO TO 89
85 CONTINUE
   CALL CDIV ( R3, S3, R2, S2, R6, S6 )
89 CONTINUE
C   PICK FIRST F = 0 FOR NORMALIZING
C   AND COMPONENT DESIRED FOR LEAST SQUARES
   CALL FINAL ( F, R6, S6, NCK, H, XK)
101 CONTINUE
   DD(1) = COU + 1.
   RETURN
   END

C   SETS UP CRR FOR NORMALIZING EACH TERM, KYLSTRA
   SUBROUTINE GUEST( B2S, DL2, T, RK, RC2, SC2 )
   TB1 = T*B2S
   DT = 1. + DL2*B2S
   A = DL2 * T
   B = ( T*DT + DL2 ) / ( A * 2.)
   C = ( DT - RK*EXPF ( -TB1 ))/A
   Q = B*B - C
   IF( Q ) 10, 20, 20
10  RC2 = B
   GO TO 50
20  RC2 = B - SQRTF ( Q )
50  SC2 = 0.
   RETURN
   END

C   CALCULATES EACH TERM, KYLSTRA
   SUBROUTINE TERM (Z,GT,M,AN,BN,RN,SN,DR,DI,CRR)
   GP = Z + GT
   ZFP = GP*AN - CRR
   CALL CEX ( - ZFP , - GP*BN, R1, S1)
   IF ( M ) 20, 20, 5
5  GP = GT - Z
   ZFP = GP*AN - CRR
   CALL CEX ( - ZFP , - GP*BN, R2, S2)
   SIG = (-1.)** M
   R1 = SIG * ( R1 + R2 )

```

```

      S1 = SIG * ( S1 + S2 )
20 CONTINUE
      CALL CMUL ( RN, SN, R1, S1, DR, DI)
      RETURN
      END

C      CALCULATES ABS. ERROR, KYLSTRA
      SUBROUTINE ERROR ( DR, DI, R, S, RAR, RAI, NR)
      DAR = ABSF(DR)
      DAS = ABSF(DI)
      R = R + DAR
      S = S + DAS
      IF( XMODF (NR,2)) 50, 20, 50
20 RAR = 1.
C      FORCES TERMINATION ON ODD ROOT
      GO TO 100
50 RAR = DAR / R
100 RAI = DAS / S
      RETURN
      END

C      SUBROUTINE CRT FOR COMPLEX ROOTS OF D.F., KYLSTRA
      SUBROUTINE CRT ( DB1, DL, TB1, T, WS, WT, RK, SK, NP
1, NR, A, B, AA, BB, E, F, F2)
C      DB1 = 1+L2*B2, DL = L2, TB1 = T*B2, T = T, WS = W* SL,
C      RK = K*(1+W2*T12*(1-B))/1+W2*T12, SK=K*W*T1*B/1+W2*T12
C      NP = 1, PRINT ROOTS, =0, DONOT, NR = ROOTS FOUND
C      A + J B = ROOTS, AA + J BB = SQRT (A + J B )
C      F = FACTOR ON TWO PI, F2 = FACTOR ON DR AND DI
C      WT = W*TL, E = ERROR ALLOWED
      DIMENSION AR(100),BR(100),AAR(100),BBR(100),CDUT(100)
      KC = 0
      F3 = F
      F1 = F2
      IF( NP) 20, 20, 2
C      NP = 1, PRINT OUT ROOTS
2 CONTINUE
      RC3 = SC3
      RC4 = SC4
      YP = ZP
      DR = DS
      WRITEOUTPUTTAPE 6, 1001,DB1,DL,TB1,T,WS,WT,RK,SK
1001 FORMAT ( 1H0 20X34HVALUES OF ROOTS FOR THE FOLLOWING
1 10H CONSTANTS
1 // 9X 3HLB1 12X 2HDL 11X 3HTB1 13X 1HT 12X 2HWS 12X
2 2HWT 12X 2HRK
2 12X 2HSK / 4X 8E14.6, // 11X 4HROOT 13X 1HA
3 15X 1HB 14X

```

```

32HAA 14X 2HBB      12X 5HCOUNT / )
DO 5 I = 1, NR
WRITEOUTPUTTAPE 6, 1002, I, AR(I), BR(I), AAR(I),
1 BBR(I), COUT(I)
1002 FORMAT ( 1H 9X I5, 5X 5E16.7 )
5 CONTINUE
GO TO 600
20 CONTINUE
IF(NR) 25, 25, 100
C IF 1 ROOT ALREADY FOUND, PROCEED FROM IT
25 CONTINUE
SKT = 6.28 * F3 / T
IF(RK - .05) 30, 30, 50
C IF -, USE DIFFUSION APPROX, OTHERWISE, GUESS ROUTINE
30 R1 = DB1 / DL
S1 = WT / DL
C EQUATION 58
IF (RK) 500, 500, 200
C RK = 0, GO TO SQRT PART, OTHERWISE, TO CONVERGENT PART
50 CONTINUE
DB2 = DB1
DL2 = DL
TB2 = TB1
T2 = T
WS2 = WS
WT2 = WT
RK2 = RK
CALL GUESS( DB2, DL2, TB2, T2, WS2, WT2, RK2, R1, S1)
GO TO 200
100 CONTINUE
C ESTIMATE NEXT ROOT FROM LAST
S2 = BR(NR)
S0 = BR(1)
S1 = - S2 + S0
IF(NR-2) 90, 90, 95
90 R1 = AR(1)
GO TO 96
95 R1 = AR(NR-1)
96 CONTINUE
IF( XMODF ( NR, 2 )) 105, 200, 105
105 CONTINUE
S1 = S1 + SIGNF(SKT, S0)
C END OF GUESSING SECTION, START CONVERGENT SECTION
200 CONTINUE
COU = 0.
201 IDY = 1
R = R1
S = S1
IF( F1 ) 210, 207, 210
207 F1 = 1.
210 CONTINUE

```

```

RC1 = DB1 - DL * R
SC1 = WT - DL * S
RC2 = TB1 - T * R
SC2 = WS - T * S
CALL CEX ( RC2, SC2, RC3, SC3 )
CALL CMUL( RC1, SC1, RC3, SC3, RC4, SC4 )
Y1= RC4 - RK
Z1= SC4 + SK
COU = COU + 1.
NCT = NCT + 1
RC5 = DL + T* RC1
SC5 = T * SC1
CALL CMUL ( RC3, SC3, RC5, SC5, YP, ZP )
C  YP AND ZP ARE DERIVATIVES OF Y AND Z
CALL CDIV (Y1,Z1, YP, ZP, DR, DS )
R1 = R + DR *F1
S1 = S + DS *F1
250 CONTINUE
RE = ABSF( DR/ R )
SE = ABSF( DS/ S )
IF( RE - E ) 255, 255, 260
255 IF( SE - E ) 270, 270, 260
260 R = R1
S = S1
IF(COU - 99.) 210, 210, 268
C RETURN FOR NEXT ITERATION
268 KC = 1
GO TO 2
270 CONTINUE
500 A = R1
B = S1
NR = NR + 1
AR(NR) = R1
BR(NR) = S1
CALL CSRT ( R1, S1, RC1, SC1)
AA = RC1
BB = SC1
AAR(NR) = RC1
BBR(NR) = SC1
COUT(NR) = COU
IF( NR -100) 610,510, 510
510 KC = 1
GO TO 2
600 IF ( KC) 610, 610, 605
605 CONTINUE
WRITEOUTPUT TAPE 6, 1005, KC, NR, COU
1005 FORMAT ( 1H0 15X 6H KC = 15, 7H. NR = 15,
1 8H. COU = F7.1, / 15X 11HSKIP ONE )
E = 10.
610 RETURN
END

```

```

C      SUBROUTINE GUESS, KYLSTRA
C      USED BY CRT FOR FIRST ROOT OF DL
      SUBROUTINE GUESS( DB1, DL, TB1, T, WS, WT, RK, R1, S1 )
      IF( WS - WT ) 1, 2, 2
C      WS GREATER THAN WT, USE EXP SCHEME
1      NW = 1
      WFAC = WT
      GO TO 5
2      NW = -1
      WFAC = WS
5      CONTINUE
      DT = DB1 - 1.
      IF( TB1 - DT ) 7, 8, 8
C      TB1 GREATER THAN DT, USE EXP SCHEME
7      NC = 1
      TFAC = DT
      GO TO 10
8      NC = -1
      TFAC = TB1
10     CONTINUE
      IF ( WFAC - TFAC ) 12, 13, 13
C      GO TO LARGEST
12     NU = NC
      GO TO 15
13     NU = NW
15     CONTINUE
      IF ( NU ) 20, 20, 50
C      NU +, USE POLY, NU -, USE EXP
20     TIG = DL + T
      R1 = ( -LOGF(RK) + DT + TB1 ) / TIG
      S1 = (WS + WT)/TIG
      GO TO 100
50     CONTINUE
      TLF = 2. *T *DL
      P1 = T*DB1 + DL
      Q1 = WT* T
      P2 = Q2
      CALL CEX ( -TB1, -WS, P2, Q2)
      P3 = DB1 - RK*P2
      Q3 = WT - RK*Q2
      P4 = Q4
      CALL CMUL ( P1, Q1, P1, Q1, P4, Q4)
      P5 = P4 - 2. * TLF * P3
      Q5 = Q4 - 2. * TLF * Q3
      CALL CSRT ( P5, Q5, P3, Q3)
      R1 = (P1 - P3) / TLF
      S1 = (Q1 - Q3) / TLF
100    CONTINUE
      RETURN
      END

```

```

C      FINAL NORMALIZES AND SETS UP L.S. COMPONENT.  KYLSTRA
      SUBROUTINE FINAL(F, R5, S5, NC, T, X)
      DBLF(X,Y) = 4.3429448 * LOGF ( X*X + Y*Y)
      R6 = R5
      S6 = S5
      NCK = NC
      IF ( F ) 520, 520, 525
520 IF ( NX ) 528, 528, 530
528 RNF = R6
      AMPN = DBLF ( R6, 0.)
      NX = 1
      GO TO 530
525 NX = 0
530 CONTINUE
C      RETURN COMPONENT DESIRED FOR LEAST SQUARES FIT
      GO TO ( 535, 535, 550, 550 ), NCK
C      CK = 1, REAL, = 2, IMAG, = 3, DB, = 4, THETA
535 R6 = R6 / RNF
      S6 = S6 / RNF
      GO TO ( 540, 545 ), NCK
540 H = R6
      XK = S6
      GO TO 101
545 H = S6
      XK = R6
      GO TO 101
550 AMP = DBLF(R6,S6) - AMPN
      TH = 57.29578 * ATANF ( S6/R6)
      GO TO ( 540, 545, 555, 560), NCK .
555 H = AMP
      XK = TH
      GO TO 101
560 XK = AMP
      H = TH
101 CONTINUE
      T = H
      X = XK
      RETURN
      END

```

```

C      SUBROUTINE CMUL, KYLSTRA
C      SOLVES  $R3 + J S3 = (R1 + J S1) * (R2 + J S2)$ 
      SUBROUTINE CMUL ( R1, S1, R2, S2, R3, S3)
      R3 = R1 * R2 - S1 * S2
      S3 = R1 * S2 + R2 * S1
      RETURN
      END

```

```

C      SUBROUTINE CDIV, KYLSTRA
C      SOLVES  $R3 + J S3 = (R1 + J S1) / (R2 + J S2)$ 
      SUBROUTINE CDIV ( R1, S1, R2, S2, R3, S3 )
      DEM = R2*R2 + S2 * S2
      R3 = (R1 * R2 + S1 * S2 ) / DEM
      S3 = (R2 * S1 - R1 * S2 ) / DEM
      RETURN
      END

```

```

C      SUBROUTINE CSRT , KYLSTRA
C      SOLVES  $R2 + J S2 = \text{SQRTF} ( R1 + J S1 )$ 
      SUBROUTINE CSRT( R1, S1, R2, S2)
      R3 = R1
      S3 = S1
      C01 = SQRTF( R3*R3 + S3*S3 )
      R2 = SQRTF ( ( C01 + R3 ) *.5 )
      S4 = SQRTF( ( C01 - R3 ) *.5 )
100  S2 = SIGNF ( S4, S3)
      RETURN
      END

```

```

C      SUBROUTINE CEX, KYLSTRA
C      SOLVES  $R2 + J S2 = \text{EXP} ( R1 + J S1 )$ 
      SUBROUTINE CEX ( R1, S1, R2, S2 )
      SA = EXPF( R1)
      R2 = SA * COSF( S1)
      S2 = SA * SINF( S1)
      RETURN
      END

```

Fourier Transform

A Fortran II subroutine named TRNS evaluates Equation (112). It is called by the general data processing program (31) to calculate the Fourier transform of the correlation functions. The majority of the input and output from TRNS is through the common storage; however, the frequencies at which the transform is calculated may be read in. The following pages contain a listing of TRNS and NXTPR, an output subroutine used to combine the results of successive runs for $H_{23}(\omega)$ (Equation (91)).

```

C      TRNS, LINEAR INTEGRATION OF FOURIER TRANSFORM, KYLSTRA
      SUBROUTINE TRNS
C      COMMON FOR VARIABLES SAME IN DIFFERENT MZ CASES
      COMMON X,H,G,NCT,ID,ID2,FNT,NRD,NDS,M,MZ,MM,MZ2,MPL
      COMMON NFILE,WMAX,NDEX,NFREQ,GT
      COMMON VCTYI,VCTYK,VCTAC
      COMMON JVA,JVB
      DIMENSION X(600),H(601),G(600)
      DIMENSION VCTYI(40),VCTYK(40),VCTAC(40)
      DIMENSION GT(18)
      DIMENSION JVA(40),JVB(40)
C      COMMON FOR VARIABLES THAT DIFFER FROM MZ TO MZ
      COMMON Y,AC
      COMMON TRR,TRI
      DIMENSION Y(750,4), AC(300,4,4), TRR(300,4,4)
      DIMENSION WWW(300), TRI(300,4,4)
      EQUIVALENCE ( X, WWW)
C
      TA = NRD * MZ
      TA2 = TA / 15000.
      FT = MM
      TAM = TA2 * FT
      READINPUTTAPE 5, 5001, NPRT, NCAL, NTRY, NWIN
5001  FORMAT ( 5I5 )
      WWW(1) = 0.
      NCT1 = 1
      IF ( NPRT ) 1980,1990, 1980
1980  CONTINUE
      NCT1= NPRT + 1
      READ INPUTTAPE 5,1981,(WWW(K), K = 2, NCT1)
1981  FORMAT ( 5E12.1 )
1990  CONTINUE
      IF( NCAL ) 1997, 1997, 1991
1997  IF( NPRT ) 1999, 1998, 1999
1998  NCAL = M
1991  FI = 1.
      NBB = NCT1 + 1
      NCT1 = NCT1 + NCAL
      DW = .5 / ( TA2 * (FLOATF( NCAL - 1 )))
      DO 1995 KK = NBB, NCT1
      WWW(KK) = DW * FI
1995  FI = FI + 1.
1999  NMT = NCT1
      WRITEOUTPUTTAPE 6, 1940, (WWW(II), II = 1,NCT1)
1940  FORMAT ( 1H0 15X 34HTHE SPECTRAL DENSITY COEFFICIENTS
145HTO FOLLOW ARE EVALUATED AT THESE FREQUENCIES
1 // ( 4X 5E20.8 ))
      DO 3000 L = 1, NDEX
      J = JVA(L)
      K = JVB(L)
      IT = K - J

```

```

FIT = IT
T = FIT / 15000.
C   FIRST DELAY POINT IS T FOR CROSSCORRELATION
C   FIRST DELAY POINT IS ZERO FOR AUTOCORRELATION
TLR = AC(M,J,K) - AC(MM,J,K)
TLI = AC(M,J,K)
C   LAST POSITIVE TAU TERMS
TCR = AC(1,J,K) - AC(2,J,K)
IF(IT) 2001, 2005, 2001
2001 TCR = TCR + AC(1,K,J) - AC(2,K,J)
C   CENTER TERMS
2003 TFI = AC(M,K,J)
TFR = AC(M,K,J) - AC(MM,K,J)
C   LAST NEGATIVE TAU TERMS
2005 CONTINUE
C   START ZERO FREQUENCY INTEGRATION
RHO = AC(M,J,K) * .5
DO 2010 KK = 1, MM
2010 RHO = RHO + AC(KK,J,K)
IF(IT) 2011, 2014, 2011
2014 RHO = RHO - .5 * AC(1,J,K)
GO TO 2013
2011 RHO = RHO + AC(M,K,J) * .5
DO 2012 KK = 2, MM
2012 RHO = RHO + AC(KK, K, J)
2013 CONTINUE
STR1 = RHO * TA2
H(L) = STR1
TRR(1,J,K) = 1.
TRI(1,J,K) = 0.
C   HAVE FREQ EQUAL ZERO RESULT
C   CALCULATE AND STORE CHANGE OF SLOPE IN AC MATRIX
C   AC(1) = AC(3) - 2AC(2) + AC(1)
PH1 = AC(1,J,K)
PH2 = AC(2,J,K)
DP1 = PH2 - PH1
DO 2020 KK = 3, M
KF = KK - 2
PH3 = AC(KK, J, K)
DP2 = PH3 - PH2
AC(KF, J, K) = DP1 - DP2
DP1 = DP2
PH2 = PH3
2020 CONTINUE
IF( IT) 2025, 2050, 2025
2025 PH1 = AC(1,K,J)
PH2 = AC(2,K,J)
DP1 = PH2 - PH1
DO 2040 KK = 3, M
KF = KK - 2
PH3 = AC(KK, K, J )

```

```

DP2 = PH3 - PH2
AC(KF,K,J) = DP1 - DP2
DP1 = DP2
PH2 = PH3
2040 CONTINUE
2050 CONTINUE
C THIS LOOP CONTROLS FREQ
DO 2500 KK = 2, NMT
W = WWW(KK) * 6.281852
IF(W) 2056, 2055, 2056
2055 TRR(KK,J,K) = 0.
TRI(KK,J,K) = 0.
GO TO 2500
2056 WT1 = W*T
C1S = COSF( WT1)
S1S = SINF( WT1)
WDT = W * TA2
DC1 = COSF( WDT)
DS1 = SINF( WDT)
COL = 1. /(W*W * TA2)
WTM = W*TAM
CMS = COSF(WTM)
SMS = SINF(WTM)
WTL = WTM
CNS = COSF ( WTL )
SNS = SINF ( WTL )
CS = 1.
SS = 0.
R1 = 0.
S1 = 0.
SH = 0.
RH = COL *{ CMS*TLR + TCR} + SMS * TLI/W
IF( IT) 2060, 2070, 2060
2060 RH = RH + CNS * TFR * COL + SNS * TFI / W
SH = {CMS*TLI - CNS*TFI}/W + COL*{-SMS*TLR+SNS*TFR}
2070 CONTINUE
M3 = M - 2
C THIS LOOP SWEEPS THROUGH CHANGE IN SLOPE CURVE
DO 2400 KF = 1, M3
CSS = CS
CS = CS * DC1 - SS * DS1
SS = SS * DC1 + CSS* DS1
R1 = R1 + CS * AC(KF,J,K)
IF( IT) 2110, 2120, 2110
2110 CONTINUE
R1 = R1 + CS *AC(KF,K,J)
S1 = S1 - SS*(AC(KF,J,K) - AC(KF,K,J) )
2120 CONTINUE
2400 CONTINUE
RPS = ( RH + R1 * COL) / STR1
SIP = ( SH + S1 * COL) / STR1

```

```

      TRR(KK,J,K) = C1S * RPS + SIP * S1S
      TRI(KK,J,K) = C1S * SIP - RPS * S1S
2500 CONTINUE
3000 CONTINUE
3050 CONTINUE
      M = NCT1
      NFREQ = NWIN
      MZ = NTRY
      RETURN
      END

```

```

C      SPECIAL NXTPR FOR COMBINING RUNS, KYLSTRA
      SUBROUTINE NXTPR
C      COMMON FOR VARIABLES SAME IN DIFFERENT MZ CASES
      COMMON X,H,G,NCT,ID,ID2,FNT,NRD,NDS,M,MZ,MM,MZ2,MPL
      COMMON NFILE,WMAX,NDEX,NFREQ,GT
      COMMON VCTYI,VCTYK,VCTAC
      COMMON JVA,JVB
      DIMENSION X(600),H(601),G(600)
      DIMENSION VCTYI(40),VCTYK(40),VCTAC(40)
      DIMENSION GT(18)
      DIMENSION JVA(40),JVB(40)
C      COMMON FOR VARIABLES THAT DIFFER FROM MZ TO MZ
      COMMON Y,AC
      COMMON TRR,TRI
      DIMENSION Y(750,4), AC(300,4,4), TRR(300,4,4)
      DIMENSION TRI(300,4,4)
      EQUIVALENCE ( X, W)
      DIMENSION DB(300), R(300), W(300), TH1(300), TH2(300)
      DIMENSION T2(300), TR2(300), TI2(300)
      CT = 57.29578
      CL = 4.34294482
      NTRY = MZ
      NWIN = NFREQ
      NTIN = 2
      NTOU = 2
      NTPU = 3
      REWIND NTIN
      IF (XABSF( NWIN) - 5) 505, 505, 502
502 DO 503 I = 1,M
503 X(I) = X(I) * 16.
505 CONTINUE
      DO 50 J = 1, NDEX
      K = JVA(J)
      L = JVB(J)
      DO 52I = 1, M
      A = TRR(I, K,L)
      B = TRI(I,K,L)
      IF ( K-L) 4, 5, 4

```

```

4 CONTINUE
  TH = CT*ATANF ( B/A)
  TH1(I) = TH
  TH2(I) = 180. - TH
  AA = SQRTF( A*A + B*B)
  R(I) = AA
  GO TO 6
5 CONTINUE
  AA = A
6 CONTINUE
  X1 = CL* LOGF(AA)
  IF(I-1) 2, 2, 3
2 XS = X1
3 CONTINUE
  DB(I) = X1 - XS
52 CONTINUE
  IF( K-L) 51, 55, 51
51 CONTINUE
  WRITEOUTPUTTAPE 6, 1001, H(J), ID, K, L
1001 FORMAT ( 1H1 10X 33HVALUES FOR CROSS POWER SPECTRUM,
1 13HNORMALIZED TO E20.8, //
1 10X 8H RUN NO. I5, 12H , CHANNELS I5, 7H , AND
1 I5, //
1 6X 4HFREQ 11X 4HREAL 11X 4HIMAG 10X 3HAMP 9X 5H DB
1 10X 5HTHETA 10X 5HTHETA )
  WRITEOUTPUTTAPE 6, 1002, (W(I), TRR(I,K,L), TRI(I,K,L)
1 , R(I), DB(I), TH1(I), TH2(I), I = 1, M)
1002 FORMAT ( 7E15.6 )
  GO TO 50
55 CONTINUE
  WRITEOUTPUTTAPE 6, 1003, H(J), ID, K, L
1003 FORMAT ( 1H1 10X 31HVALUES FOR AUTO POWER SPECTRUM
1 14H NORMALIZED TO E20.8, //
1 10X 8H RUN NO. I5, 12H , CHANNELS I5, 7H , AND
1 I5, //
1 2X 4HFREQ 12X 5HRTATIO 13X 2HDB 24X 4HFREQ 12X
1 5HRTATIO 13X 2HDB )
  WRITEOUTPUTTAPE 6, 1004, (W(I), TRR(I,K,L), DB(I), I=1,M)
1004 FORMAT ( 4X 3E17.8, 10X 3E17.8 )
50 CONTINUE
  IF (NTRY) 100, 150, 126
C = -, WRITE, = +, READ
100 CONTINUE
  WRITETAPE NTOU, ID, M
  WRITETAPE NTOU, ( TRR(I,1,2), TRI(I,1,2), TRR(I,1,1),
1 I = 1, M)
  GO TO 500
126 CONTINUE
  READ TAPE NTIN, ID2, M
  READ TAPE NTIN, (TR2(I), TI2(I), T2(I), I =1,M)
  NTRY = NTRY - 1

```

```

      IF( NTRY) 150, 150, 127
127  NTRY = NTRY * M * 4
      DO 128 I = 1, NTRY
128  READ INPUTTAPE NTPU, 1115, ITT
1115 FORMAT (I1)
150  CONTINUE
      DO 53I = 1, M
          F3 = TRR(I, 1, 1)
          FR3 = TRR(I, 1, 2) / F3
          FI3 = TRI(I, 1, 2) / F3
          F2 = T2(I)
          FR2 = TR2(I) / F2
          FI2 = TI2(I) / F2
          DEM = FR2*FR2 + FI2*FI2
          RR = ( FR3*FR2 + FI3*FI2) / DEM
          SS = ( FI3*FR2 - FR3*FI2 ) / DEM
          R(I) = RR
          G(I) = SS
          AM = RR*RR + SS*SS
          DB(I) = CL * LOGF ( AM)
          H(I) = SQRTF ( AM)
          THE = CT * ATANF ( SS/RR)
          TH1(I) = THE
          TH2(I) = 180. - THE
53  CONTINUE
      WRITEOUTPUTTAPE 6, 1006, ID , ID2
1006 FORMAT ( 1H1 20X 30HTRANSFER FUNCTION BETWEEN TWO
1 10HDETECTORS /
1 10X 42HRATIO OF CROSS POWER SPECTRUM FOR RUN NO.
1 15, 22H TO THAT OF RUN NO. 15, // 10X 4HFREQ 13X
1 4HREAL 13X 4HIMAG 13X 3HAMP 15X 2HDB 13X 5HTHETA 12X
1 5HTHETA )
      WRITEOUTPUTTAPE 6, 1007, (W(I), R(I), G(I), H(I),
1 DB(I), TH1(I), TH2(I), I = 1, M)
1007 FORMAT ( 1H 7E17.8 )
      ITT = 0
      ITH = 0
      ID3 = ID*10 + ID2
C  PUNCH TAPE B3 FOR LEAST SQUARES INPUT
      DO110 I = 1, M
          WRITEOUTPUTTAPE NTPU, 1010, ITT, ITH, W(I), R(I), I, ID3
110  CONTINUE
          ID3 = ID3 * 10
          DO115 I = 1, M
              WRITEOUTPUTTAPE NTPU, 1010, ITT, ITH, W(I), S(I), I, ID3
115  CONTINUE
1010 FORMAT ( 2I1, 2E20.8, 2I10 )
      ID3 = ID3 * 10
      DO 120 I = 1, M
          WRITEOUTPUTTAPE NTPU, 1010, ITT, ITH, W(I), DB(I), I, ID3
120  CONTINUE

```

```

      ID3 = ID3 * 10
      DO 125 I = 1, M
      WRITEOUTPUTTAPE NTPU,1010,ITT,ITH,W(I),TH1(I),I,ID3
125  CONTINUE
      IF ( NWIN ) 146, 146, 135
C      = 0, DONOT REWIND, = 1, DO
135  REWIND NTPU
      PRINT 1127
1127 FORMAT ( 31HOMAY DISMOUNT TAPE B3 AND SAVE )
146  CONTINUE
500  CONTINUE
      RETURN
      END

```

APPENDIX E

COUNT RATE CIRCUIT DESIGN

The count rate circuit is basically a simple diode pump and storage capacitor network, as described in standard textbooks on electronic circuits (34). However, the specifications of a fast response circuit and little ripple on the output signal cannot be satisfied by the conventional count rate meter design.

Conventional meters use large time constant circuits to obtain an average count rate, whereas in this study, the ability of the circuit to accurately follow the random fluctuations of the neutron density is important. The frequency response of the count rate circuit is an indication of how closely the output signal of the count rate circuit approximates the instantaneous variation of the neutron density. The circuit shown in Figure 32 satisfies the specifications, if the design criteria listed below are used in selecting the values of the resistors and capacitors in the circuit. References (35, 36) also provide information applicable to count rate circuit design.

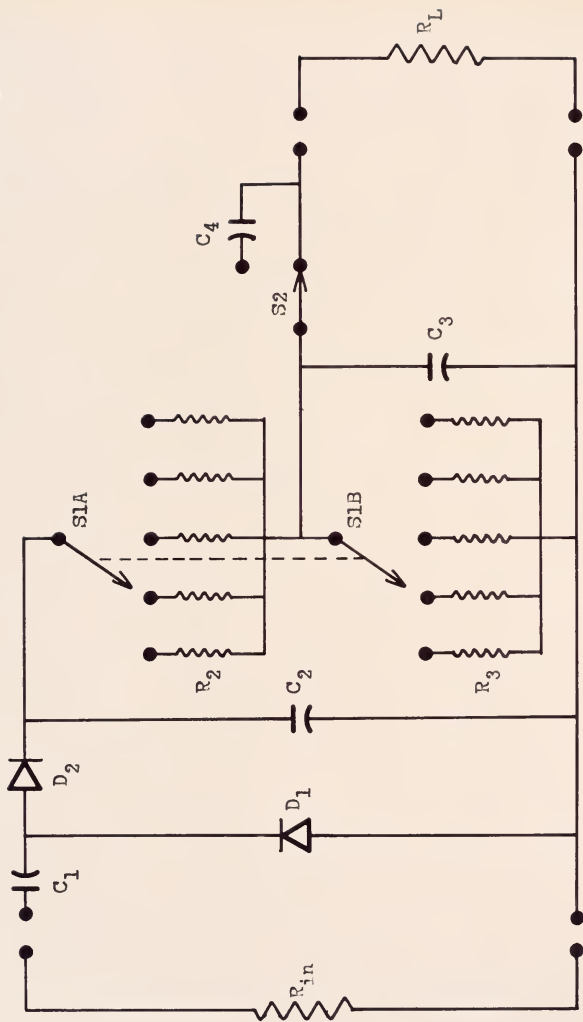


Figure 32. Count rate circuit diagram

TABLE 4
Design Criteria

1. pulse width = 1 μ sec
2. $R_{in} = 10^3 \text{ ohm}$
3. $R_L = 10^6 \text{ ohm}$
4. $R_{in} C_1 = 10^{-7} \text{ sec}$
5. $(C_1 + C_2) / (C_1 C_2 R_{in} f_{\max}^*) > 10$
6. $C_2 (R_2 + R_3) = 4 / f_{\min}^*$
7. $C_1 (R_2 + R_3) = 1 / f_{\max}^*$
8. $C_3 = C_2 / 2$
9. $R_3 / R_2 = 2 / 3$
10. $R_3 \text{ used} = (R_2 + R_3 \text{ cal}) / (R_L - R_3 \text{ cal})$
*f = counts/sec

Design Criteria 1, 2, and 3 were established by the expected input and output impedance of the equipment connected to the count rate circuit and by the characteristics of the input pulse. In practice, R_{in} may have any value up to 10^4 ohms. The circuit will continue to operate for higher values of R_{in} , but the output voltage will be less for the same count rate. The value of the load resistor, R_L , is also flexible. However, to prevent loading of the count rate circuit, R_L should not be much less than 1 megohm, particularly for the low count rate ranges. It may have any value above 1 megohm.

The operation of the circuit is as follows. A negative voltage pulse enters the circuit and starts charging C_1 .

As C_1 is charging, the arrangement of the diodes is such that D_1 shorts C_1 to ground. The equivalent circuit is a series circuit of R_{in} and C_1 . Thus, if Design Criterion 4 is satisfied, C_1 is completely charged by the one micro-second long pulse supplied by the linear amplifier. When the pulse stops, C_1 discharges through D_2 , transferring part of its charge to C_2 . If Design Criterion 5 is satisfied, this transfer is easily made before the next pulse occurs. Although C_2 continuously discharges through R_2 and R_3 , Design Criterion 6 prevents complete discharge of C_2 before the next pulse occurs.

Design Criterion 7 is used to insure that the output of the circuit is approximately proportional to the input pulse rate. The output voltage is generally less than 25 per cent of the peak voltage of the incoming pulses.

If C_3 is not in the circuit, the output signal fluctuates considerably between pulses. This fluctuation is caused by the fast response of C_2 and the bypass resistors R_2 and R_3 . The presence of C_3 adds a low pass filter that smooths the ripple without reducing the frequency response of the circuit. Choosing the values of R_2 , R_3 , and C_3 according to Design Criteria 8 and 9 will reduce the ripple on the signal from the basic circuit by more than 95 per cent and increase the frequency response of the circuit one and one half to two times. Design Criterion 10 adjusts the value of R_3 to compensate for the loading effect of R_L .

Switch 1 has two rotary wafers, allowing simultaneous changing of R_2 and R_3 to obtain a different count rate

range. If desired, C_4 may be included in the circuit by Switch 2 to remove the dc level from the output signal. The values of the components used in the count rate circuit are tabulated in Table 5.

TABLE 5
Count Rate Circuit Components

<u>Range</u>	<u>Counts per sec</u>	<u>R_2, ohm</u>	<u>R_3, ohm</u>	<u>-3db point</u>
1	100 K to 250 K	24 K	16 K	5400 cps
2	40 K to 100 K	60 K	42 K	2000 cps
3	20 K to 50 K	120 K	87 K	1000 cps
4	10 K to 25 K	240 K	196 K	600 cps
5	4 K to 10 K	600 K	667 K	350 cps

$$C_1 = 100 \mu\mu f$$

$$C_2 = 1000 \mu\mu f$$

$$C_3 = 500 \mu\mu f$$

$$C_4 = 2 \mu\mu f$$

D_1 and D_2 are high speed silicon computer diodes.

Figure 33 shows the attenuation of the circuit when on Ranges 1, 3, and 5.

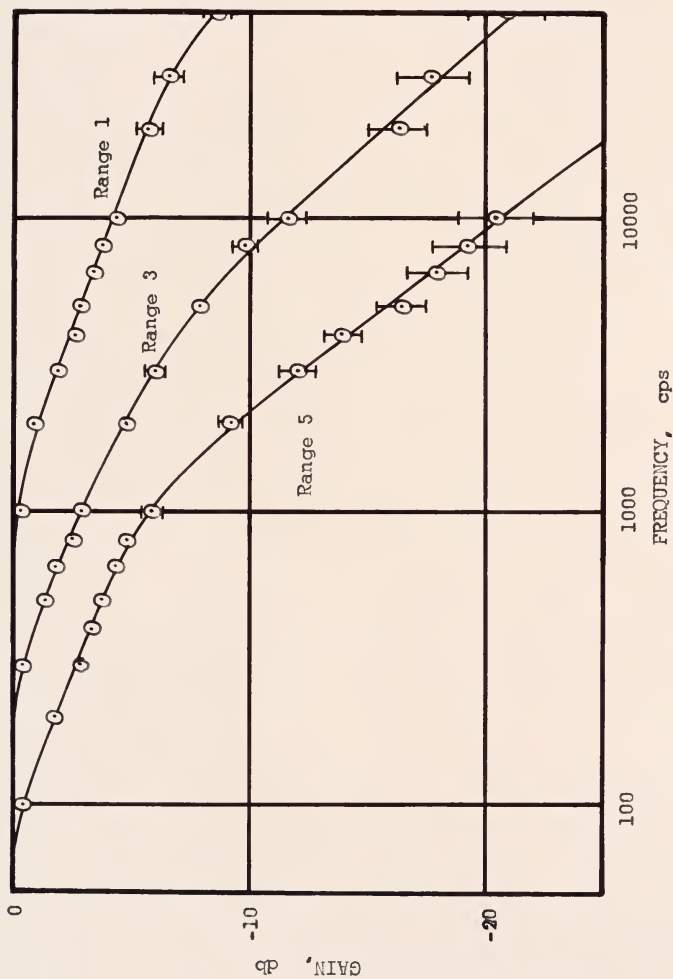


Figure 33. Amplitude of the transfer function for the count rate circuit

BIBLIOGRAPHY

1. Schultz, M. A., Control of Nuclear Reactors and Power Plants, 2nd ed., McGraw-Hill, New York, 1961.
2. Glasstone, S., and M. C. Edlund, The Elements of Nuclear Reactor Theory, C. VanNostrand Co., Inc., Princeton, N. J., 1952.
3. Harrer, J. M., R. E. Boyer, and D. Krucoff, "Transfer Functions of Argonne CP-2 Reactor," Nucleonics, Vol. 10, no. 8, pp 32, 1952.
4. Weinberg, A. M., and H. C. Schweinler, The Physical Review, Vol. 74, no. 8, pp. 851, Oct. 15, 1948.
5. Uhrig, R. E., "Neutron Waves in a Subcritical Assembly," Summary published in Trans. of the ANS, Vol. 2, no. 2, Nov., 1959.
6. Perez, R. B., and R. E. Uhrig, "Propagation of Neutron Waves in Moderating Media," Summary published in Trans. of the ANS, Vol. 5, no. 2, Nov., 1962.
7. Badgley, R. W., "Power Spectral Density of the University of Florida Training Reactor Operating in the Subcritical Region," unpublished M. S. thesis, University of Florida, Gainesville, Florida, Aug., 1962.
8. Boynton, A. R., "Evaluation of Parameters in a Two Slab Reactor by Random Noise Measurements," unpublished Ph. D. dissertation, University of Florida, Gainesville, Florida, Dec., 1962.
9. deHoffman, F., "Intensity Fluctuations of a Neutron Chain Reactor," MDD-C-382, LADA-256 (declassified October 7, 1946).
10. Albrecht, R. W., "The Measurement of Dynamic Nuclear Reactor Parameters by Methods of Stochastic Processes," Trans. of the ANS, Vol. 4, no. 2, pp. 311, 1961.
11. Velez, C., "Autocorrelation Functions of Counting Rate in Nuclear Reactors and Their Application to the Design of Reactor Control Instrumentation," Ph. D. dissertation, University of Michigan, 1959.

12. Moore, M. N., "The Determination of Reactor Transfer Functions from Measurements at Steady Operation," Nuclear Sci. and Eng., Vol. 3, pp. 387-394, 1958.
13. Moore, M. N., "The Power Noise Transfer Function of a Reactor," Nuclear Sci. and Eng., Vol. 6, pp. 448-452, 1959.
14. Cohn, C. E., "Determination of Reactor Kinetic Parameters by Pile Noise Analysis," Nuclear Sci. and Eng., Vol. 5, pp. 331-335, 1959.
15. Griffin, C. W., and J. G. Lundholm, "Measurement of the SRE and KEWB Prompt Neutron Lifetime Using Random Noise and Reactor Oscillating Techniques," NAA-SR-3765, Oct., 1959.
16. Balcomb, J. D., et al., "A Cross Correlation Method for Measuring the Impulse Response of Reactor Systems," Nuclear Sci. and Eng., Vol. 11, pp. 159-166, 1961.
17. Rajagopal, V., "Determination of Reactor Transfer Functions by Statistical Correlation Methods," Nuclear Sci. and Eng., Vol. 12, pp. 218-224, 1962.
18. Meghreblian, R. V., and D. K. Holmes, Reactor Analysis, McGraw-Hill, New York, 1960.
19. Sokolnikoff, I. S., and R. M. Redheffer, Mathematics of Physics and Modern Engineering, McGraw-Hill, New York, 1958.
20. Wallace, P. R., and J. LeCaine, "Elementary Approximations in the Theory of Neutron Diffusion," AECL no. 336, Chalk River, Ontario, Aug., 1943.
21. Wylie, C. R., Jr., Advanced Engineering Mathematics, McGraw-Hill, New York, 1951.
22. Lee, Y. W., Statistical Theory of Communication, John Wiley & Sons, Inc., New York, 1960.
23. Stern, T. E., A. Blaquiere, and J. Valat, "Reactivity Measurements Using Pseudo-Random Source Excitation," Reactor Science and Technology (Journal of Nuclear Energy Parts A/B), Vol. 16, pp. 499-508, 1962.
24. Cockrell, R. G., Private Communication, June, 1963.
25. Poortvliet, D. C. J., "The Measurement of System Impulse Response by Means of Cross-Correlation with Binary Signals," Technological University, Delft, Netherlands.

26. Peterson, W. W., Error Correcting Codes, The MIT Press and John Wiley & Sons, Inc., New York, 1961.
27. Morse and Feshbach, Methods of Theoretical Physics, McGraw-Hill, New York, 1953.
28. Bendat, J. S., Principles and Applications of Random Noise Theory, John Wiley & Sons, Inc., New York, 1958.
29. Fry, D. N., "Pulsed Neutron Measurements in Proton Moderated Media," unpublished M.S. thesis, University of Florida, Gainesville, Florida, Aug., 1962.
30. Smith, S. P. D., "The Construction and Calibration of a Heavy Water Moderated Subcritical Assembly," unpublished M. S. thesis, University of Florida, Gainesville, Florida, April, 1963.
31. Selfridge, R., Private Communication, June, 1963.
32. Neutron Generator, PW 5300, Series D611, D630, Phillips Service, New York, N. Y; Operating Manual.
33. Crandall, J. L., "Status of the United States Effort in D₂O Reactor Physics," Paper prepared for submission to the European-American Reactor Physics Committee, June, 1962.
34. Elmore and Sands, Electronics, McGraw-Hill, New York, 1949.
35. Randall, R. L., "Results of the S2DR Reactor Noise Experiments," NAA-SR 6662, Sept., 1961.
36. Thomas, S., "N-Decade Count Rate Meter with Automatic Scale Change Feature and Resolution of One Decade," IEEE Transactions on Nuclear Science, Vol. NS-10, no. 1, Jan., 1963.
37. Hodgman, C. D., editor, Handbook of Chemistry and Physics, 36th ed., Chemical Rubber Publishing Co., Cleveland, Ohio, 1954.
38. Moore, M. N., Private Communication, July, 1963.
39. Diaz, N. J., Private Communication, July, 1963.
40. McInerney, J. J., "Some Aspects of Neutron Slowing-Down Distributions in Hydrogeneous Media," unpublished paper, Nuclear Engineering Department, Pennsylvania State University, July, 1963.

41. Foderaro, A., and H. L. Garabedian, "A New Method for the Solution of Group Diffusion Equations," Nuclear Sci. and Eng., Vol. 8, no. 1, July, 1960.
42. Moore, M. N., "The Role of the Dispersion Law in Space Dependent Kinetics," Proceedings of the Symposium on Reactor Kinetics and Control, AEC Symposium Series (in press), 1963.
43. Jenkins, F. A., and H. E. White, Fundamentals of Physical Optics, McGraw-Hill, 1937.
44. Edlington, H., "Nuclear Engineering Handbook," McGraw-Hill, 1958.

BIOGRAPHY

Chester D. Kylstra was born November 15, 1936, in Santa Rosa, California. He completed his secondary education at Fossil, Oregon, in May, 1954, and entered Oregon State University the following fall. He received the degree of Bachelor of Science in Mechanical Engineering in June, 1958, and at the same time was commissioned as a Second Lieutenant in the United States Air Force.

He served two years of active duty as a Propulsion Engineer at Patrick Air Force Base, Florida, where he participated in the flight testing of the Goose and Titan missiles at Cape Canaveral.

In September, 1960, he entered the Graduate School of the University of Florida, and received the degree of Master of Science in Engineering the following August. While pursuing his graduate studies, he has held three successive Atomic Energy Commission Special Fellowships in Nuclear Science and Engineering.

Chester D. Kylstra is married to the former Patricia Lee Camp. He is a student member of the American Nuclear Society and a member of Phi Kappa Phi and Tau Beta Pi.

This dissertation was prepared under the direction of the chairman of the candidate's supervisory committee and has been approved by all members of that committee. It was submitted to the Dean of the College of Engineering and to the Graduate Council, and was approved as partial fulfillment of the requirements for the degree of Doctor of Philosophy.

December, 1963.

Thomas L. Hartman, Jr.
Dean, College of Engineering

Dean, Graduate School

Supervisory Committee:

Robert E. Ullrich
Chairman

W. W. W. W. W.

E. R. Parker

John Schussman

John H. H. H.